
Improved Genetically-Encoded Calcium Indicators Based on Troponin C

Marco Mank

Dissertation
an der Fakultät für Biologie
der Ludwig-Maximilians-Universität
München

vorgelegt von
Marco Mank
Naila

München, den 05.02.2008

Erstgutachter:
Zweitgutachter:
Tag der mündlichen Prüfung:

Prof. Dr. Alexander Borst
Prof. Dr. Rainer Uhl
05.03.2008

'Don't study life in order to miss it'

Table of Contents

Table of Contents	V
Table of Figures	IX
Abbreviations	XIII
Abstract	1
Introduction	3
2.1. <i>Fluorescence</i>	4
2.2. <i>Fluorescence Resonance Energy Transfer (FRET)</i>	7
2.3. <i>Fluorescent Proteins</i>	10
2.4. <i>Genetically-Encoded Calcium Indicators (GECIs)</i>	13
Material and Methods	23
3.1. <i>Molecular biology</i>	23
3.1.1. Polymerase Chain Reaction (PCR).....	23
3.1.2. Site-directed mutagenesis via PCR	24
3.1.3. Restriction of DNA	25
3.1.4. Ligation of DNA fragments.....	26
3.1.5. Transformation of chemically-competent <i>E. coli</i>	27
3.1.6. Transformation of electro-competent <i>E. coli</i>	27
3.1.7. Preparation of chemically-competent <i>E. coli</i>	28
3.1.8. Preparation of electro-competent <i>E. coli</i>	28
3.2. <i>Proteinbiochemistry</i>	29
3.2.1. Protein expression using the <i>E. coli</i> BL21 strain.....	29
3.2.2. Purification of recombinantly expressed proteins.....	29
3.3. <i>Spectroscopy</i>	30
3.3.1. Fluorescent spectra of purified proteins	30

Table of Contents

3.3.2. Spectroscopic determination of Kd-value.....	31
3.3.3. Stopped-flow measurements	32
3.4. <i>Cell culture</i>	33
3.4.1. Preparation of dissociated hippocampal neuronal culture.....	33
3.4.2. Transfection of neuronal cell culture using lipofectamine.....	34
3.4.3. Transfection of neuronal cell culture using phosphate-precipitation	34
3.5. <i>Imaging Setup</i>	35
3.6. <i>Transgenic animals</i>	35
3.6.1. Transgenic flies.....	35
3.6.1.1. Spin dialysis	35
3.6.1.2. Injection of fly embryos with DNA.....	36
3.6.1.3. Generation of transgenic fly stocks	36
3.6.1.4. Crossing	37
3.6.1.5. Breeding and husbandry	37
3.6.2. Transgenic mice	37
3.6.2.1. DNA preparation for pronucleus injection.....	37
3.6.2.2. Injection and breeding	38
3.6.2.2. Genotyping	38
3.7. <i>Materials</i>	40
3.7.1. Instruments	40
3.7.2. Consumables.....	40
3.7.3. Buffers, solutions and media.....	41
3.7.4. Chemicals	44
3.7.5. Plasmids, bacterial strains, cell-lines and flies	46
Results	47
4.1. <i>Development of TN-XL, a Mg²⁺-insensitive GECI based on troponin C with fast kinetics</i>	47
4.1.1. Removing Mg ²⁺ -induced FRET signals in troponin C-based GECIs	47
4.1.2. Characteristics of TN-XL.....	51

Table of Contents

4.1.3. Expression of TN-XL in cultured hippocampal neurons	52
4.2. <i>Red-shifted variants of TN-XL</i>	53
4.3. <i>Point mutating the csTnC backbone of TN-XL to lower the Kd for calcium</i>	55
4.3.1. Tuning the troponin C backbone of TN-XL by introducing point mutations in the N-terminal part of csTnC.....	56
4.3.2. Effect of the mutation I130T in csTnC's C-terminal part of TN-XL	57
4.4. <i>Development of TN-XXL, a genetically-encoded calcium indicator with enhanced signal strength</i>	58
4.4.1. Doubling the csTnC's C-terminal part of TN-XL I130T.....	59
4.4.2. Doubling the csTnC's C-terminal part of TN-L15 N108D D110N I130T Citrine cp174	61
4.5. <i>Comparison of TN-L15, TN-XL and TN-XXL with respect to decay time constant τ</i>	64
4.6. <i>Performance of TN-XXL in cell culture</i>	66
4.6.1. Detection of calcium signals in primary hippocampal neurons with TN-XXL.....	67
4.6.2. Imaging calcium oscillations in HEK293 cells	68
4.7. <i>Applying different strategies to improve the troponin C-based GECI TN-XXL</i>	69
4.7.1. Expanding the C-terminal doubling strategy to variants of troponin C from different species	70
4.7.2. Reducing the calcium binding site in TN-XXL to one C-terminal domain.....	72
4.7.3. Introducing aspartic acid to glutamic acid (D \rightarrow E) conversion to the -X position of chelating loops III and IV in the TnC backbone of TN-XXL	74
4.8. <i>Comparison of TnC-based with CaM-based GECIs and one synthetic calcium indicator (OGB-1)</i>	78
4.9. <i>Transgenic animals</i>	80
4.9.1. Transgenic expression of TN-XXL in <i>Drosophila melanogaster</i>	80

4.9.2. Creating transgenic mice with TN-XL and TN-XXL using the human GFAP-Promoter	82
Discussion.....	85
<i>5.1. Enhancing signal strength in TN-L15</i>	<i>85</i>
<i>5.2. Reducing the calcium binding moiety in troponin C-based GECIs to a single EF-hand domain</i>	<i>93</i>
<i>5.3. In vivo comparison of troponin C-based GECIs at the Drosophila NMJ</i>	<i>94</i>
<i>5.4. Determination of TN-XXL's detection threshold in organotypic hippocampal slices</i>	<i>102</i>
<i>5.5. In vivo detection of sensory evoked calcium transient in mouse visual cortex</i>	<i>104</i>
<i>5.6. Outlook</i>	<i>107</i>
References.....	109
Acknowledgements	119
Curriculum Vitae	121
Versicherung	123

Table of Figures

Figure 1: Jablonski diagram	5
Figure 2: Dependency of κ^2 on the directions of the transition dipoles.....	9
Figure 3: Three dimensional structure of GFP (pdb entry 1Q4A) and the mechanism of chromophore formation.....	11
Figure 4: Calcium coordination to the first EF-hand of calmodulin.....	16
Figure 5: Structural change in EF-hands I and II of calmodulin upon calcium binding.....	17
Figure 6: Fluorescence excitation and emission spectra of CFP and Citrine.	19
Figure 7: Three dimensional structure of chicken skeletal troponin C.....	21
Figure 8: Fluorescence emission spectra of TN-L15 and TN-L15 Citrine cp174, two troponin C-based GECIs.....	48
Figure 9: Ribbon and stick representation of the calcium binding loops III and IV in csTnC.	48
Figure 10: Fluorescence emission spectra of different variants with disrupted Z-acid pairs of EF-hand III and IV.	49
Figure 11: Schematic of the substitutions in the calcium binding loops III and IV in TN-XL.	50
Figure 12: Characteristics of TN-XL.....	51
Figure 13: Performance of TN-XL and TN-L15 in primary hippocampal neurons.....	53
Figure 14: Fluorescent emission spectra of red-shifted TN-XL variants.....	54
Figure 15: Comparison of the red-shift approach to CFP/YFP FRET indicators.	55
Figure 16: Substitution of single hydrophobic residues in the N-terminal lobe of csTnC in TN-XL.	56
Figure 17: Effect of the I130T mutation in the C-terminal part of csTnC in TN-XL.	58
Figure 18: Doubling the C-terminal part of csTnC in TN-XL I130T.....	60

Figure 19: Kd and ΔR/R values obtained from the C-terminal doubling variants of TN-XL I130T	60
Figure 20: Characteristics of TN-L15 Citrine cp174 variants with single mutated EF-hand loops.....	62
Figure 21: Schematic drawing of the strategy used to develop TN-XXL	63
Figure 22: Comparison of selected troponin C-based GECIs	63
Figure 23: Comparison of decay time constants obtained from TnC-based GECIs	65
Figure 24: Comparison of the parameters obtained from TnC-based GECIs.	66
Figure 25: Activity of a primary hippocampal cell reported by TN-XXL	67
Figure 26: Inhibition of the calcium signals produced by primary hippocampal neurons with TTX.....	68
Figure 27: Eliciting calcium oscillations in HEK293 cells.....	69
Figure 28: Amino acid alignment of the C-terminal parts of wild type chicken skeletal, mouse skeletal and zebrafish skeletal troponin C.....	70
Figure 29: Titration curves of nine different indicators based on the C-terminal doubling of troponin C from different animals.	71
Figure 30: Kd and ΔR/R values obtained from the C-terminal doubling of troponin C from different species.	72
Figure 31: Reducing the calcium binding moiety of TnC-based GECIs to one EF-hand domain.	73
Figure 32: Schematic drawing of the aspartic acid to glutamic acid substitution in -X position of chelating loops in EF-hand III and IV of csTnC.	74
Figure 33: Titration curves obtained from the different aspartic acid to glutamic acid substitutions in EF III and IV of TN-XXL.	75
Figure 34: Comparison of the actual ΔR/R values in [%] of the aspartic acid to glutamic acid substitutions elicited by all permutations.	76
Figure 35: Selected variants of the aspartic acid to glutamic acid substitution compared to TN-XXL.	78
Figure 36: Comparison of TnC-based with CaM-based GECIs and OGB-1. .	79
Figure 37: Comparison of ΔF/F and ΔR/R values from different calcium indicators at 65 nM free Ca ²⁺	79

Table of Figures

Figure 38: Transgenic expression of TN-XXL in <i>Drosophila melanogaster</i> using the Gal4/UAS-system.	81
Figure 39: Schematic of the constructs used to create transgenic mice.	83
Figure 40: Glial calcium signals detected with TN-XL using the hGFAP promoter.	83
Figure 41: Dependency of FRET-efficiency on the distance of two chromophores with a Förster radius (R_0) of 50 Å.	88
Figure 42: Effect of the I130T mutation in csTnC -based calcium indicators.	90
Figure 43: Comparison of the basal FRET in two TnC-based GECIs with different amount of calcium binding sites.	94
Figure 44: <i>In vivo</i> comparison of troponin C-based GECIs at the <i>Drosophila</i> NMJ.	96
Figure 45: Comparison of actual $\Delta R/R$ values in [%] obtained from different csTnC-based GECIs in two different systems.	97
Figure 46: Effect of mimicking <i>in vivo</i> conditions to the spectra of the calcium titrations of purified TN-XXL obtained from cuvette data.	98
Figure 47: Comparison of <i>in vivo</i> mimicked data of calcium titrations to <i>in vivo</i> data obtained at the <i>Drosophila</i> NMJ for three TnC-based GECIs.	99
Figure 48: Signal strength of OGB-1 obtained at different resting calcium values.	101
Figure 49: <i>In vitro</i> responses of TN-XXL in organotypic hippocampal slices.	103
Figure 50: <i>In vivo</i> detection of sensory evoked calcium transients using TN-XXL.	106

Abbreviations

AM	acetoxyethyl
AM	acetoxyethyl
AtoA	area to area
ATP	adenosine 5'-triphosphate
ATP	adenosine 5'-triphosphate
BAPTA	1,2-bis-[2-aminophenoxy]ethane-N,N,N',N'-tetraacetic acid
BAPTA	1,2-bis-[2-aminophenoxy]ethane-N,N,N',N'-tetraacetic acid
BBS	BES-buffered saline
BES	N,N-bis[2-hydroxyethyl]-2-aminoethanesulfonic acid
BFP	blue mutant of GFP
BSA	bovine serum albumin
CaM	calmodulin
CCD	charge-coupled device
CFP	cyan fluorescent protein
CMV	cytomegalovirus
CP	circularly permuted
csTnC	chicken skeletal muscle troponin C
DMEM	Dulbecco's Modified Eagle Medium
DMSO	dimethyl sulfoxide
DNA	desoxyribonucleic acid
DsRed	red fluorescent protein from <i>Discosoma</i> sp.
E18	embryonic day 18
EDTA	ethylenediamine tetraacetic acid
EGTA	ethylene glycol-bis[β-amino-ethyl ether] N,N,N',N'-tetraacetic acid
F	fluorescence light intensity

FCS	fetal calf serum
FRET	fluorescence resonance energy transfer
Gal4	yeast transcription factor Gal4
GFAP	glial fibrillary acidic protein
GFP	green fluorescent protein
HBSS	Hanks' balanced salt solution
HEK	human embryonic kidney
HEPES	N-(2-hydroxyethyl)piperazine-N'-(2-ethanesulfonic acid)
IPTG	isopropyl-β-D-thiogalactopyranoside
Kd	dissociation constant
K_{off}	dissociation rate constant
K_{on}	association rate constant
LB	Lysogeny broth, Luria broth or Luria-Bertani broth
MOPS	3-(N-morpholino)propanesulfonic acid
mTnC	mouse troponin C
NMJ	neuromuscular junction
NTA	nitriloacetic acid
OD₆₀₀	optical density (absorption) at 600 nm
OGB-1	oregon green BAPTA, synthetic calcium indicator
PBS	phosphate-buffered saline
PBT	phosphate-buffered saline with Triton-X-100
PCR	polymerase chain reaction
PIPES	piperazine-1,4-bis(2-ethanesulfonic acid)
PMSF	phenylmethylsulfonylfluoride
PtoP	peak to peak
R	ratio; fluorescence intensity of acceptor emission over donor emission
R_{max}	ratio R at highest ligand concentration
R_{min}	ratio R in ligand-free conditions

Abbreviations

SDS	sodium dodecyl sulfate
SFV	semliki forest virus
TAE	tris-acetate-EDTA electrophoresis buffer
TE	tris-EDTA buffer
TnC	troponin C
TTX	tetrodotoxin
UAS	upstream activation sequence
WT	wildtype
XCaM	xenopus calmodulin
YC	yellow cameleon
YFP	yellow fluorescent protein
zTnC	zebrafish troponin C
ΔF/F	fractional change in fluorescent light intensity
ΔR	difference of ratio R under Ca^{2+} -saturated and Ca^{2+} -free conditions

Abstract

Calcium imaging is one of the standard methods used in physiology and cell biology to report activity of various cell-types, with a special class of calcium sensors called the Genetically-Encoded Calcium Indicators (GECIs) being developed during the last ten years.

Our lab created a GECI that makes use of Fluorescence Resonance Energy Transfer (FRET) using spectral variants of GFP, namely CFP and YFP. Both fluorescent proteins enwrap the chicken skeletal troponin C (csTnC) that is able to bind calcium and therefore modulates FRET which is used as fluorescence readout. The first generation of troponin C-based GECIs, TN-L15, reported calcium changes in cell culture and transgenic animals but showed insufficient signal strength to small calcium fluctuations and poor kinetics. The aim of this research was to enhance the response properties of TN-L15 with respect to signal strength and kinetics. By using a circularly permuted acceptor variant, the introduction of point mutations inside the csTnC backbone and a ‘doubling’ of the mutated C-terminal domain of csTnC, new troponin C-based GECIs could be developed. Point mutating the calcium binding loops III and IV of the csTnC backbone in TN-L15 led to an indicator with fast kinetics, named TN-XL. Additionally, a profound rearrangement of the calcium binding domain, the doubling of the C-terminal part of csTnC, yields another version of troponin C-based GECIs. This indicator, named TN-XXL, showed a 2.4 fold increase in signal strength according to the calcium regime up to 1.35 μM when compared to TN-L15. Transgenic expression of TN-XL and TN-XXL at the *Drosophila* larval neuromuscular junction (NMJ) confirmed the improvement of these indicators when comparing the response properties of troponin C-based GECIs *in vivo*. Furthermore by using TN-XXL it was possible to record single action potentials in organotypic hippocampal slices using patch clamp techniques. Finally, by viral expression of TN-XXL in the primary visual cortex of mice, the indicator was able to detect sensory evoked calcium transients *in vivo*.

Introduction

Fluorescence imaging has become one of the most powerful tools in biology during the last few decades, in part due to the event of fluorescence occurring at a time scale of about 10^{-9} s, making it suitable for detecting various biological and biochemical processes. Among these, shuttling of proteins between distinct cellular organelles or changes in intracellular messengers such as calcium can be detected by using fluorescence techniques. Fluorescence microscopy is a very sensitive method since it enables the detection of low levels of light that is emitted by a fluorescent probe. The high sensitivity of fluorescence microscopy is provided by the separation of the fluorescent probe and an (ideally) non-fluorescent background which does not contribute to emitted photons that are detected.

Fluorescence microscopy techniques have undergone many improvements over the last few years. On the one hand fluorescence microscopy has improved in terms of single photon microscopy such as STED (1) or PALM (2) microscopy. These two techniques allow for nanoscale fluorescence microscopy down to 20 nm lateral resolution (2, 3) that, in turn, shows that the diffraction limit as described by E. Abbe in 1873 is not longer valid. On the other hand multiphoton microscopy like 2P-microscopy (2-photon) exploits longer wavelength excitation light and therefore achieves larger penetration depths into biological tissue by using a pulsed laser to excite a given chromophore ‘in two steps’ (4). This technique highlights a milestone for biological imaging since it expanded the access to deeper structures. In that line the use of fiber optics has led to an even higher penetration of biological systems in terms of implanting a fiber coupled lens directly to a given structure like the hippocampus (5).

Beside these technical improvements innovations in the field of fluorescent dyes (small synthetic dyes, fluorescent proteins, small synthetic indicators or genetically-encoded sensors of biological processes) has led to a new era of visualizing biological processes. Fluorescent tagging of proteins can be

achieved by simply expanding the protein's DNA of interest with the coding sequence of a given fluorescent protein. Additionally fluorescent highlighting can be attained with small biarsenical synthetic dyes attached to the protein via a tetracysteine motif (6, 7). Up to now fluorescent compounds, synthetic or genetically-encoded, have been developed into functional biosensors to monitor a variety of biological processes.

2.1. Fluorescence

Fluorescence can be grouped together with phosphorescence to form the phenomenon called luminescence. Hereby we will define an event exploiting the conversion of energy evoked by an appropriate molecule that absorbs a photon of a given energy level. The energy of this photon elicits a transition of an electron in the ground state to an excited singlet state (absorption) whereby the electron in the excited orbital is of opposite spin to the electron in the ground state orbital. From this excited state the electron returns to its ground state within a short period of time, with a typical fluorescence lifetime (τ) of $1 - 10 \times 10^{-9}$ s. During this time between excitation and the return to the ground state a photon is released (emission) (Figure 1). Absorption usually takes place at the lowest vibrational level ($v = 0$) of the lowest energy state (S_0), thus, after light absorption an electron is shifted to higher vibrational levels (e.g. $v = 1, 2$) in higher energy states (e.g. S_1, S_2). Return from higher vibrational levels to the lowest vibrational level in the excited energy state (S_1) is called 'Internal Conversion' and occurs within 10^{-12} s. This is much faster than the fluorescence lifetime and the return of the excited electron to the lowest vibrational level in S_1 is completed before emission and results in a thermally equilibrated state. From this state the electron drops back to the ground state where it usually occupies a higher vibrational level before it returns to the lowest vibrational level in S_0 (within 10^{-12} s, in terms of heat). As a result of the energy difference of the electron that is excited by an absorbed photon ($h\nu_A$) compared to the electron that cause emission of a photon ($h\nu_E$)

Introduction

the required wavelength of the absorbed photon is smaller than that of the emitted photon. This red-shift between excitation and emission is called 'Stokes' Shift'. Since excitation occurs on a very fast time scale (10^{-15} s) the distance of the nuclei will not change during excitation, an observation called the 'Franck-Condon Principle'. Distinct transitions of an electron to vibrational levels in the excited electronic state are occurring proportionately to the overlap of their vibrational wave functions. After relaxation to the lowest vibrational level of S_1 transitions to distinct vibrational levels in S_0 (e.g. $S_1, v = 0$ to $S_0, v = 2$) occur at the same frequency as transitions after excitation to distinct vibrational levels in S_1 (e.g. $S_0, v = 0$ to $S_1, v = 2$). Therefore emission spectra are red-shifted to the corresponding excitation spectra and often display mirror symmetry.

An alternative way for the excited state electron to decay is provided by an 'Intersystem Crossing'. This action comes along with a spin conversion and ends in the first triplet state (T_1) (Figure 1). Transition from T_1 to S_0 is forbidden due to the same spin orientation of the electrons in both states resulting in a longer lifetime of the triplet electron (10^2 s - minutes) compared to the lifetime of the singlet excited state. This phenomenon is called phosphorescence.

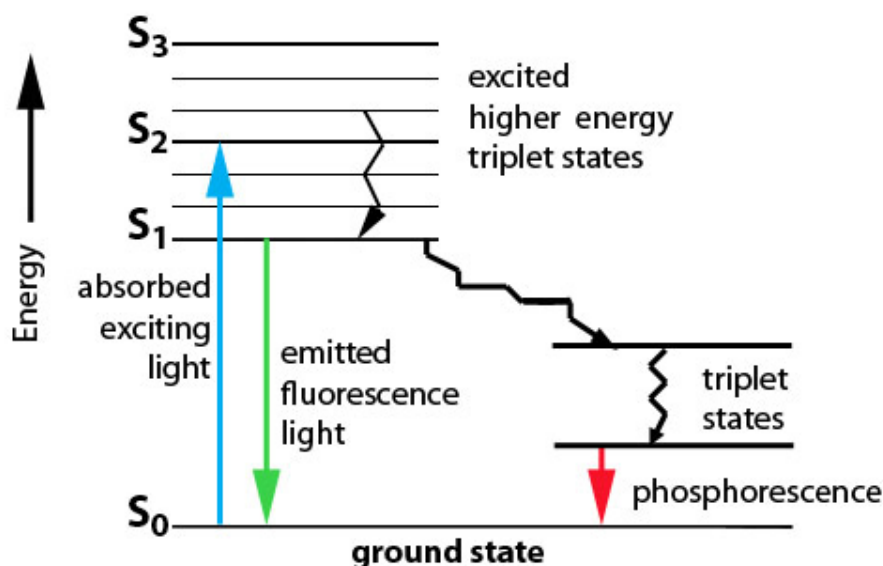


Figure 1: Jablonski diagram

One important characteristic of a fluorophore is its quantum yield (Q) that can be defined as the ratio between emitted and absorbed photons. It can be determined by the rates of emissive (relaxation of the excited state electron to the ground state by emission of a photon) and non-emissive (relaxation of the excited state electron to the ground state by non-emissive processes, e.g. quenching) decay properties:

$$Q = \frac{\Gamma}{\Gamma + k_{ne}}$$

Q = quantum yield

Γ = rate of emissive decay [s^{-1}]

k_{ne} = rate of non-emissive decay [s^{-1}]

If the rate of non-emissive decay is much smaller than the emissive decay of the excited electron this equation reaches approximately 1, that in turn resembles an almost 100 % conversion of all absorbed photons to emitted photons. A number of different events can cause a reduction of the quantum yield and hence the intensity of fluorescence and such processes are referred to the ‘Quenching Phenomenon’. Collisional Quenching (deactivation of the excited state through contact with other molecules), Fluorescence Resonance Energy Transfer (FRET, non-radiative transfer of the excited state energy to an acceptor molecule) or Static Quenching (formation of non-fluorescent complexes with other molecules) are the most common mechanisms to reduce the quantum yield of a fluorophore. In addition, another important factor that should be considered when describing a fluorescent probe is its molar extinction coefficient (ϵ). This defines the amount of absorbed photons of a given substance at a defined wavelength measured in an absorption photometer (at a concentration of 1 mol/l with a pathlength of 1 cm). Combined, both factors together determine the overall brightness of a fluorophore.

Reduction of the fluorescence of a given species can also be due to a particular mechanism called Photoisomerization. As describe for the wild type

Introduction

Green Fluorescent Protein (GFP), which possesses two absorption peaks (395 nm and 475 nm), strong illumination of the 395 nm excitation peak causes the decline of this particular excitation peak and shifts the absorption towards the second peak at 475 nm because of the isomerization to the anionic form of the chromophore and hence a loss of fluorescence (8). For a detailed description of the wild type GFP the reader is referred to the 'Fluorescent Proteins' section (2.3.).

Besides quenching and photoisomerization, one additional phenomenon can be observed in fluorescence spectroscopy namely Photobleaching. Usually the excitation/emission cycle of a fluorophore occurs over ten thousand times before photobleaching takes place (9). As mentioned above the excited state of a fluorophore can come in two forms: the short lived singlet state and the long-lived triplet state. It is thought that the triplet state interacts with other molecules (also in the triplet state) especially molecular oxygen. Transfer of energy from the fluorophore to oxygen will cause activation of the latter to its singlet excited state that is capable of proceeding chemical reactions, e.g. with the chromophore itself. This can lead to an irreversible destruction of the fluorophore and hence loss of fluorescence (9).

2.2. Fluorescence Resonance Energy Transfer (FRET)

The first description of Fluorescence Resonance Energy Transfer (FRET) was provided by Theodor Förster in the middle of the 20th century (hence FRET can also be referred to as Förster Resonance Energy Transfer) and can largely be regarded as a special case of quenching. In this case an excited state fluorophore (donor) transfers its energy to an acceptor molecule that in turn reaches its excited state without emission of a photon from the donor. For FRET to occur the spectral properties of donor and acceptor have to fulfill some important criteria that will be described in this part.

FRET-efficiency strongly depends on the distance of two chromophores and can be described as follows:

$$E_{FRET} = \frac{R_0^6}{R_0^6 + r^6}$$

E_{FRET} = FRET-efficiency

R_0 = Förster radius [nm]

r = distance [nm]

The constant R_0 (also named Förster radius) defines the distance of a given FRET pair at which the efficiency of energy transfer reaches half-maximum. It can be calculated according to the equation:

$$R_0^6 = 8.79 * 10^{-25} [\kappa^2 n^{-4} Q_D J(\lambda)]$$

R_0^6 = Förster distance [cm^6]

n = refractive index of the medium

Q_D = quantum yield of donor in the absence of acceptor

$J(\lambda)$ = overlap integral [$\text{M}^{-1} \text{cm}^3$]

Note: The factor 8.79×10^{-25} is calculated from physical constants among them the Avogadro's number that occurs in the denominator and therefore provides the dimension [mol].

There are two important factors that define the Förster distance and hence the FRET-efficiency, namely the overlap integral $J(\lambda)$ of donor emission and acceptor excitation and the orientation factor κ^2 that describes the orientation of the transition dipoles of the two fluorophores. The overlap integral can be described as follows:

$$J(\lambda) = \int_0^\infty F_D(\lambda) \varepsilon_A(\lambda) \lambda^4 d\lambda$$

Introduction

- $J(\lambda)$ = overlap integral [$M^{-1} \text{ cm}^3$]
 $F_D(\lambda)$ = normalized fluorescence intensity of the donor
 $\epsilon_A(\lambda)$ = extinction coefficient of the acceptor at λ [$M^{-1} \text{ cm}^{-1}$]
 λ = wavelength [cm]

The second dependence of FRET-efficiency is defined by the orientation of the transition dipoles that abstract the fluorophores (emission transition dipole of donor and absorption transition dipole of acceptor). This relation is expressed by the orientation factor κ^2 that can be calculated from:

$$\kappa^2 = (\cos \theta_T - 3 \cos \theta_D \cos \theta_A)^2$$

- θ_T = angle between transition dipole of emission of donor and transition dipole of absorption of acceptor
 $\theta_{D/A}$ = angle between the depicted transition dipole and the vector joining donor and acceptor

Figure 2 represents a schematic diagram of the vectors and angles that define the orientation factor κ^2 . It is interesting to note that κ^2 can have values from 0 to 4. If the transition dipoles are oriented perpendicular to each other κ^2 becomes 0 and subsequently FRET does not occur.

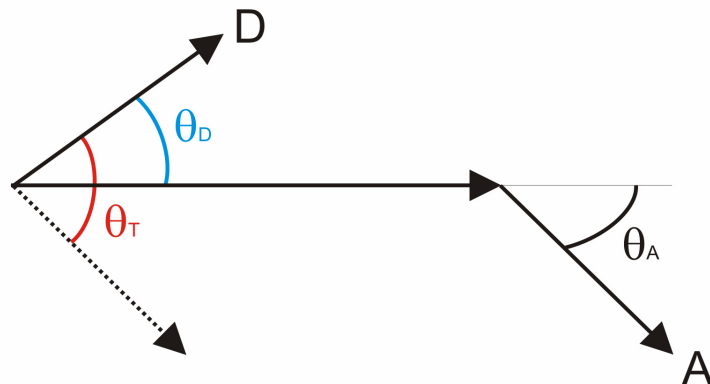


Figure 2: Dependency of κ^2 on the directions of the transition dipoles.

For practical use one has to mention that distance is the primary factor that varies FRET-efficiency. For small fluorescent dyes (particularly in solution and freely diffused but also attached via a freely rotating covalent bond) the orientation factor can be defined as constant 2/3. Additionally the overlapping integral is fixed for a given FRET pair and consequently this is the reason why FRET was primarily used as a ‘molecular ruler’ to measure distances. One exception to this rule is the intramolecular fusion of two fluorescent proteins that are suitable for FRET. In this case the orientation is relatively rigid according to the protein structure and allows tuning of FRET-efficiency by altering the orientation of donor and acceptor transition dipoles.

2.3. Fluorescent Proteins

Beside the well established small fluorescent synthetic compounds like fluorescein a number of Fluorescent Proteins (FPs) have emerged during the last few decades. In this context the discovery of the Green Fluorescent Protein (GFP) set a milestone for biological imaging. First described by Shimomura and colleagues in 1962 (10) it took approximately 40 years until the cDNA was cloned and GFP could be used as a molecular marker in cell biology (11, 12). GFP variants were discovered in two different organisms with the most commonly used being GFP (which acted as template for mutagenesis that yielded the famous EGFP) that was extracted from the jellyfish *Aequoria victoria* (Victoria, British Columbia, Canada) (13). GFP also occurs in the sea pansy *Renilla reniformis* (Georgia, USA) (14). Interestingly GFP was discovered as a co-factor that transduces the blue emission of aequorin into a greenish light. The mechanism that is utilized refers to RET (Resonance Energy Transfer), an energy transfer from the bioluminescent aequorin to GFP. Solving the crystal structure revealed that GFP consist of 11 β -sheets building up a so called β -barrel (or β -can) (Figure 3A).

This cage-like structure covers a central α -helix at which the matured chromophore is tethered (15, 16). The fluorophore of GFP is built from three

Introduction

subsequent amino acid residues namely serine65 (S65), tyrosine66 (Y66) and glycine67 (G67). The generation of the fluorescent part, a so called 4-(*p*-hydroxybenzylidene)imidazolidin-5-one, is carried out in an autocatalytic manner without any external co-factors except of molecular oxygen (8) (Figure 3B) and allows easy labeling of cells by delivering the DNA that encodes GFP. An interesting phenomenon of wild type GFP is its complex spectral characteristic.

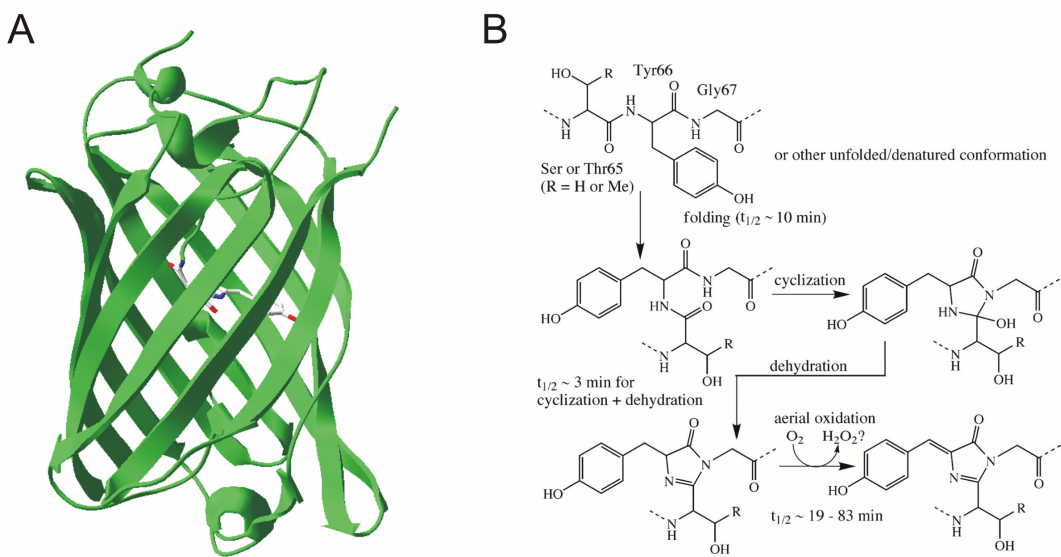


Figure 3: Three dimensional structure of GFP (pdb entry 1Q4A) and the mechanism of chromophore formation.

Picture in (A) was redrawn using DeepView/SwissPdbViewer 3.7. Picture in B is taken from (8).

The fluorescence excitation spectrum contains two peaks (395 nm and 475 nm) that give rise to almost identical emission peaks at 508 nm and 503 nm respectively. The two distinct excitation maxima correspond to two different populations of the chromophore. The deprotonated or anionic (phenolate) form of the fluorophore (R^-) gives rise to the 475 nm peak whereas the 395 nm peak comes from the protonated form (RH) (8). The excited state of the neutral form is thought to be much more acidic. An Excited State Proton Transfer (ESPT) occurs giving rise to a deprotonation and therefore a highly similar emission spectrum with regard to direct excitation of the deprotonated fluorophore (8). Both deprotonated states are not equal i.e. there exist two

different stabilized forms. An intermediate I-state formed by excitation and subsequent deprotonation (ESPT) of RH and an equilibrated B-state that is due to excitation of R⁻. This results in the slightly variation in emission peaks formed by wild type GFP (17) and represents the photophysical basis for direct stabilization of the two states that has been achieved by mutating wild type GFP to EGFP and the Sapphire variant. EGFP exploits the S65T mutation that is known to stabilize the anionic form of the fluorophore and hence a single absorption peak at 489 nm (18). On the other hand a sole excitation peak at 399 nm is achieved in the Sapphire variant of GFP due to the mutation T203I (19).

Since chromophore formation is realized by the three adjacent amino acids wavelength alteration can be obtained by replacing aromatic residues. For example the variants CFP (Cyan Fluorescent Protein, indole chromophore, Y66W) and BFP (Blue Fluorescent Protein, imidazole chromophore, Y66H) emerged by changing a single amino acid residue inside the chromophore forming positions (19). In addition of changing an aromatic side one can achieve a red shift by a so-called π-stack. A structurally nearby amino acid residue (T203Y) gives rise to a stack of two independent π-systems that yield the group of YFPs (Yellow Fluorescent Proteins) (8). YFP is sensitive to environmental factors like fluctuations in pH or halide concentration (20, 21) that can be exploited to record pH or halide changes in cells (22, 23). Nevertheless for a biosensor that depends on FRET one would like to have a stable variant of YFP that acts as an acceptor. For this reason mutagenesis was applied to the YFP that yielded two pH and halide stable variants referring to as Citrine and Venus (24-26), both of which are successfully used in FRET-based biosensors.

A plethora of different FPs were discovered and subcloned from different species during the last years. Particular attention was paid to the discovery of red shifted FPs in order to enhance the color spectrum. This has the advantage of e.g. multicolor labeling. Most famous among these proteins is DsRed from *Discosoma striata*, the first Red Fluorescent Protein (RFP) that has been discovered (27). This obligate tetramer was finally engineered to the monomer mRFP1 (λ_{PeakExc} 584 nm/ λ_{PeakEm} 607 nm) (28) which marked the

Introduction

basis of a more recent broadening of the FP spectrum. Using the technique of somatic hypermutation and random mutagenesis the group of Roger Tsien could develop the so called mFruits, fluorescent proteins that cover almost the entire visible spectrum (29, 30).

2.4. Genetically-Encoded Calcium Indicators (GECIs)

To decipher various system or cell biological events one has to possess the capability of detecting these. In neurobiology the standard method to obtain information about the activity of distinct neurons is electrophysiology; with the use of patch clamping or sharp electrode techniques allowing the time course of electrical activity from individual nerve cells to be recorded.

Although changes in the membrane potential are directly linked to activity of neurons, they are hard to detect by optical means. Optical imaging of the membrane potential would have the advantage to record the activity of a huge number of neurons simultaneously. This in turn would make this technique superior to electrophysiology where only a single or a few cells can be recorded at the same time. There exist a number of optic voltage sensors mainly synthetic ones (31-34) but none of these sensors provided the basis for practical usage in neuroscience so far.

To circumvent these problems an alternative approach has emerged in the last few years. In order to detect activity of neurons directly one can use the visualization of calcium transients that correspond to electrical activity. Also here the first sensors were based on small organic compounds like EGTA. A couple of different synthetic calcium sensors were developed among these e.g. OGB-1 (35), the stil-, fura-, indo-family (36) and the rhod- and fluo-family (37).

Synthetic dyes can be applied to a cell by loading with electrodes. In this case only one or a small subset of cells will be labeled (usually when more than one electrode is used). Alternatively the so-called AM-derivatives (acetoxymethyl esters) of small molecule sensors can be used to incorporate

the indicator of choice in more than one particular cell. AM-derivatives of synthetic indicators can pass biological membranes and undergo cleavage inside the cytosol by intracellular esterases. The cleaved form of the AM-ester is eventually trapped inside the cell. A novel approach to yield *in vivo* labeling for a population of cells - the so called bulk loading technique - was recently developed by Stosiek and colleagues (38).

A different method to increase the amount of neurons from which signals can be recorded is genetic labeling. Therefore a genetically-encoded calcium sensor (GECI) can be used that additionally allows, by using an appropriate promoter system, labeling of a distinct population or sub-population of neurons. A GECI is a calcium biosensor with a fluorescent and a calcium binding domain that are entirely genetically-encoded. Another important advantage of using GECIs is that they can be targeted to defined compartments inside a cell. In that respect the labeling of Golgi (24), mitochondria (39), nucleus (40) or the plasma membrane (41) has been achieved.

Protein-based calcium chelation is the initial step in the cascade leading to manipulation of a biosensor's fluorescence output. The nature of the appropriate binding sites determines the properties of a biosensor and the design options for sensor construction. It is therefore worthwhile to have a closer look at the molecular constitution and functional characteristics of these motifs. Apart from some unconventional calcium binding sites (for example in calpains (42)) there are two prominent types of intracellular calcium binding motifs that are able to chelate calcium in the physiologically relevant range, the C2 domain and the EF-hand.

The C2 domain is found in a huge variety of different proteins e.g. phospholipase A₂ (PLA₂), phospholipase C (PLC), protein kinase C (PKC) or synaptotagmin (43). A feature of many C2 domains is that they bind calcium and phospholipids although there are variants that have evolved to bind other targets. PKC was the first protein where the C2 domain was found. It consists of ~130 amino acid residues and the structure reveals a scaffold consisting of eight β-sheets. On top of this scaffold three loops are attached that promote calcium and phospholipid binding. It is interesting to note that the coordination

Introduction

sphere is provided by residues that are not neighbored in the linear sequence and that the phospholipid can act as a ligand for calcium binding as it has been shown for the PKC-C2 domain (44). Calcium can be bound in the absence of a phospholipid although presence of the latter increases the affinity for this particular ion. For example, the Kd value for calcium of the C₂A domain of synaptotagmin I is >1 mM but is decreased about 1000-fold in the presence of phospholipids (43). C2 domains apparently do not display a significant structural rearrangement of the protein backbone upon calcium binding as shown for the C₂A domain of synaptotagmin I (45). Due to the interrelationship between phospholipid and calcium binding, the large domain size with chelating residues distributed far apart and the possible binding to other targets C2 domains appear not a first choice for indicator construction. Thus a more suitable candidate for GECIs is the well-known calcium binding protein domain called EF-hand. It was first described in parvalbumin (46) and represents a helix-loop-helix motif of ~30 amino acids that is capable of coordinating one calcium (or magnesium) ion. Usually EF-hands occur as pairs in proteins so that most EF-hand containing polypeptides have 2, 4, 6 or more EF-hand domains. The most important part of the domain is the loop region that gives rise to the coordination space through predominantly negatively charged amino acid residues. Most EF-hand containing proteins possess the so called canonical EF-hand. This version of the domain exhibits a 12 residue calcium binding loop consisting of 9 residues in the loop region and 3 residues in the exiting helical part of the EF-hand. The canonical EF-hand co-ordinates the calcium ion via a pentagonal bipyramid i.e. through 7 co-ordinating ligands (Figure 4A). The positions inside the 12 residue binding loop are referred to as:

$$1(+X), 3(+Y), 5(+Z), 7(-Y), 9(-X), 12(-Z)$$

Numbers indicate the position along the linear sequence of the loop whereas letters indicate the position in the 3D-geometry of the pentagonal bipyramid (Figure 4B). Amino acid residues in the Y and Z positions belong to the planar pentagon with a glutamic acid at -Z that provides two chelating groups as a

bidentate side chain. The X positions complete the coordination space for calcium and correspond to the tips of the bipyramid (47).

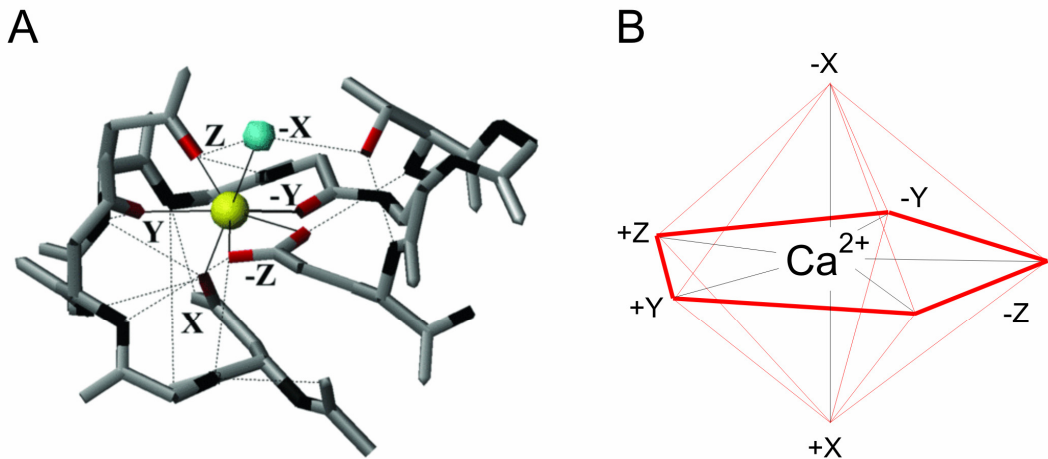


Figure 4: Calcium coordination to the first EF-hand of calmodulin.

Picture in (A) taken from (47).

Although most chelating groups arise from the amino acid residues there is one exception found in the canonical EF-hand. This exclusion is displayed by position 7(-Y) that coordinates the calcium ion with its carbonyl group of the peptide backbone. Additionally the amino acid residue at position 9(-X) is able to coordinate the ion either directly or through a bridged water molecule. A hydrophobic amino acid residue at position 8 (Ile, Val or Leu) plays another important role: as mentioned before, EF-hands are usually found as pairs in EF-hand containing peptides and this residue stabilizes the paired EF-hand domain via a short anti-parallel β -sheet formed with the corresponding hydrophobic residue in the second EF-hand (48) (Figure 5).

In contrast to the C2 domain many EF-hands display a structural rearrangement, elicited by the calcium coordination. The EF-hand pair undergoes a transition of almost parallel helices of each EF-hand in the apo (unbound or closed) state to perpendicular helices in the bound (open) state. In case of calmodulin this conformational change exposes a hydrophobic surface that is the basis of target recognition (47) (Figure 5).

Some of the EF-hands are able to bind not only calcium but also magnesium. They are referred to as $\text{Ca}^{2+}/\text{Mg}^{2+}$ EF-hands. Two crucial features can be

Introduction

observed in such EF-hands, namely a Z-acid pair (49) or an aspartic acid in position 12 (47).

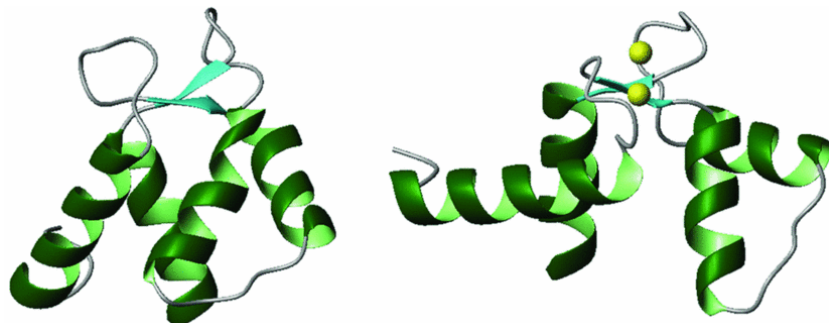


Figure 5: Structural change in EF-hands I and II of calmodulin upon calcium binding.

Picture taken from (47).

The coordination space for the magnesium ion exhibits an octahedral geometry thus in some of the $\text{Ca}^{2+}/\text{Mg}^{2+}$ EF-hands the bidentate amino acid residue at position 12 co-ordinates the ion through one of its oxygens, while calcium binding is promoted with both oxygens of the side chain. For example, in EF-hands III and IV of troponin C magnesium binding can induce a structural change and interferes with calcium binding (50, 51).

According to their effector function essentially two categories of EF-hands can be discriminated: ‘regulatory’ EF-hands that undergo a conformational change after calcium binding and ‘structural’ EF-hands that do not (48). The regulatory hands are typical of proteins with important regulatory function such as calmodulin, troponin C or recoverin. These proteins usually mediate effects of calcium on physiology and biochemistry of a cell. The structural EF-hands occur in buffer proteins such as calbindin D9K or parvalbumin and serve to shape the profile and duration of calcium signals within cells.

EF-hands generally occur as pairs in proteins that are stacked against each other and provide mutual stabilization. As a consequence, calcium binding to EF-hands is co-operative. In general positive co-operativity is observed because calcium binding to an EF-hand has positive structural effects on the ‘partner’ hand, facilitating calcium binding to this hand. A certain challenge therefore may lie in tuning a sensor in a way that linear reporters of calcium and neuronal activity can be obtained. Due to the paired functional EF-hand

domain EF-hand containing polypeptides are often built in a modular fashion and have 2, 4, 6 or more EF-hand domains (52). Some of the smaller calcium binding proteins such as troponin C and calmodulin are constituted almost exclusively of 4 EF-hand motifs. Each pair of hands in these proteins form a globular lobe domain named the N-terminal and C-terminal lobe. The domains are structurally independent and differ considerably in terms of calcium binding properties and biological function (50, 53). The different nature of these domains should be kept in mind when using such a protein as binding domain within a biosensor.

The strategy to develop genetically-encoded calcium indicators has followed two main ways. One set of indicators is based on a single chromophore whereas a second one uses FRET exploiting the GFP variants CFP and YFP. Typical members of the single chromophore indicators are the Camgaroos, Pericams, and GCaMPs that all rely on calmodulin (CaM) as calcium sensing domain.

The Camgaroo family uses YFP (Camgaroo-1) (54) or Citrine (Camgaroo-2) (24) as fluorescent protein. The fluorophore has an insertion of *Xenopus* calmodulin at position Y145 that enables the modulation of fluorescence in a calcium dependent manner. The reported Kd values are 7 μM (Camgaroo-1) and 5.3 μM (Camgaroo-2) which list them amongst the low affinity calcium indicators.

The Pericam family exploits a circularly permuted (cp) variant of YFP (at position 145). This cpYFP was fused between the M13 peptide and *Xenopus* CaM to yield a functional calcium indicator (55). The Kd values for calcium in this family vary between 0.2 μM - 1.7 μM which should make them suitable of detecting cytosolic calcium dynamics inside active neurons.

In contrast to Pericams the GCaMPs are based on cpGFP (the same position is used namely amino acid 145). During the last years performance of this kind of GECI was improved yielding the state to the art GCaMP2 (56). The reported Kd is 146 nM which means that GCaMP2 is one of the most affine GECIs known so far.

Beside single chromophore calcium indicators a number of various indicators exists that exploit the FRET-mechanism. For that purpose so far almost all of

Introduction

these so-called ratiometric biosensors are using variants of the CFP and YFP since their fluorescence spectra show significant overlap (from donor emission and acceptor excitation) and excellent separation (of donor and acceptor excitation spectra) that allows for exclusive excitation of the donor without direct excitation of the acceptor (e.g. at 432 nm as depicted in Figure 6, black line).

Ratiometric imaging has some advantages in contrast to single wavelength imaging. Instead of having an intensity change of a single wavelength, ratiometric indicators make use of fluorescence change in two channels. For CFP/YFP dependent calcium biosensors the binding of calcium usually promotes the FRET from CFP to YFP that can be detected by a decrease in intensity of the CFP and an increase in intensity of the YFP channel.

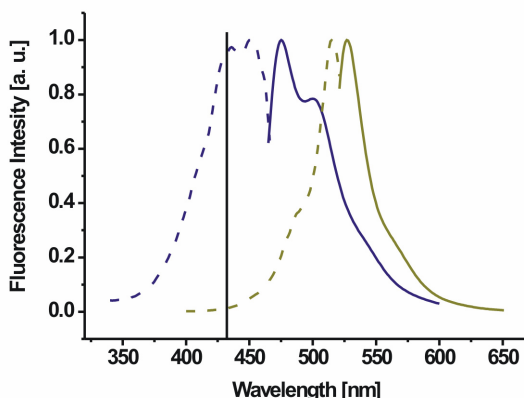


Figure 6: Fluorescence excitation and emission spectra of CFP and Citrine.

As readout the ratio of these two wavelengths is build and the relative change in their ratio reports the calcium binding to the indicator. Since two channels display the signal overall changes in fluorescence of both wavelengths, as elicited by movement or fluctuation of the excitation light source, cancel out yielding a more stable readout for the measurement.

Among the FRET indicators two different calcium binding moieties are used. One group also exploits calmodulin whereas another family relies on troponin C. Since most of the calmodulin-based GECIs showed poor performance when they were used in *in vivo* experiments it has been thought that the calmodulin/M13 complex that exists in these sensors interact with the cellular

machinery particularly of neurons which in turn diminishes their activity (57). Therefore calmodulin was replaced by troponin C to build a second class of GECIs based on the FRET-mechanism that should not interfere with the cellular machinery.

Calmodulin/M13 dependant ratiometric biosensors are the so called Cameleons among them Yellow Cameleon 2.0, 3.0 and 4.0 (YC 2.0, 3.0 and 4.0) (40). YC 2.0 exploits wild type CaM, YC 3.0 the E104Q and YC 4.0 the E31Q mutation. Replacement of the acceptor protein YFP with Citrine (a pH stable YFP derivative, (24)) led to the variants YC 2.3, YC 3.3 and YC 4.3. As mentioned before FRET-efficiency depends not only on the distance but also on the orientation of the transition dipoles of the chromophores. This has been exploited in various FRET-based biosensors to increase the signal obtained with GECIs by introducing a circularly permuted acceptor protein (57, 58). In that respect the overall signal strength could be increased in the new sensors YC 2.60 (Kd is 40 nM), YC 3.60 (Kd is 250 nM) and YC 4.60 (Kd is 60 nM/14 µM for the biphasic titration curve) (57).

As mentioned before calmodulin-based indicators often did not show a good performance when they were expressed in the nervous system of transgenic animals (57). This is likely to be due to the fact that calmodulin plays an essential role in the cellular signaling machinery and that additionally expressed calmodulin or the calmodulin-target M13 peptide will interfere with this machinery and hence perturb the performance of calmodulin dependant GECIs. Additionally, overexpression of the CaM-peptide could promote activation of endogenous CaM-targets and disrupt the cellular homeostasis.

Two different approaches emerged to circumvent these problems. The group of Roger Tsien mutated the calmodulin and the M13 peptide inside the cameleons to prevent interaction with intrinsic binding partners yielding so-called ‘design variants’ of Cameleons (D-series) (39). They could show that wild type calmodulin (CaM) does not diminish the overall signal strength of these indicators. For example the design variant D3cpv (Kd is 600 nM) retains 90% of its $\Delta R/R_{max}$ in the presence of 800 µM wild type CaM. This redesign should retain their functionality when expressed in the nervous tissue. A different way to avoid unwanted cellular/biosensor interactions was achieved

Introduction

in our lab by replacing the calcium binding moiety of the cameleons with troponin C. This protein is exclusively expressed in the muscle tissue so that interaction with the cellular machinery inside neurons is unlikely to happen. The regulatory complex of muscle contraction consists of actin, tropomyosin and the troponin complex. The latter one consists of troponin C (TnC which binds Ca^{2+} and therefore displays the calcium sensor of the complex) together with troponin I (TnI that binds to actin and inhibits the actomyosin ATPase) and troponin T (TnT which links the troponin complex to tropomyosin). Binding of calcium to the N-terminal part of troponin C will remove the TnI inhibition of the ATPase, allowing subsequent hydrolysis of ATP and eventually the movement of the two filaments (actin and myosin) (59).

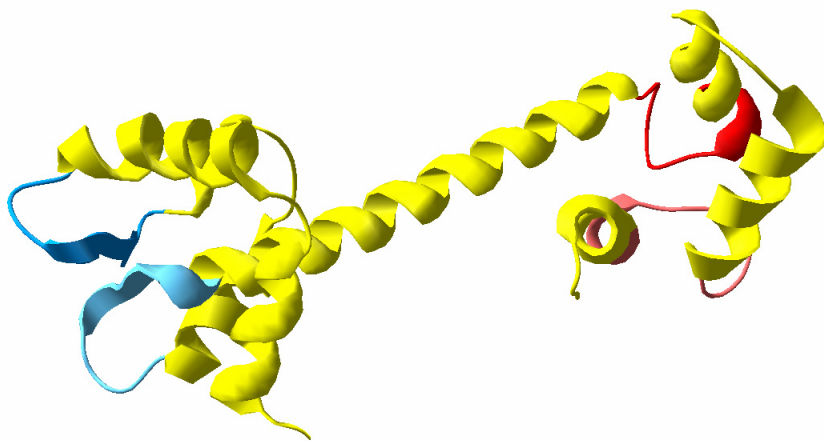


Figure 7: Three dimensional structure of chicken skeletal troponin C.

Figure was redrawn according to the pdb entry 1TOP. Calcium chelating loops are colored (loops of EF-hand I and II in blue and loops of EF-hand III and IV in red).

Troponin C consists of four EF-hands with two of them residing in each terminus (Figure 7). The protein displays a dumbbell-shaped occurrence consisting of about 160 amino acids with different calcium binding properties for each terminus. The N-terminal EF-hands (EF I and EF II) bind calcium with low affinity (K_d is 3 μM) and are insensitive to magnesium whereas the C-terminal EF-hands (EF III and EF IV) bind calcium with high affinity (K_d is 50 nM) and competitively bind magnesium (K_d is 0.2 mM) (49).

One of the first troponin C-based indicators used a truncated (starting at leucine14) variant of chicken skeletal troponin C. This indicator named TN-

L15 successfully expresses in mammalian cells and in transgenic animals where it reliably reports cytosolic calcium changes (41, 60, 61). Nevertheless improvement of TN-L15 with respect to signal strength and kinetics would be desirable. The most important characteristic of a given GECI is presumably signal strength i.e. the signal that is provided by the indicator at a given change in the calcium level. For example, it is important to have a GECI that is capable of sensing the small changes of cytosolic free calcium elicited by a single action potential which is not detected by TN-L15 (61).

The aim of this research was to improve TN-L15 with respect to signal strength and hence to close the gap of non-responsiveness to small calcium changes. For that purpose different strategies were applied that ranges from point mutating the calcium binding domain of TN-L15 to profoundly rearranging the troponin C by doubling the C-terminal domain to yield an indicator that was suitable to detect single action potentials and sensory evoked calcium transients *in vivo*.

Material and Methods

3.1. Molecular biology

3.1.1. Polymerase Chain Reaction (PCR)

Originally developed by Kary Mullis, this method allows the amplification of a distinct strand of DNA. For that purpose one makes use of a thermal-stable variant of DNA polymerase. This can be Taq (*Thermus aquaticus*), Vent (*Thermococcus litoralis*) or Pfu (*Pyrococcus furiosus*). The different enzymes vary in speed and accuracy of amplifying DNA. Pfu polymerase is known to have a high proof-reading capacity and is the choice for subsequent cloning.

PCR-reaction mix (50 µl):

0.5 - 1 µl DNA template (~50 ng)

2 µl primer #1 (50 µM)

2 µl primer #2 (50 µM)

5 µl polymerase buffer (10 x)

5 µl DMSO

1 µl dNTP solution (12.5 mM)

33 µl H₂O

0.7 µl Pfu polymerase (~2 U)

Addition of DMSO to the reaction mix often enhances the yield of DNA obtained by the PCR especially when the reaction initially produces too little DNA.

Reaction cycle:

1. 5 min at 95°C
2. 30 s at 95°C (melting of double stranded DNA)
3. 2 min at 52°C (annealing of primers)
4. 2 min/1kb of target DNA at 68°C (synthesis of DNA)

29x (2. - 4.)

5. 5min at 68°C
6. incubate at 15°C

PCR-reaction mix was prepared on ice and put into thermal-cycler when a temperature of 95°C was reached.

3.1.2. Site-directed mutagenesis via PCR

Polymerase chain reaction can not only be used to amplify a defined stretch of DNA but is also suitable to introduce base substitutions. For that purpose a distinct base in the primer region is replaced by a different base so that in the translated protein one will find an amino acid replacement.

Mutagenesis primers were designed in such a way that the replacing base resides in the middle of the oligonucleotide primer with an average length of ~45 bases (roughly 7 triplets flanking the region to mutate on each side).

Mutagenesis-reaction mix (50 µl):

- 0.5 - 1 µl DNA template (5 - 50 ng)
- 2.5 µl primer #1 (50 ng/µl)
- 2.5 µl primer #2 (50 ng/µl)
- 5 µl polymerase buffer (10 x)
- 0.8 µl dNTP solution (12.5 mM)
- 37.5 µl H₂O

Material and Methods

0.7 µl Pfu polymerase (~2 U)

Reaction cycle:

7. 30 s at 95°C
8. 30 s at 95°C (melting of double stranded DNA)
9. 1 min at 55°C (annealing of primers)
10. 2 min/1kb of target DNA at 68°C (synthesis of DNA)

16 x (2. - 4.)

11. 5 min at 68°C
12. incubate at 15°C

Usually mutation was achieved by applying the method to the target DNA in the pRSETB backbone. The whole vector was amplified and used to transform a bacterial strain of choice.

To get rid of the template vector DNA, a DpnI digest was applied that degrades the methylated template DNA.

DpnI-treatment:

20 µl mutagenesis-mix

1 µl DpnI (20 U)

Incubate for 2 h at 37°C

3.1.3. Restriction of DNA

Restriction sites consist of a short sequence that usually comes along in a palindromic manner and have a length of 6 bp although longer restriction sites exist. These sites can be recognized by a specialized restriction

endonuclease that breaks the double strand and often leaves a single stranded (sticky) end. Restriction of DNA was used to prepare the vector backbone/PCR fragment for subsequent cloning or to analyze a given DNA for the correct introduction of a desired DNA-fragment after ligation.

Control digests for checking the successful incorporation of a DNA stretch was done with 1 - 2 µl (100-200 ng) of DNA.

1 - 2 µl DNA (100-200 ng)

0.1 - 0.3 µl of restriction enzyme (~2 U)

0.2 µl BSA (bovine serum albumine 100 x, NEB)

2 µl restriction buffer for restriction enzyme (10 x, NEB)

Add 20 µl H₂O

Incubate for 1 h at 37°C

Preparative digests for subsequent cloning were performed as follows:

2 - 10 µl DNA (2-10 µg)

1 - 3 µl of restriction enzyme (~10 U)

0.8 µl BSA (bovine serum albumin 100 x, NEB)

8 µl restriction buffer for restriction enzyme (10 x, NEB)

Add 80 µl H₂O

Incubate for 3 h - 16 h at 37°C (dependant on the restriction enzymes that were used and on the manufacturer's advice [NEB]).

3.1.4. Ligation of DNA fragments

A prerequisite for an easy introduction of a new stretch of DNA into a vector backbone is to place different restriction site at each end of the desired DNA. Treatment of the vector backbone and the DNA of choice with the same set of

Material and Methods

restriction enzymes enable the directed introduction of the desired fragment into the vector backbone.

The molar ratio of vector to insert should be 1:3 to 1:5. Amount of DNA to use was determined by agarose gel electrophoresis of the desired DNA.

0.5 - 1 µl vector DNA (~50 ng)

1 - 3 µl insert (dependant of the size and concentration)

1.5 µl T4 ligase buffer (10 x)

0.75 µl T4 DNA ligase (300 U)

Add 15 µl H₂O

Incubate for 1 h at room temperature

3.1.5. Transformation of chemically-competent *E. coli*

Chemically competent cells (50 µl aliquots, storage -80°C) were thawed on ice and transformed with desired DNA. Cells were kept on ice for 20 min and heat-shocked for 1 min in a water bath (42°C). Before striking out on LB-agar plates cells were additionally stored on ice for 2 min. When working with ampicillin resistance bacteria were immediately plated, for other resistance transformed bacteria were added with 150 µl of LB-medium and let grow without antibiotics for 1 h at 37°C in a shaker before plating onto LB-agar plates with the appropriate antibiotic.

3.1.6. Transformation of electro-competent *E. coli*

In order to increase the yield of transformed bacteria, one can make use of electroporation. For that purpose electro-competent cells were used as follows: put the desired DNA to electro-competent cells on ice. Place the cells into a pre-cooled cuvette and apply an electric pulse (1800 V). Add 150 µl of

SOC medium and let the bacteria grow for 1 h at 37°C in a shaker. Plate the suspension onto LB-agar plates supplemented with the appropriate antibiotic.

3.1.7. Preparation of chemically-competent *E. coli*

4 ml LB medium were inoculated with the desired strain of *E. coli* and grown overnight without supplementing with antibiotics. The next day culture was transferred into 300 ml LB medium and grown to an OD₆₀₀ of 0.6. Next the suspension was placed on ice for 20 min followed by harvesting the cells by centrifugation at 2500 g for 20 min (4°C). Supernatant was discarded and the cells were resuspended with 60-80 ml of cooled Inoue transformation buffer. Again cells were harvested by centrifugation at 2500 g for 15 min (4°C). Once more cells were resuspended with cooled Inoue transformation buffer but this time with 20 ml supplemented with 1.5 ml DMSO. Suspension was incubated on ice for 10 min. Cells were aliquoted (50 µl) and stored at -80°C until usage.

3.1.8. Preparation of electro-competent *E. coli*

20 ml LB medium were inoculated with the desired strain of *E. coli* and grown overnight without supplementing with antibiotics. The next day culture was transferred into 1 l LB medium (37°C) and grown to an OD₆₀₀ of 0.6. Next the suspension was cooled ice followed by harvesting the cells by centrifugation at 2500 g for 10 min (4°C). Supernatant was discarded and the cells resuspended with 50 ml of cooled H₂O (sterile). This procedure was repeated 5-6 times to remove all traces of ions. After the 4th washing step all cells were pooled into one 50 ml falcon tube. Eventually cells were resuspended with 4 ml of cooled glycerol (10 %). Electro-competent *E. coli* were aliquoted (50 µl) and stored at -80°C until usage.

3.2. Proteinbiochemistry

3.2.1. Protein expression using the *E. coli* BL21 strain

DNA for the protein of interest was cloned in the pRSETB vector that is optimized for protein expression and carries a 6 x His-tag 5' of the multiple cloning site. The vector containing the DNA of interest was transformed in the *E. coli* strain BL21. 5 ml of LB medium containing 10 µl of ampicillin (50 mg/ml) were inoculated with 25 µl of the transformed bacterial culture. Starting culture was grown overnight at 37°C. The next day starter culture was used to inoculate 400 ml LB medium containing 50 µg/ml ampicillin. This bacterial culture was grown to an OD₆₀₀ of 0.6 to 0.8 at 37°C and protein expression was induced with 0.5 mM IPTG (Isopropyl-β-D-Thiogalactosid) for 3 h at 37°C. Bacterial cells containing the protein were harvested by centrifugation at 6000 g for 10 min (4°C).

3.2.2. Purification of recombinantly expressed proteins

Purification of the protein of interest was achieved via a fused N-terminal 6 x His tag that is capable of being chelated by a Ni-NTA column. Bacterial pellet was resuspended with 10 ml of protein resuspension buffer supplemented with 1 mM PMSF, 5 µg/ml Pepstatin and 1 µg/µl Leupeptin to inhibit protease activity. Resuspension was put to a freezer (-80°C) for 10 min to induce cell lysis. After thawing, 1 mg of lysozyme was added to break up the bacterial cell wall (30 min on ice). In a next step 0.1 % Triton-X-100, 5 µg/ml DNasel and 5 µg/ml RNase were added and lysis was proceed in an ultrasound bath containing ice for 20 min. Protein was harvested by centrifugation for 30 min at 13.000 rpm. Supernatant containing the protein of interest was removed and 300 µl of Ni-NTA agarose was added. Binding was allowed for 2 h at 4°C. For purification the bound protein/Ni-NTA agarose suspension was put in a

polypropylene column and exposed to gravity. Suspension was washed with 20 ml of column washing buffer containing 10 mM of imidazole. Protein was eluted by replacing the bound protein with imidazole using column elution buffer containing 150 mM imidazole.

3.3. Spectroscopy

3.3.1. Fluorescent spectra of purified proteins

Fluorescent spectra were taken using a fluorescent spectrophotometer. Purified proteins were diluted in MOPS (10 mM) buffer containing 100 mM KCl and 25 µM EGTA to set the free ion concentration to zero. CFP/YFP FRET constructs were excited at 432 nm (bandwidth 5 nm) and the emission was recorded from 450 nm to 600 nm (bandwidth 5 nm). After taking the Ca²⁺-free spectrum the indicator was exposed to different values of free ion concentrations (e.g. 1 mM Mg²⁺ or 10 mM Ca²⁺) by adding the appropriate amount of MgCl₂ or CaCl₂. Again an emission spectrum was taken. To calculate the ΔR/R value elicited by a given ion the following formula was used:

$$\Delta R/R_{\text{desired ion value}} [\%] = \frac{\text{Ratio}_{\text{desired ion value}} - \text{Ratio}_{\text{zero ion}}}{\text{Ratio}_{\text{zero ion}}} * 100$$

where Ratio = Peak_{YFP}/Peak_{CFP} (527nm/432nm).

3.3.2. Spectroscopic determination of Kd-value

For determination of Kd-value only freshly purified protein was used. For titration a prewarmed (room temperature) titration kit was applied as follows. Two stock solutions were prepared:

- Zero calcium: mix 1ml of zero calcium buffer with 1 volume of protein solution (~0.2 - 1 µM protein, directly in cuvette)
- High calcium: mix 5.4 ml of 39.8 µM free calcium buffer with 5.4 volumes of protein solution (use a 15 ml Falcon tube)

Subsequently the zero calcium stock was put into the fluorescence spectrophotometer to take a spectrum of baseline. Excitation wavelength for a CFP/YFP FRET-pair again was 432 nm. The emission was determined in the range from 450 nm to 600 nm (all bandwidths 5 nm).

Adjustment of the free calcium values was achieved by reciprocal dilution (replacing same amount of zero calcium buffer with the high calcium stock) to the desired concentrations. Usually 0, 0.065, 0.100, 0.225, 0.350, 0.600, 0.850, 1.35, 1.73, 2.85, 4.87, 7.37, 14.9, 29.9 and 39.8 µM free calcium was used as reference points to determine the Kd-value. Calculation of the volumes that had to be replaced was along the manufacturer's manual (<http://probes.invitrogen.com/media/pis/mp03008.pdf>).

CaEGTA [mM]	Free Ca ²⁺ [µM]	Volume to replace [µl]
0.00	0.000	
3.00	0.065	300
4.00	0.100	143
6.00	0.225	333
7.00	0.351	250
8.00	0.602	333
8.50	0.853	250
9.00	1.35	333

9.20	1.73	200
9.50	2.85	375
9.70	4.87	400
9.80	7.37	333
9.90	14.9	500
9.95	29.9	500
10.0	39.8	1000

After taking the spectra the $\Delta R/R$ at distinct calcium concentrations was calculated.

Extraction of the Kd-value was achieved by fitting a sigmoidal curve to the plotted \log_{10} values of the free calcium points (in M) versus the normalized signal (normalized to 39.8 μM free calcium). For this purpose OriginLab 7.5 was used.

3.3.3. Stopped-flow measurements

Experiments were carried out in a Varian Cary Eclipse Fluorescence Spectrophotometer with an Applied Photophysics RX Pneumatic Drive Accessory. Two stock solutions were prepared as follows:

- Calcium saturated indicator (5 ml): 10 mM MOPS, 4 mM CaCl_2 , 2 mM MgCl_2 , 50 mM KCl, ~0.2 - 1 μM indicator pH 7.5
- BAPTA solution (5 ml): 10 mM MOPS, 50 mM KCl, 20 mM BAPTA pH 7.5

Two separate 5 ml syringes were filled with both solutions and the stopped-flow experiment was performed at room temperature (injection pressure 3.5 bar). Excitation of the indicator was again set to 432 nm (bandwidth 5 nm). Emission spectra of the two individual channels were taken in an alternated manner at 475 nm (for CFP, bandwidth 10 nm) and 527 nm (for YFP, bandwidth 10 nm) respectively. Acquisition time was set to 12.5 ms, duration

to >10 s, mixing volume to 400 µl with a mixing dead time of the instrument of 8 ms.

An average of the individual channel was built and a resulting YFP/CFP ratio was calculated. To determine the decay time value the resulting 527 nm/475 nm ratio decay was fitted with a single or double-exponential using OriginLab 7.5. For calculation of the ratio decay, each channel was recorded at least nine times. This procedure was repeated three times with independently purified proteins.

3.4. Cell culture

3.4.1. Preparation of dissociated hippocampal neuronal culture

E18 pregnant Wistar rats were killed using CO₂. Embryos were obtained by removing the uterus and placing it into a Petri dish filled with PBS. By opening the skull, brains were excised and placed into cold HBSS. After removing the meninges the region of the hippocampus was prepared and placed into HBSS containing 1 mg/ml dispase for 20 min at 37°C. Subsequently the medium was replaced with the same volume of DMEM/10 % FCS. By triturating the solution the tissue was finally dissociated.

For cultivating the cells, glass-bottom culture dishes (35 mm, MatTek) were incubated overnight with Poly-L-Lysine. The next day dishes were washed with PBS and filled with 2 ml of DMEM/10 % FCS and placed into the incubator (37°C; 5 % CO₂). Freshly triturated cells were plated into the culture dishes overnight. The next day medium was replaced by Neurobasal supplemented with B27. Neurons were kept up to 4 weeks by changing the medium every week.

3.4.2. Transfection of neuronal cell culture using lipofectamine

Delivering DNA of interest to neuronal cell cultures can be achieved using the lipofectamine approach. For that purpose 2 µg of plasmid DNA were solved in 250 µl of Opti-MEM I. In parallel 10 µl of Lipofectamine were mixed with 250 µl of Opti-MEM I and this mixture was incubated for 5 min at room temperature. After this incubation time the DNA-mix and the Lipofectamine-mix were combined and let stand for additional 20 min. Eventually 500 µl of the mix were added to the neuronal cell culture and the transfection was allowed to proceed for 2 - 3 hours (37°C, 5% CO₂). After the incubation, cells were washed with 1 volume of Neurobasal medium.

3.4.3. Transfection of neuronal cell culture using phosphate-precipitation

To drive expression of the indicator in neuronal cell culture, the calcium phosphate precipitation method was used. For that purpose 100 µl of CaCl₂ (250 mM) were mixed with 10 µg of plasmid DNA and 100 µl of 2x BBS. The mix was incubated for 20 min. From the cell culture 500 µl of conditioned medium was put aside before the DNA was added (all 200 µl per 35 mm dish). Subsequently the cells were placed back to the incubator and transfection was allowed to proceed for 2-3 hours. After transfection was completed the dishes were rinsed 2 - 3x with prewarmed Neurobasal medium to remove the residual precipitates. Next 1.5 ml of Neurobasal medium and 0.5 ml of the conditioned medium were added to the dishes.

3.5. Imaging Setup

Imaging experiments were performed on a Zeiss Axiovert 35M fluorescence microscope including a 40x objective. Setup was controlled by a Metafluor 4.6 imaging software. For excitation, the light of a xenon lamp passed a 440/20 nm excitation filter. Fluorescence of the individual channels was collected subsequently through two emission filters placed in a filterwheel (485/35 nm for CFP and 535/25 nm for Citrine cp174). Acquisition time was set to 500 ms per channel and every channel was imaged with a frequency of 0.5 Hz.

3.6. Transgenic animals

3.6.1. Transgenic flies

The elav^{C155}-Gal4 and elav-Gal4 driver lines allow expression of the indicators in the whole nervous system. In the line elav^{C155}-Gal4, the elav promoter is fused to Gal4 that is located on the X-chromosome.

3.6.1.1. Spin dialysis

The DNA has to be cleaned by spin dialysis before injection. Little columns were prepared by cutting the lid of plastic tubes and poking a hole in the bottom with a thin needle. The tube was filled with 25 µl of glass beads and placed into a second tube. It was filled with 10 x Sepharose CL6B and centrifuged at 3000 rpm for 3 minutes. Subsequently the second tube was replaced by a fresh one. DNA was incubated at 65°C for 10 min and applied carefully onto the glass beads and centrifuged at 3000 rpm for 3 min. DNA-precipitation and injection mix spin dialysed DNA (approx. 6 µg) and spin dialysed Δ2 - 3 (approx. two µg) were diluted in 100 µl H₂O. For precipitating

the DNA mix, 1/10 % vol. of 3 M NaAcetat was added to the solution. After mixing, 2.5 x EtOH (100 %) was added and the sample was incubated in a freezer at -70°C for 30 min and centrifuged at 15 000 rpm for 30 min. The supernatant was discarded and the sample washed with 100 µl 70 % EtOH. After centrifugation at 15 000 rpm for 30 min, supernatant was discarded and the DNA was dried by exposing to air. The DNA was diluted in 20 µl 1 x injectionbuffer.

3.6.1.2. Injection of fly embryos with DNA

Wildtype flies (Bayreuth w⁻) were collected in a collection tube placed on apple agar plates and held overnight at room temperature with light. The apple agar plate was changed every 30 min and the laid eggs collected. After washing of eggs with PBT, they were put in Klorix for three minutes to remove the chorion. As a next step they were washed again with PBT and rowed up in a line on a piece of apple agar. A coverslip coated with custom made glue based on tape and heptan was pressed on the eggs to pick them up.

A glass electrode was filled with Voltalef 3S oil and the injection mix was sucked in. The strung embryos were dried in silica gel, covered with Voltalef 10S oil and put under the microscope. Small amounts of injection mix were injected into the dorsal part of the eggs by exerting pressure on the syringe. The DNA was inserted in the genome of the germ line cells by p-element mediated transfection (62). After injection, embryos were placed on apple agar plates and incubated at 18°C until the embryos developed to larvae. The larvae were collected and put in a vial containing food until the flies hedged.

3.6.1.3. Generation of transgenic fly stocks

Every single male fly that hedged from the injected embryos was crossed to 10 wild type virgins. The progeny was screened for colored eyes and single

flies were crossed to the balancer line rl/Sm6Tm6 that carries the two markers ‘curly wings’ and ‘tubby larvae’ on a fused 2nd and 3rd chromosome. The hedging flies were transferred into a new vial to breed a new fly stock.

3.6.1.4. Crossing

Five to ten virgin female elav^{C155}-Gal4-driver flies were crossed to three male flies carrying UAS-TN-XXL. They were put in a vial containing fly food and yeast. Because *D. melanogaster* adults do not mate for about 10 hours after eclosion, virgin females can be obtained by collecting them within 8 - 10 hours after the vial has been cleared from adults.

3.6.1.5. Breeding and husbandry

About 5 female and 5 male flies were collected in vials containing food and yeast. Generation time (from egg to adult) takes approximately seven days at 29°C, nine days at 25°C, eleven days at 22°C, 19 days at 18°C (source: Bloomington stock center).

3.6.2. Transgenic mice

3.6.2.1. DNA preparation for pronucleus injection

The genetically-encoded calcium indicators TN-XL and TN-XXL were subcloned into the (human) hGFAP_CFP plasmid by replacing the CFP coding sequence (plasmid kindly provided by Frank Kirchhoff). For that purpose the restriction sites AgeI (5') and EcoRI (3') were used. Linearization of the promoter/indicator DNA was achieved by overnight digestion of ~40 µg

plasmid DNA with Drdl. Purification was performed by agarose gel electrophoresis followed by electroelution into a Spectra/Por dialysis membrane. An additional ion exchange purification step was applied using an Elutip-D Minicolumn. After equilibration of the column for 1 h with Low Salt DNA Purification Buffer, the DNA was bound to the column. After washing with Low Salt Buffer, elution of the linearized DNA was achieved with the High Salt DNA Purification Buffer. For injection, DNA was adjusted to 100 ng/µl.

3.6.2.2. Injection and breeding

Microinjection of purified DNA was in pronuclei of mouse oocytes performed by the Transgenic Service Facility of the MPI for Biochemistry in Martinsried/Germany. Strains for oocyte injection were FVB and FVB:C57BL/6 (F₁-hybrids) which have large oocytes and therefore allow a high percentage of transgenes (63).

3.6.2.2. Genotyping

Purification of genomic DNA for PCR was achieved with the Proteinase K/isopropanol precipitate method of mouse tail tissue. Roughly 5 mm of tail tissue was removed from each individual mouse and dissolved in 250 µl of Mouse Tail Lysis Buffer 55°C (overnight). The next day dissolved mouse tails were centrifuged for 6 min in an Eppendorf microcentrifuge to pellet the debris. Subsequently the supernatant was placed into new eppendorf reaction tubes and the DNA was precipitated with equal amount of isopropanol. Precipitated DNA was again centrifuged and the supernatant was discarded followed by drying for 1 h at 50°C in a heating block. As final step the DNA was dissolved in 200 µl TE buffer and incubated overnight at 4°C.

PCR for genotyping was performed as follows (one reaction):

Material and Methods

0.5 µl DNA
0.2 µl dNTP (12.5 mM)
0.6 µl GFAP_for (20 µM)
0.6 µl CFP_ChR_rev (20 µM)
0.3 µl IL-2_for (20 µM)
0.3 µl IL-2_rev (20 µM)
1.2 µl Taq Polymerase Buffer (10x, NEB)
0.5 µl Taq Polymerase (5 U/µl)
7.3 µl H₂O

Reaction mixture was prepared on ice and subsequently placed into the preheated thermal cycler. PCR was performed as follows:

1. 1 min 30 s at 94°C
2. 30 s at 94°C
3. 1 min at 60°C
4. 30 s at 72°C
5. go to step 2 for 35 times

10°C forever

Primers:

GFAP_for 5'- CTC GCG GGG ATC CTC TAG-3'

CFP_ChR_rev 5'- TGC ACG CCC CAG GTC AG-3'

IL-2_for 5'-CTA GGC CAC AGA ATT GAA AGA TCT-3'

IL-2_rev 5'-GTA GGT GGA AAT TCT AGC ATC ATC C-3'

3.7. Materials**3.7.1. Instruments**

Name	Supplier
Autoflow CO ₂ Water-Jacketed Incubator	NuAire, Plymouth (USA)
Cary 100 Scan UV-Visible Spectrophotometer	Varian, Mulgrave (Australia)
Cary Eclipse fluorescence spectrophotometer	Varian, Mulgrave (Australia)
CCD-Camera Cool Snap HQ	Roper Scientific, Tucson (USA)
Dissecting Microscope	Leitz, Stuttgart (Germany)
Dyad DNA Engine Peltier Thermal Cycler	MJ Research Inc., Waltham (USA)
Metafluor 4.6 imaging software	Universal Imaging, Downingtown (USA)
Microscope Axiovert 35M	Zeiss, Oberkochen (Germany)
Shutter Lambda 10-2	Sutter Instruments, Novato (USA)
Stopped Flow RX2000 Rapid Kinetics Accessory Unit	Applied Photophysics, Leatherhead (UK)

3.7.2. Consumables

Name	Supplier
Domed Cap Strips for 48 Well Plates	AB-Gene, Epsom (UK)
Eartags for mice, Monel Nr. 1005-1	National Band & Tag Company, Newport (USA)
Elutip-D Minicolumns	Schleicher & Schüll, Keene (USA)

Material and Methods

Falcon Tissue Culture Plate, 12 Well	Becton Dickinson, Franklin Lakes (USA)
Glass Bottom Culture Dishes 35mm, Nr. P35G-0-14-C	MatTek Corp., Ashland (USA)
Polypropylene Columns	Qiagen, Hilden (Germany)
QIAquick Gel Extraction Kit	Qiagen, Hilden (Germany)
QIAquick PCR Purification Kit	Qiagen, Hilden (Germany)
Spectra/Por Dialysis Membrane, MWCO 3500, Nr. 132111	Spectrum Labs Inc., Rancho Dominguez (USA)

3.7.3. Buffers, solutions and media

Name	Recipe
BAPTA Buffer for dissociation kinetics	10 mM MOPS, pH 7.5 50 mM KCl 20 mM BAPTA
BBS (2 x)	50 mM BES (acid), pH 6.96 280 mM NaCl 1.5 mM Na ₂ HPO ₄
CaCl ₂ solution for phosphate transfections	250 mM CaCl ₂ in H ₂ O
DMEM/10 % FCS	500 ml DMEM 50 ml FCS, heat-inactivated
DNA Gel Loading Buffer (10 x)	100 mM Tris/HCl, pH 7.5 10 mM EDTA 50 % Glycerol 1 % Orange G
DNA Purification Buffer: High Salt	20 mM Tris/HCl, pH 7.4 1 M NaCl 1 mM EDTA

Material and Methods

Name	Recipe
DNA Purification Buffer: Low Salt	20 mM Tris/HCl, pH 7.4 200 mM NaCl 1 mM EDTA
Fly Injection Buffer (10 x) pH 6,8	0,2 ml 0,5 M NaPi 5 ml 1 M KCl 94,8 ml H ₂ O
Glue (based on heptan)	Tape (Tesa) in 50 ml n-Heptan
HBSS for imaging	25 mM HEPES pH 7.4 140 mM NaCl 5 mM KCl 1 mM CaCl ₂ 1 mM MgCl ₂ 1 mM Glucose 0.25% BSA
HBSS with high KCl for imaging	25 mM HEPES, pH 7.4 40 mM NaCl 100 mM KCl 1 mM CaCl ₂ 1 mM MgCl ₂ 1 mM Glucose 0.25% BSA
Inoue Transformation Buffer for competent cells	10 mM PIPES, pH 6.7 250 mM KCl 15 mM CaCl ₂ 55 mM MnCl ₂
LB (Luria-Bertani) medium pH 7,0	20 g/l LB broth base in ddH ₂ O
LB Agar	LB Medium 15 g Agar in 1 l ddH ₂ O

Material and Methods

Name	Recipe
Mouse Tail Lysis Buffer	100 mM Tris/HCl, pH 8 250 mM NaCl 1 mM EDTA 0.2% SDS 200 µg/ml Proteinase K added freshly
MOPS Buffer for fluorescence spectroscopy	10 mM MOPS, pH 7.5 100 mM KCl
Neurobasal/B27	500 ml Neurobasal medium 10 ml B27 supplement
PBS (10 x)	100 mM Na ₂ HPO ₄ , pH 7.4 20 mM KH ₂ PO ₄ 1.37 M NaCl 27 mM KCl
PBT (1 x)	0.05 % Triton X-100 in 1x PBS
Poly-L-Lysine	0.01 % (w/v) Poly-L-Lysine Hydrobromide in H ₂ O
Protein Buffer for dissociation kinetics	10 mM MOPS, pH 7.5 50 mM KCl 4 mM CaCl ₂ 2 mM MgCl ₂
Protein Resuspension Buffer	20 mM NaPO ₄ , pH 7.8 300 mM NaCl
TAE (10 x)	48.4 g Tris base 11.4 ml glacial acetic acid 20 ml of 0.5 M EDTA, pH 8.0 add H ₂ O to 1 liter
TAE (1 x)	40 mM Tris-acetate 1 mM EDTA
TE (1 x)	10 mM Tris/HCl, pH 8.4; 1 mM EDTA

3.7.4. Chemicals

Name	Supplier
Agar	Sigma, St. Louis (USA)
Ampicillin, sodium salt	Roth, Karlsruhe (Germany)
BAPTA, AM-ester	Molecular Probes, Eugene (USA)
BAPTA, tetrapotassium salt	Molecular Probes, Eugene (USA)
BES	Roth, Karlsruhe (Germany)
Bovine Serum Albumin (BSA)	Sigma, St. Louis (USA)
Calcium Calibration Buffer Kit with Magnesium #1	Molecular Probes, Eugene (USA)
Calcium Chloride, dihydrate	Sigma, St. Louis (USA)
Carbachol	Sigma, St. Louis (USA)
Deoxyribonuclease	Sigma, St. Louis (USA)
Dispase	Gibco, Grand Island (USA)
Dithiothreitol	Sigma, St. Louis (USA)
DMSO (Dimethylsulfoxide)	Sigma, St. Louis (USA)
Dulbecco's modified Eagle's medium (DMEM) w/o Sodium Pyruvate; w/ 4500 mg/ml Glucose; w/ Pyridoxine-HCl	Invitrogen, Carlsbad (USA)
Dulbecco's modified Eagle's medium /F12	Invitrogen, Carlsbad (USA)
EGTA (Ethylene glycol bis(beta-amino ethyl ether tetra-acetic acid)	Sigma, St. Louis (USA)
Fetal Bovine Serum	Gibco, Grand Island (USA)
Glucose (D-(+)-Glucose anhydrous, min 99%)	Sigma, St. Louis (USA)
Glycine	Merck, Darmstadt (Germany)
HEPES free acid	Sigma, St. Louis (USA)

Material and Methods

Name	Supplier
Imidazole	Merck, Darmstadt (Germany)
Ionomycin, calcium salt	Sigma, St. Louis (USA)
Leupeptin hydrochloride	Sigma, St. Louis (USA)
L-Glutamic acid	Roth, Karlsruhe (Germany)
Lipofectamine	Invitrogen, Carlsbad (USA)
Lysozyme	Sigma, St. Louis (USA)
Magnesium chloride hexahydrate	Merck, Darmstadt (Germany)
MES monohydrate	Sigma, St. Louis (USA)
MOPS	Merck, Darmstadt (Germany)
NeuroBasal medium	Gibco, Grand Island (USA)
Ni-NTA Agarose	Qiagen, Hilden (Germany)
Opti-MEM I	Invitrogen, Carlsbad (USA)
Penicillin-Streptomycin	Gibco, Grand Island (USA)
Pepstatin A	Sigma, St. Louis (USA)
Pfu polymerase	Stratagene, La Jolla (USA)
Phenylmethylsulfonylfluoride (PMSF)	Sigma, St. Louis (USA)
Poly-L-lysine hydrobromide	Sigma, St. Louis (USA)
Potassium chloride	Merck, Darmstadt (Germany)
Ribonuclease A	Sigma, St. Louis (USA)
Saccharose	Merck, Darmstadt (Germany)
Sephadex CL6B	Sigma, St. Louis (USA)
Sodium bicarbonate	Sigma, St. Louis (USA)
Sodium chloride	Sigma, St. Louis (USA)
Sodium phosphate monobasic, anhydrous	Sigma, St. Louis (USA)
T4-Ligase	New England Biolabs, Beverly (USA)
Triton-X-100	Sigma, St. Louis (USA)
Trizma Base	Sigma, St. Louis (USA)

Name	Supplier
Trypsin	Sigma, St. Louis (USA)
Trypsin-EDTA	Gibco, Grand Island (USA)
Voltalef 3S oil	Lehmann & Voss & Co., Hamburg (Germany)
Yeast extract	Sigma, St. Louis (USA)

3.7.5. Plasmids, bacterial strains, cell-lines and flies

Plasmid name	Supplier
pcDNA3	Invitrogen, Carlsbad (USA)
pRSETB	Invitrogen, Carlsbad (USA)
Strain name	Supplier
BL21(DE3)	Invitrogen, Carlsbad (USA)
DH5 α	Invitrogen, Carlsbad (USA)
XL-1 Blue	Invitrogen, Carlsbad (USA)
HEK 293T	Invitrogen, Carlsbad (USA)
Fly strain	Provider and engineer
WT Bayreuth w ⁻	provided by C. Lehner, University of Bayreuth (Germany)
elav ^{C155} -Gal4	gift from C. S. Goodman, University of California Berkeley, Berkeley (USA) (64)

Results

4.1. Development of TN-XL, a Mg^{2+} -insensitive GECI based on troponin C with fast kinetics

In order to enhance FRET signals in troponin C-based calcium biosensors I have made use of the circularly permuted (cp) protein variants. These variants display the same structural geometry as the wild type protein but have different N- and C-termini. In cp variants the linear sequence of the wild type protein is broken up at one site and the resulting parts are exchanged yielding a protein with new C- and N-termini. Using a distinct variant of the acceptor protein Citrine, namely Citrine cp174, I could enhance FRET-efficiency in TN-L15 Citrine cp174 and thereby enhance the signal strength of this indicator presumably due to the reorientation of the transition dipoles of the two chromophores (58). Unfortunately signal enhancement was not confined to calcium-induced signals but was also seen with magnesium. In the following chapter, I will present the strategy applied to circumvent magnesium binding to the TnC backbone of our GECIs to retain a high fractional fluorescent change elicited exclusively by the calcium ion.

4.1.1. Removing Mg^{2+} -induced FRET signals in troponin C-based GECIs

As mentioned in the introduction, troponin C is capable of not only binding calcium but also magnesium. For this reason TN-L15 Citrine cp174 shows an enhanced signal produced by 1 mM Mg^{2+} in contrast to the signal elicited by the same amount of Mg^{2+} in TN-L15 (Figure 8).

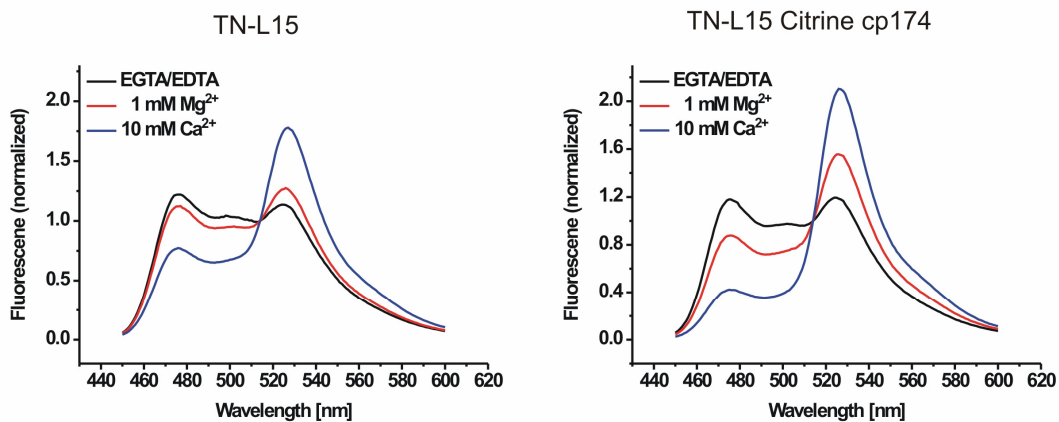


Figure 8: Fluorescence emission spectra of TN-L15 and TN-L15 Citrine cp174, two troponin C-based GECIs.

Spectra were recorded in MOPS buffer supplemented with 25 μ M EGTA/100 μ M EDTA to set free calcium and magnesium to zero (black lines). Excitation took place at 432 nm and emission was recorded from 450 nm to 600 nm (all bandwidths 5 nm). Red lines correspond to magnesium-induced FRET after adding 1 mM of $MgCl_2$ to the solution. Note that the magnesium-induced signals are more pronounced in TN-L15 Citrine cp174. Signals obtained after saturating the indicators with 10 mM $CaCl_2$ are indicated with blue lines. All spectra are normalized to the isosbestic point at 514 nm.

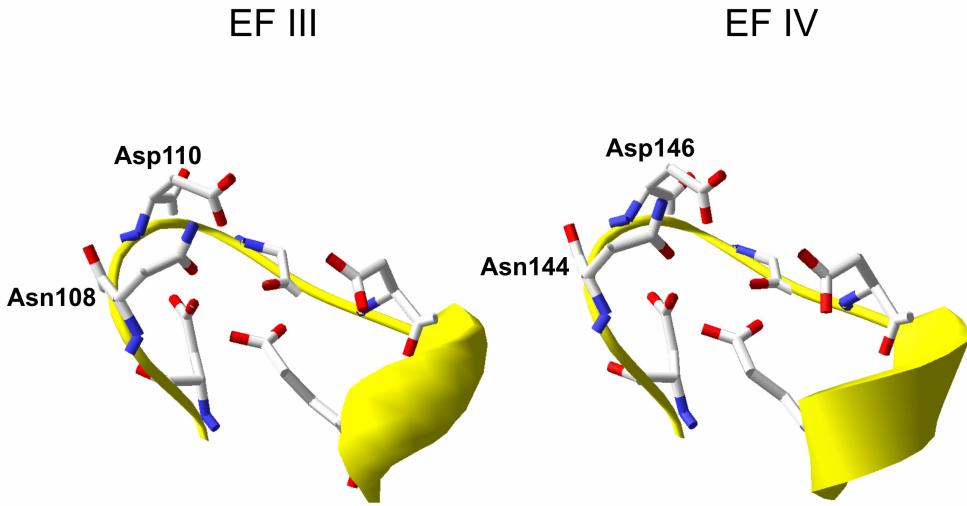


Figure 9: Ribbon and stick representation of the calcium binding loops III and IV in csTnC.

Shown are the chelating positions in each of the C-terminal calcium binding loops. Amino acids in TN-L15 Citrine cp174 chosen for mutagenesis are highlighted (Asn108, Asp110, Asn144 and Asp146). Structures were redrawn according to the pdb entry 1TOP using DeepView/SwissPdbViewer 3.7. Ribbon representation of the protein backbone is depicted in yellow.

Results

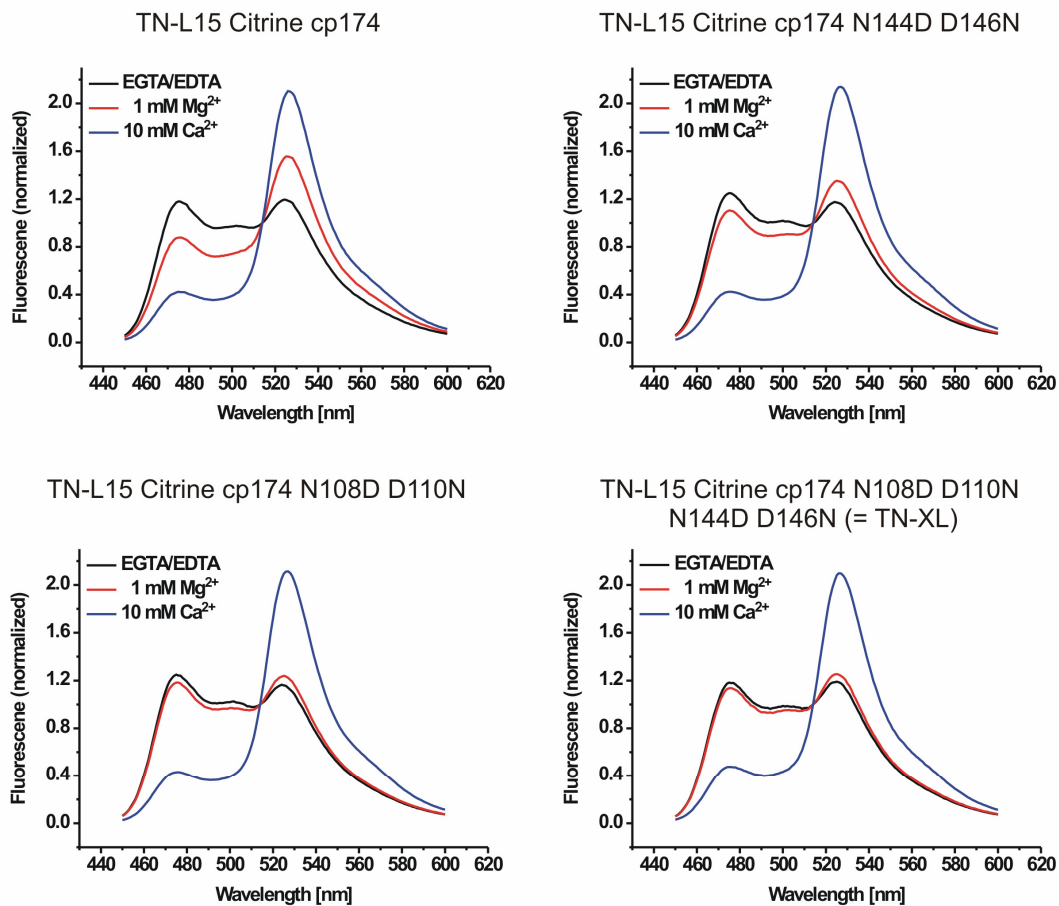


Figure 10: Fluorescence emission spectra of different variants with disrupted Z-acid pairs of EF-hand III and IV.

Overview of the development to remove magnesium-induced FRET signals in TnC-based calcium indicators. As seen in Figure 8 TN-L15 Citrine cp174 exhibit a huge signal with 1 mM Mg^{2+} . Subsequent disruption of the Z-acid pair in the loop region of EF III and IV yielded indicators with reduced magnesium-induced signals. TN-L15 Citrine cp174 N108D D110N and TN-L15 Citrine cp174 N144D D146N correspond to indicators in which only one binding loop is mutated (EF III and EF IV respectively). Almost no magnesium-induced FRET is detectable in the double mutant TN-L15 Citrine cp174 N108D D110N N144D D146N (TN-XL). Again spectra were obtained by exciting the indicators at 432 nm and recording the emission from 450 nm to 600 nm. Black curves correspond to the ion-free indicator at 25 μM EGTA/100 μM EDTA. Magnesium- (red curve) and calcium- (blue curve) induced FRET signals were obtained by adding 1 mM $MgCl_2$ and 10 mM $CaCl_2$. All spectra are normalized to the isosbestic point at 514 nm.

To avoid magnesium-induced FRET signals I introduced different point mutations in the calcium binding domains EF III and EF IV of chicken skeletal troponin C in TN-L15 Citrine cp174. These mutations disrupt the Z-acid pair relying in each EF-hand's calcium binding loop and at the same time restore the overall amount of negatively charged amino acid residues. It has been

shown that a Z-acid pair plays an important role in chelating the magnesium ion (49). The particular mutations refer to N108D/D110N for EF-hand III and N144D/D146N for EF-hand IV (Figure 9). Positions depicted in this thesis refer to the sequence of chicken skeletal troponin C according to the NCBI accession number NM_205450. Numbering of the amino acids starts with alanine1, the first residue that is encoded after the initial start codon for methionine.

I introduced all variations of the mutated EF-hands into the TN-L15 backbone, leading to indicators named TN-L15 Citrine cp174 N108D D110N (EF III mutated), TN-L15 Citrine cp174 N144D D146N (EF IV mutated) and TN-L15 Citrine cp174 N108D D110N N144D D146N (both hands mutated). The purified indicator proteins displayed different magnesium-induced signals but always showed a significantly reduced FRET elicited by Mg^{2+} according to TN-L15 Citrine cp174 (Figure 10).

Disruption of the Z-acid pair in EF III lead to the lowest magnesium-induced FRET signal in the two sensors where just one calcium binding loop was mutated. Best performance was achieved by mutating both EF-hands.

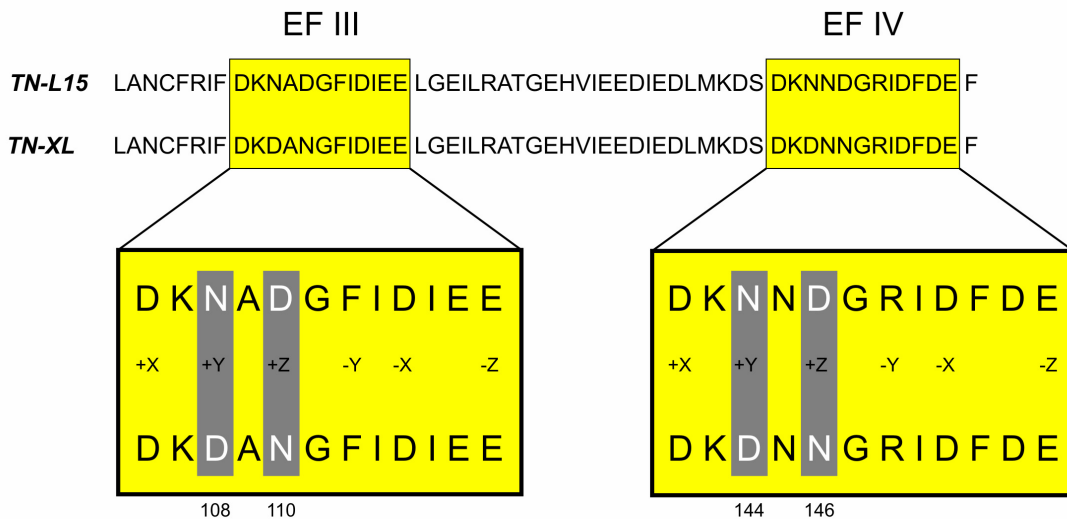


Figure 11: Schematic of the substitutions in the calcium binding loops III and IV in TN-XL.

Shown is the C-terminal part of csTnC from leucine98 to phenylalanine154. Yellow boxes highlight the chelating loops of EF-hand III and IV of csTnC. In the blow up boxes the chelating residues of TN-XL are compared to TN-L15. In TN-XL the Z-pair consists of an asparagine/glutamic acid which refers to the disrupted Z-acid pair.

Results

The indicator TN-L15 Citrine cp174 N108D D110N N144D D146N displayed almost no magnesium-induced signal thereby providing a huge $\Delta R/R_{\max}$ elicited by calcium in the presence of magnesium. Therefore it was named TN-XL (for X-Large). Figure 11 shows a schematic of the substitutions that were made according to the TN-L15 backbone. Shown is the C-terminal part including the ion binding loops of EF-hand III and IV.

4.1.2. Characteristics of TN-XL

In the next step TN-XL was characterized with respect to its dissociation constant (K_d) and decay time constant (τ). To determine the K_d -value of TN-XL we used a commercially available calcium titration kit that is supplemented with 1 mM free Mg^{2+} . Figure 12A shows the result of four different titrations performed on four independently purified TN-XL proteins. A dose response curve fit to the data in Figure 12A yielded a calcium dissociation constant for TN-XL of 2.2 μM (in presence of 1 mM free magnesium).

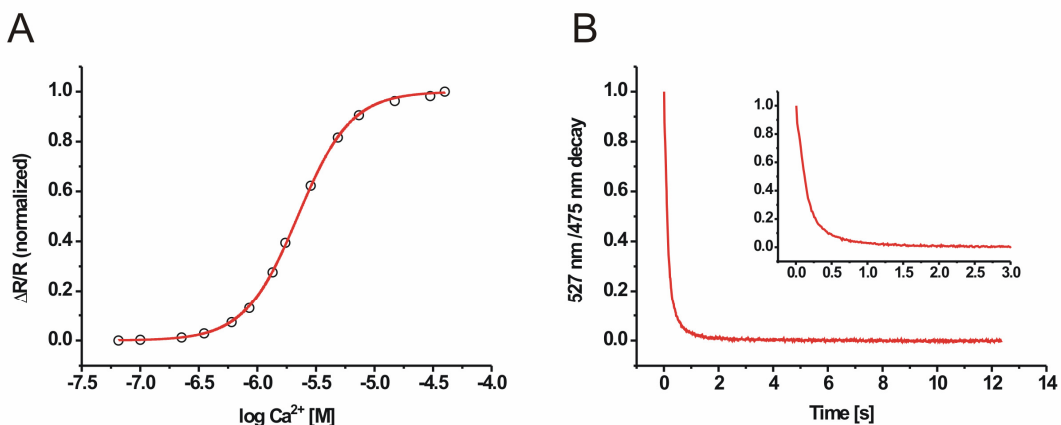


Figure 12: Characteristics of TN-XL.

(A) Calcium titration curve for determination of the dissociation constant. Data points reflect the average of four titrations from four different purified proteins. Dose response fit to the data yielded a K_d for TN-XL of 2.2 μM . (B) Stopped-flow measurement for determination of the decay time constant of TN-XL. Data represent the average 527 nm/475 nm decay of three measurements. In each experiment the ratio decay was calculated by averaging the CFP rise and YFP decay from at least nine runs. Resulting τ was 180 ms for single exponential fit and 143 ms (91 %)/864 ms (9 %) for double exponential fit. Inset shows a blowup of the first three seconds.

Aside from the calcium range where a given indicator displays its dynamic range, kinetics are of particular interest. The decay time constant of calcium saturated (2 mM Ca²⁺, 1 mM Mg²⁺) TN-XL indicator protein was determined by a stopped-flow experiment. Rapid mixing of the indicator with 10 mM BAPTA led the indicator return to the calcium-free state. This was displayed by a decrease in the Citrine cp174 channel and an increase in the CFP channel. Figure 12B shows the resulting mean 527 nm/475 nm ratio decay extracted from three independently purified proteins (with at least nine measurements per channel). Resulting dissociation time constants are 180 ms (for single exponential fit) and 143 ms/864 ms (for double exponential fit) and represent the Koff since [BAPTA] >> [indicator] and Kd (BAPTA) << Kd (indicator). Inset in Figure 12B shows a blow up of the first 3 seconds.

4.1.3. Expression of TN-XL in cultured hippocampal neurons

To test the *in vitro* performance of TN-XL primary hippocampal neurons were transfected with either the TN-XL or TN-L15 constructs. Before this could be performed both constructs were subcloned into the pcDNA3 vector to allow cytosolic expression that is driven by the CMV promoter. Both indicators show stable expression filling the neuron's cytosol and are excluded from the nucleus (Figure 13C).

To compare the response properties, neurons were stimulated with high potassium (50 mM KCl) that promoted depolarization of the membrane and subsequent opening of voltage gated calcium channels.

Repeated stimuli of transfected hippocampal neurons led to stable signals obtained with both indicators. TN-XL showed about twice the signals compared to TN-L15 (Figure 13A and Figure 13B respectively). Fluorescent responses obtained from the individual cells rely on the FRET-mechanism as it can be seen in the individual FRET channels (Figure 13A and Figure 13B, lower traces). Upon stimulation with KCl one can observe a decrease in the donor/CFP channel (485/35 nm) with a simultaneously increase in the acceptor/Citrine cp174 channel (535/25 nm). Enhanced signals produced by

Results

TN-XL are in line with the increased $\Delta R/R_{\max}$ that can be seen in the purified indicator proteins (Figure 8 and Figure 10).

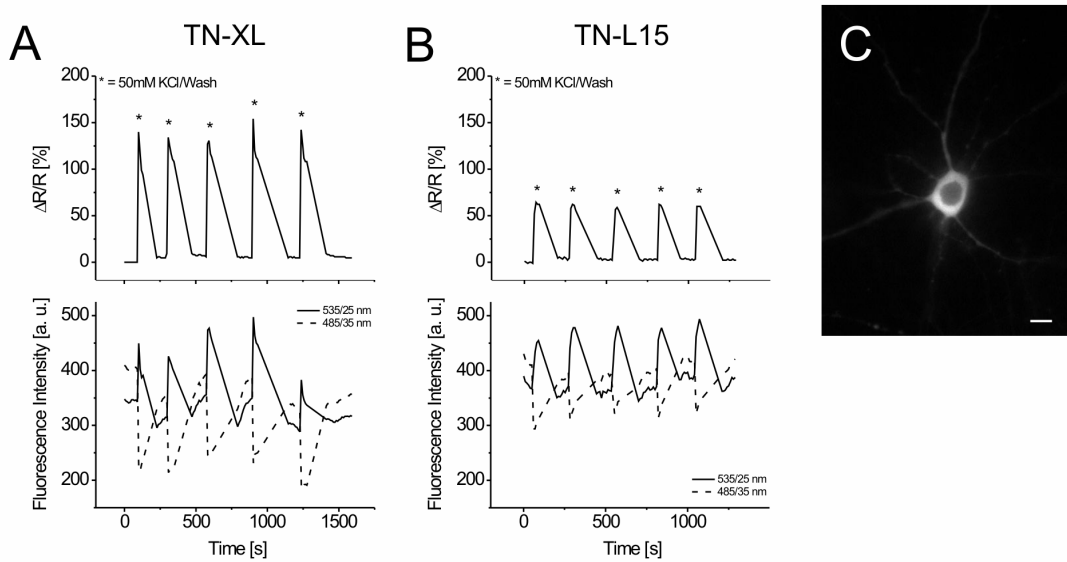


Figure 13: Performance of TN-XL and TN-L15 in primary hippocampal neurons.

(A) Traces obtained from a rat hippocampal neuron transfected with TN-XL. Upper trace shows the changes of the YFP/CFP ratio depicted in [%]. The cell was repeatedly stimulated by high potassium (50 mM) followed by washout (asterisks). Lower trace shows the corresponding changes in intensities of the YFP (535/25 nm) and the CFP (485/35 nm) channel. Time axes for ratio and intensities have the same time scale. (B) Responses of a primary hippocampal neuron transfected with TN-L15 treated like A. (C) Primary hippocampal neuron expressing TN-XL. The image shows the Citrine cp174 emission at 535/25 nm upon excitation at 440/20 nm. Scale bar 10 μ m.

4.2. Red-shifted variants of TN-XL

Shifting the emission spectra of genetically-encoded calcium indicators is a prerequisite for multicolor and deeper *in vivo* imaging. In the following I present the results of exchanging donor and acceptor proteins in TN-XL with longer emitting species of fluorescent proteins.

During this thesis a variety of new red-shifted proteins were developed (29, 30). To yield a red-shifted variant of our genetically-encoded calcium sensor, I replaced the donor (CFP) with Citrine and the acceptor (Citrine cp174) with

mOrange and tdTomato respectively. Figure 14 shows spectra of both purified indicator proteins before and after calcium saturation.

TN-XL_Citrine_mOrange showed a $\Delta R/R$ from zero calcium to calcium saturation of 15 % (peak values: 562 nm/527 nm) whereas TN-XL_Citrine_Tomato displayed a $\Delta R/R$ value of 50 % (peak values: 581 nm /527 nm). Excitation took place at 495 nm (for Citrine) and the emission spectra were taken between 505 nm and 650 nm. Both indicators displayed a calcium-induced FRET although their signal strength was not comparable to the CFP/Citrine cp174 variant of TN-XL ($\Delta R/R = 400$ % from zero calcium to calcium saturation).

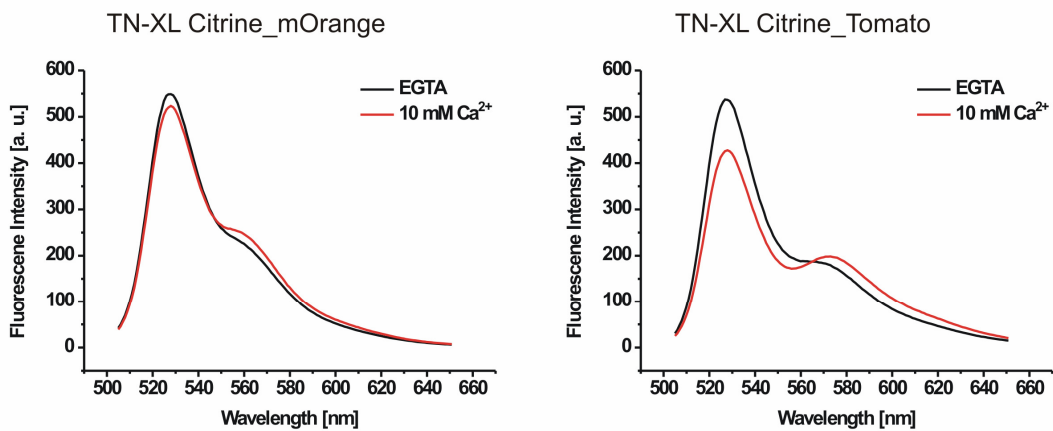


Figure 14: Fluorescent emission spectra of red-shifted TN-XL variants.

Donor and acceptor replacement yielded indicators TN-XL_Citrine_mOrange and TN-XL_Citrine_Tomato. Both indicators display only moderate FRET signals upon calcium saturation. For both constructs excitation took place at 495 nm. Emission spectra were taken from 505 nm to 650 nm.

To illustrate the red-shift, spectra of TN-XL and TN-XL_Citrine_Tomato are drawn into the same plot (Figure 15A). The gain of such a red-shifted indicator would be 52 nm the difference between Citrine cp174 emission peak (527 nm) and CFP emission peak (475 nm). Figure 15B displays the fluorescence spectra of the individually purified fluorescent proteins (Citrine and tdTomato). Note that the excitation spectra of Citrine and tdTomato overlap to a high degree which hardly allows for excitation of the donor without simultaneous direct excitation of the acceptor and therefore a high degree of fluorescence in the acceptor channel that is not elicited by the resonance energy transfer.

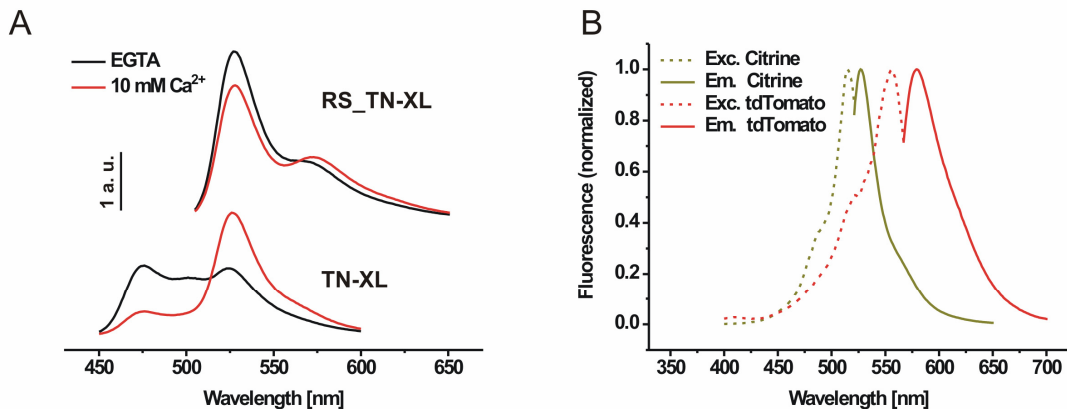


Figure 15: Comparison of the red-shift approach to CFP/YFP FRET indicators.

(A) Fluorescence emission spectra of calcium free and calcium saturated TN-XL and TN-XL Citrine_Tomato (RS_TN-XL) are plotted in the same graph to illustrate the gain in wavelength shift. Such a shift would be 52 nm to the ‘red-side’. All spectra are normalized to their isosbestic point (514 nm for CFP/YFP and 565 nm for YFP/Tomato). The huge discrepancy in signal production after calcium saturation can be easily seen between the two donor/acceptor variants. (B) Normalized fluorescence excitation and emission spectra of Citrine and tdTomato.

4.3. Point mutating the csTnC backbone of TN-XL to lower the Kd for calcium

This paragraph describes the results obtained by point mutating the csTnC backbone of TN-XL. Point mutations were introduced to the calcium binding moiety in order to reduce the Kd value of TN-XL for calcium and to enhance signal strength this troponin C-based GECI. These point mutations are not applied to positions inside the calcium binding loop of the EF-hand domains. This shows that altering the Kd-value of a calcium binding protein can also be achieved by changing amino acids that are not directly involved in calcium coordination.

4.3.1. Tuning the troponin C backbone of TN-XL by introducing point mutations in the N-terminal part of csTnC

Compared to TN-L15, the magnesium insensitive calcium biosensor TN-XL displays a higher Kd value for calcium (0.7 μM vs. 2.2 μM). To increase calcium affinity in TN-XL, I applied different point mutations in the unmutated N-terminal part that is known to be less calcium sensitive than the C-terminal lobe. For that purpose I tried to exchange hydrophobic residues in the N-terminal lobe with more polar groups. This should promote the transition of the apo (calcium free state) to the calcium bound state due to increased solvent accessibility and therefore the reduction of energy that is needed to drive this transition (65, 66). Point mutations were inserted at position Phe22, Val45, Met46, Leu49, Val65, Met82 and Met86. Figure 16 gives a summary of the mutated and purified sensor proteins with respect to their calcium dissociation constants.

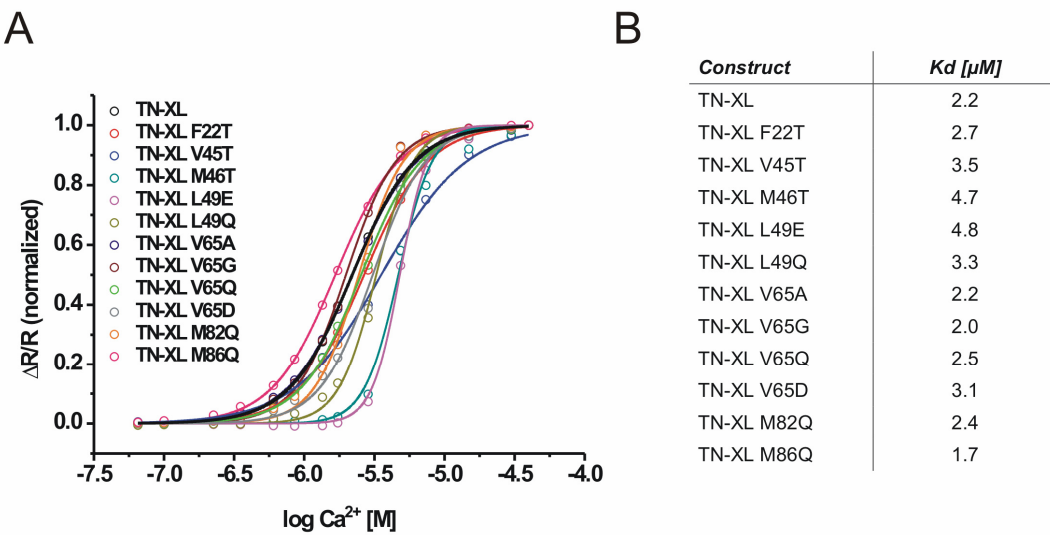


Figure 16: Substitution of single hydrophobic residues in the N-terminal lobe of csTnC in TN-XL.

Normalized calcium titration curves (A) and extracted Kd values (B) of different amino acid substitutions in the N-terminal lobe of the csTnC backbone in TN-XL. Residues that were used to mutate refer to as F22, V45, M46, L49, V65, M82 and M86. Except for TN-XL (average of four different titrations of four purified proteins) data represents one titration.

As it can be seen in Figure 16 only the mutations V65G and M86Q led to a decrease of the Kd value although both mutations provided only small effects

Results

on the dissociation constant (2.0 μM for V65G, 1.7 μM for M86Q compared to 2.2 μM in the unmutated TN-XL).

4.3.2. Effect of the mutation I130T in csTnC's C-terminal part of TN-XL

As mentioned before the C-terminal part of troponin C displays a higher calcium affinity than the N-terminal lobe. Dissociation constant of a given EF-hand not only depends on the chelating residues that bind the calcium inside the loop region. It has been recognized that particular amino acid residues outside the binding-loop can have a strong effect on calcium chelation like position 130 in csTnC. In wild type csTnC this position is occupied by an isoleucine. One particular study by Trigo-Gonzalez and colleagues showed that replacement of this side chain with threonine leads to a stabilization of the two C-terminal EF-hands and to an increase in calcium affinity for that EF-hand domain (67). I introduced this particular amino acid substitution to our mutated csTnC backbone of TN-XL with the aim of lowering the K_d value for calcium of TN-XL. Figure 17A shows the normalized titration curves of TN-XL and TN-XL I130T. Spectra show a shift of TN-XL I130T to the left side representing a lower K_d value for TN-XL I130T (1.6 μM) compared to TN-XL (2.2 μM).

To further increase calcium affinity of our biosensor I introduced the M86Q mutation to yield the double mutant TN-XL M86Q I130T. Since the M86Q substitution worked well in TN-XL the intention was to further lower the K_d value with the combined substitution. As it can be seen in Figure 17A, this approach indeed led to a decreased K_d value of 740 nM for TN-XL M86Q I130T. For a more profound comparison of TN-XL, TN-XL M86Q, TN-XL I130T and TN-XL M86Q I130T the actual $\Delta R/R$ values in [%] are depicted in Figure 17B. For each indicator the signals are plotted against free calcium values from zero to 1.35 μM (in presence of 1 mM Mg^{2+}), a range that might best reflect the cytosolic $\Delta[\text{Ca}^{2+}]_i$ of a stimulated cell.

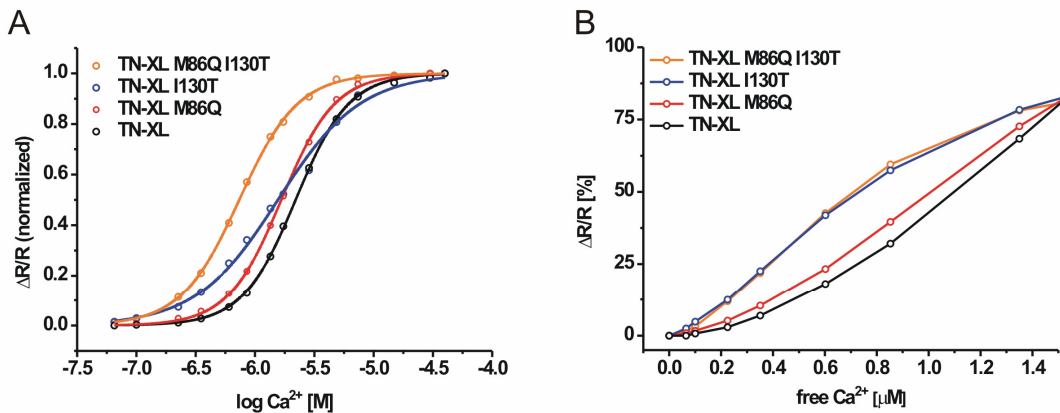


Figure 17: Effect of the I130T mutation in the C-terminal part of csTnC in TN-XL.

(A) Comparison of normalized calcium titration curves obtained from TN-XL, TN-XL M86Q, TN-XL I130T and the double mutant TN-XL M86Q I130T. A dose response fit to the individual curves yielded Kd values of 1.7 μM (TN-XL M86Q), 1.6 μM (TN-XL I130T), 0.74 μM (TN-XL M86Q I130T) and 2.2 μM (TN-XL). (B) Signals obtained with the different indicators as $\Delta R/R$ in [%] according to the calcium regime from zero to 1.35 μM free Ca^{2+} . Signals obtained from TN-XL I130T and TN-XL M86Q I130T show similar values and exceed the values obtained from TN-XL and TN-XL M86Q. Except for TN-XL (average of four different titrations of four purified proteins) and TN-XL I130T (average of three different titrations of two purified proteins) data represents one titration.

In contrast to the pure Kd values it becomes clear that lowering the Kd value not necessarily displays an improvement according to signal strength as the $\Delta R/R_{\max}$ also varies between the different sensors. In this case one can observe an almost equal enhancement of signal obtained with TN-XL I130T and the double mutated TN-XL M86Q I130T according to TN-XL. This makes the significant difference of the Kd value of these two sensors negligible. In other words the single mutation I130T in TN-XL is sufficient to increase the signal strength of this biosensor.

4.4. Development of TN-XXL, a genetically-encoded calcium indicator with enhanced signal strength

In the following section I will introduce the ‘doubling strategy’ that led to a genetically-encoded calcium indicator with enhanced signal strength. The strategy was to double a high affinity EF-hand domain consisting of two

Results

calcium binding EF-hands. The strategy was applied to the C-terminal part of csTnC carrying different point mutations.

4.4.1. Doubling the csTnC's C-terminal part of TN-XL I130T

Instead of introducing point mutations to enhance signal strength I tried to perform a more profound rearrangement of the csTnC backbone. For that purpose a doubling of the high affinity C-terminal part was considered to be suitable of lowering the Kd-value by simultaneously preserve the high $\Delta R/R_{max}$ obtained with TN-XL.

I decided to double the C-terminus with different starting and ending points. As one starting point I chose serine94 (S94, **S**) and, additionally, added two amino acids in front of serine94 namely threonine and aspartic acid (**TDS**) that are found to precede the according serine positioned in wild type CaM. As ending points methionine158 (M158, **M**) and glutamine162 (Q162, **Q**) were chosen. The C-terminal domain of csTnC was shortened by four amino acids (when stop is at Met158) because the crystal structure (pdb entry 1TOP) shows the end of the exiting helix of EF-hand IV at this position. Figure 18A displays the graph of normalized titration curves obtained from the investigated doublings. All doublings were performed on the mutated C-terminal part of csTnC as it was used for TN-XL I130T. Names of the biosensors reflect the overall building scheme. For example S-Q_S-Q can be described as follows:

CFP - Ser94 - Glu162 - Gly Thr - Ser94 - Glu162 - Citrine cp174

The domains are linked together by a KpnI restriction site that encodes for glycine/threonine (underlined). In case of starting with TDS as second part the threonine was used from the restriction site to avoid doubling of this particular amino acid residue.

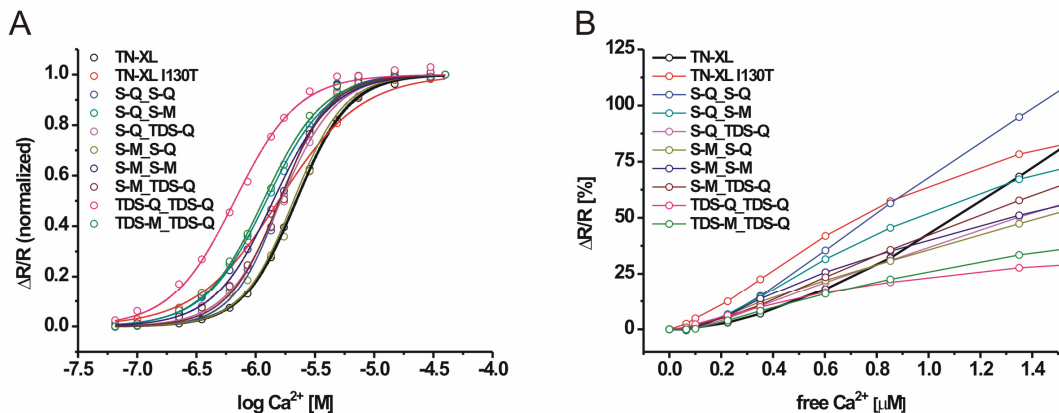


Figure 18: Doubling the C-terminal part of csTnC in TN-XL I130T.

(A) Normalized titration curves obtained from different C-terminal doublings of the C-terminal lobe of csTnC as used in TN-XL I130T. For K_d values see Figure 19. (B) $\Delta R/R$ values in [%] acquired from the individual C-terminal doublings according to zero up to 1.35 μM free Ca^{2+} . None of the doublings display a significant enhancement in strength compared to the TN-XL I130T variant (red curve). Note that of all doublings the S-Q_S-Q variant shows the highest $\Delta R/R$ values (blue curve). Except for TN-XL (average of four different titrations of four purified proteins) and TN-XL I130T (average of three different titrations of two purified proteins) data represents one titration.

With respect to the calcium regime from zero to 1.35 μM from all tested doublings the S-Q_S-Q variant displayed the best improvement according to TN-XL (Figure 18B). Unfortunately none of the doublings provided a higher actual signal than TN-XL I130T according to small calcium changes (65 nM to 800 nM).

Construct	K_d [μM]	$\Delta R/R$ [%], 39.8 μM Ca^{2+}
TN-XL	2.2	250
TN-XL I130T	1.6	170
S-Q_S-Q	1.6	250
S-Q_S-M	1.2	130
S-Q_TDS-Q	1.6	130
S-M_S-Q	2.1	170
S-M_S-M	1.4	110
S-M_TDS-Q	1.6	150
TDS-Q_TDS-Q	0.7	40
TDS-M_TDS-Q	1.2	60

Figure 19: K_d and $\Delta R/R$ values obtained from the C-terminal doubling variants of TN-XL I130T.

Calcium dissociation constants were extracted by a dose response fit of the curves depicted in Figure 18A. $\Delta R/R$ represents the ratio change obtained from the variants at 39.8 μM free Ca^{2+} . Except for TN-XL (average of four different titrations of four purified proteins) and TN-XL I130T (average of three different titrations of two purified proteins) data represents one titration.

Results

Compared to TN-XL, S-Q_S-Q displayed no significant enhancement in $\Delta R/R$ values up to 100 nM free Ca^{2+} . In contrast, a significant improvement in signal strength can be observed from 225 nM up to 1.35 μM (on average a 1.9 fold enhancement). Figure 19 gives a summary of all K_d values extracted from the individual doublings and the $\Delta R/R_{\max}$ value obtained at 39.8 μM free calcium (in presence of 1 mM magnesium).

4.4.2. Doubling the csTnC's C-terminal part of TN-L15 N108D D110N I130T Citrine cp174

Among all tested variants of TN-XL introduction of the single mutation I130T alone led to the most dramatic improvement of signal strength. As mentioned before disruption of the Z-acid pairs of EF-hand III and IV not only removed magnesium-induced FRET signals in TN-XL but also lowered the K_d value for calcium. As shown in Figure 10, the single mutations of EF-hand III and EF-hand IV alone showed a significant disruption in magnesium binding. Both indicators display lower K_d values than TN-XL as it can be seen in Figure 20A. Compared to TN-L15 N144D D146N Citrine cp174 in which EF-hand IV is mutated, TN-L15 N108D D110N Citrine cp174 exhibits a much more diminished magnesium-induced FRET signal (Figure 10). Interestingly, this biosensor showed the smaller K_d value of both single mutated EF-hand sensors (1.3 μM vs. 1.6 μM). A closer look at the actual $\Delta R/R$ values gives rise to a signal enhancement of TN-L15 N108D D110N Citrine cp174 that reaches and eventually exceeds the TN-XL I130T values (Figure 20B).

As a next step I introduced the mutation I130T in the TN-L15 N108D D110N Citrine cp174 backbone to see if this mutation has the same effect on signal strength as in TN-XL. Again a dramatic increase can be observed especially in the low calcium regime from 65 nM up to 600 nM. Only above this value the signals were similar or smaller than omitting the I130T mutation. With the knowledge about the C-terminal doubling of TN-XL I130T, I also tried to apply this strategy to the csTnC's C-terminal part from TN-L15 N108D D110N I130T

Citrine cp174. For that purpose I again used the start and end points serine94 and glutamine162. The resulting building scheme is depicted in Figure 21.

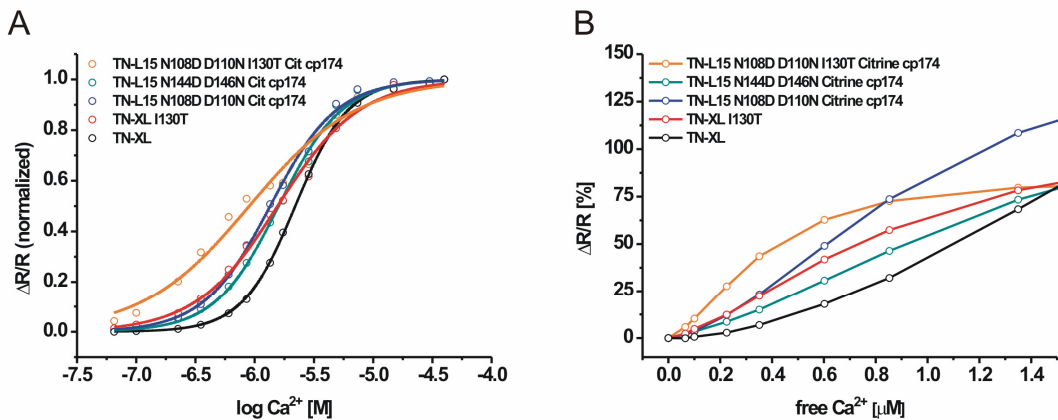


Figure 20: Characteristics of TN-L15 Citrine cp174 variants with single mutated EF-hand loops.

(A) Comparison of normalized calcium titration curves of different sensors with mutated EF-hand loops. Among those the double disrupted Z-acid pair variants are TN-XL and TN-XL I130T. Single mutated EF-hand sensors are TN-L15 N108D D110N Citrine cp174, TN-L15 N108D D110N I130T Citrine cp174 (Z-acid pair in EF loop III disrupted) and TN-L15 N144D D146N Citrine cp174 (Z-acid pair in EF loop IV disrupted). TN-L15 N108D D110N I130T Citrine cp174 shows an unusual titration curve that roughly displays biphasic characteristics (see also Figure 42). (B) Comparison of signal strength obtained from the variants in A according to the calcium concentration from zero to 1.35 μM . Note the significant enhancement of the signals obtained from TN-L15 N108D D110N I130T Citrine cp174 in the low calcium regime of 65 nM to 600 nM. Except for TN-XL (average of four different titrations of four purified proteins) and TN-XL I130T (average of three different titrations of two purified proteins) data represents one titration.

I determined the calcium dissociation constant of this indicator by titration which yielded a K_d value of 800 nM (Figure 22A). This reflects a tremendous lowering of the dissociation constant in contrast to TN-XL (2.2 μM) by almost retaining the $\Delta R/R_{\max}$ (230 % vs. 250 %, in presence of 1 mM Mg^{2+}). Therefore this indicator was named TN-XXL. Improvement of TN-XXL is best displayed by comparison of the actual signals produced by defined calcium values. As depicted in Figure 22B TN-XXL performs superior to all the other promising indicators tested so far. Comparing the $\Delta R/R$ values elicited by the different TnC-based indicators TN-L15, TN-L15 N108D D110N I130T Citrine cp174, TN-XL and TN-XXL one can observe a dramatic increase in signal strength obtained with TN-XXL.

Results

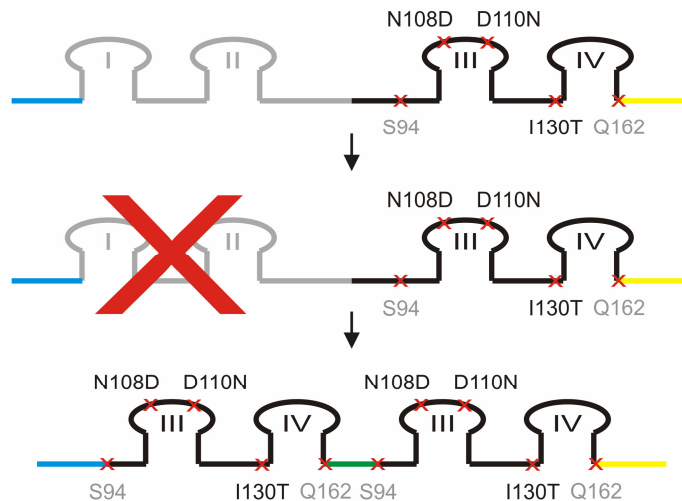


Figure 21: Schematic drawing of the strategy used to develop TN-XXL.

Upper row shows positions of interest according to the wt_csTnC (wild type chicken skeletal troponin C) as it is used in TN-L15. These positions are serine94 (start), asparagine108, aspartic acid110, isoleucine130 and glutamine162 (end). Note that each of these amino acids resides in the C-terminal part of troponin C. The individual EF-hands are depicted in roman numerals. Blue and yellow lines in front and behind the schematic of TnC resemble the fusion of CFP and Citrine cp174 respectively. The whole C-terminal fragment between serine94 and glutamine162 was doubled and sandwiched between CFP and Citrine cp174. As linker between the fragments a KpnI site was used that encodes for the amino acids GlyThr (green).

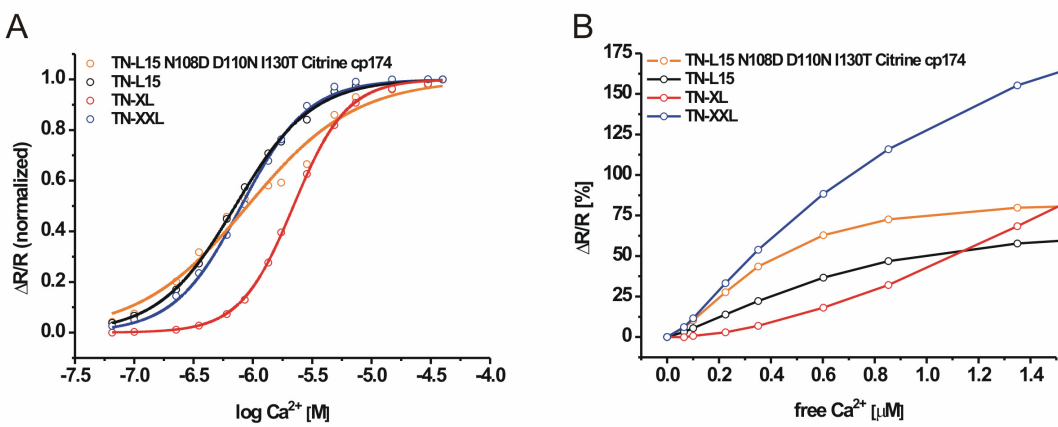


Figure 22: Comparison of selected troponin C-based GECIs.

(A) Calcium titration curves obtained from TN-L15, TN-L15 N108D D110N I130T Citrine cp174, TN-XL and TN-XXL. Note that TN-L15 and TN-XXL almost display the same Kd value (710 nM vs. 800 nM) but with a different $\Delta R/R_{max}$ (80 % vs. 230 %). (B) Actual signals in [%] elicited by the different variants in the low calcium regime. Note that the signal enhancement of TN-L15 N108D D110N I130T, as it can also be seen in Figure 20, is preserved in TN-XXL and stays above all other troponin C-based calcium indicators investigated so far. On average one finds a 2.4 fold enhancement in signal strength of TN-XXL according to TN-L15. Except for TN-L15 N108D D110N I130T Citrine cp174 (one titration) data represents the average of four measurements from four different purified proteins.

The values even exceeded those of TN-L15 N108D D110N I130T Citrine cp174 which displayed the highest reached so far.

Apart from the enhancement seen with TN-L15 N108D D110N I130T Citrine cp174, TN-XXL preserved the signals in the low calcium regime of 65 nM to 600 nM and did not show a decline above these values. When compared to TN-L15, TN-XXL showed a 2.4 fold enhancement in signal strength according to free calcium values of 65 nM to 1.35 µM.

4.5. Comparison of TN-L15, TN-XL and TN-XXL with respect to decay time constant τ

As mentioned before actual signal strength is not the only parameter that is of importance when describing a calcium indicator as, in addition, how fast a given calcium signal can be transduced into a FRET signal must also be considered. For that purpose I performed stopped-flow measurements of the purified indicator proteins to determine the decay time constant of selected TnC-based indicators. Again purified proteins were rapidly mixed with 10 mM BAPTA to measure the decay time constant. This time constant reflects the K_{off} rate since the buffer system exceeds the indicator concentration and the K_d value for BAPTA is much smaller than the dissociation constants of the indicators. Having measured the K_d and K_{off} values, one can extract the K_{on} rates by the relation $K_d = K_{off}/K_{on}$.

Figure 23 shows the 527 nm/475 nm ratio decay of the individual troponin C-based calcium indicators that has been calculated from the measurements of three independent (three purifications) experiments per indicator. Single and double exponential fits were applied to the data obtained from the different indicators. As seen in Figure 23, all curves can be best described by a double exponential fit that might reflect uneven calcium binding properties of the different calcium binding sites in each indicator. Of all troponin C-based indicators TN-XL possess the fastest decay time constant and hence K_{off} . It is followed by TN-XXL that in turn shows a smaller τ than TN-L15.

Results

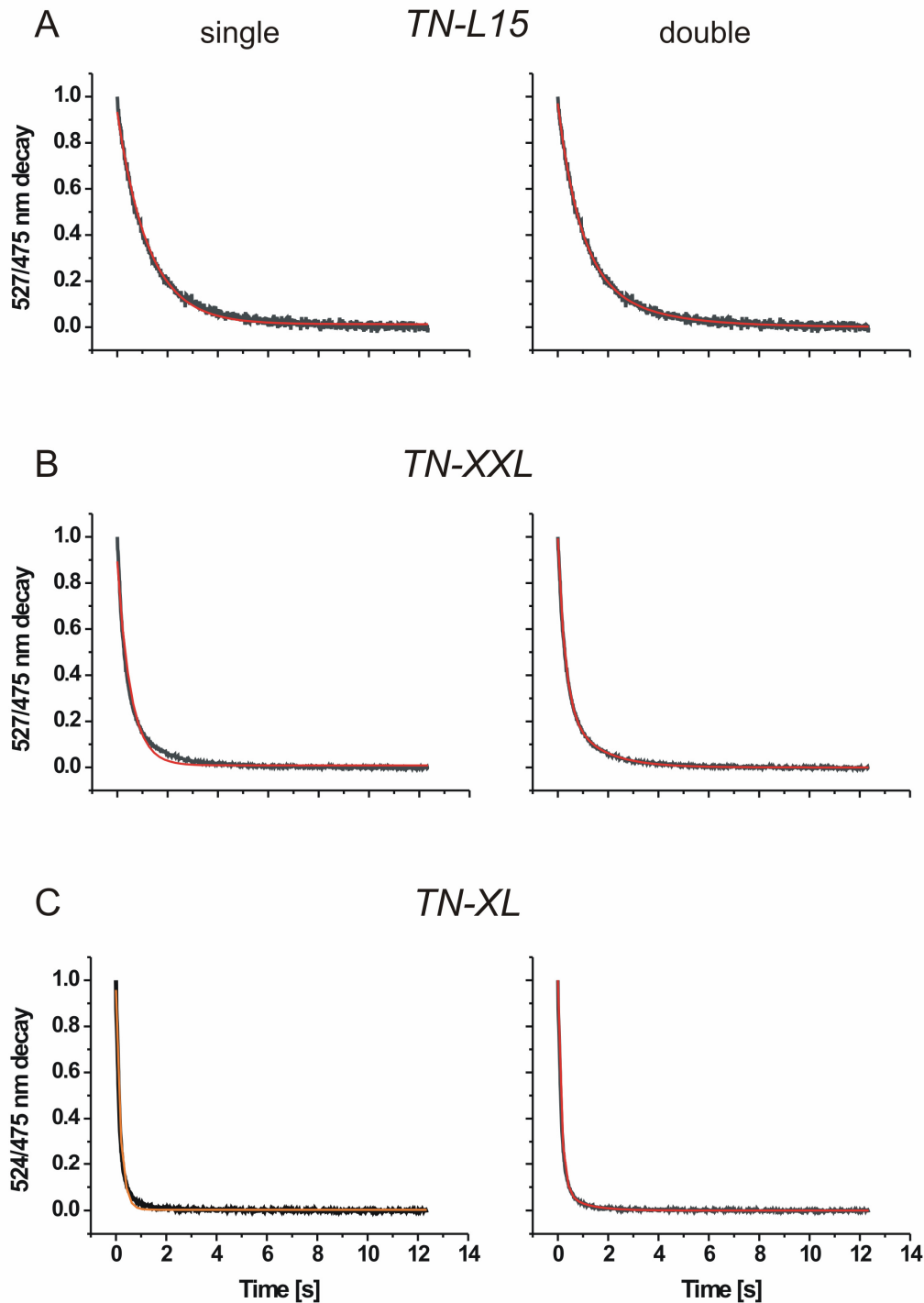


Figure 23: Comparison of decay time constants obtained from TnC-based GECIs.

Stopped-flow measurements for determination of the decay time constant of (A) TN-L15, (B) TN-XXL and (C) TN-XL. Data represent the average 527 nm/475 nm decay of three measurements. In each experiment the ratio decay was calculated by averaging the CFP rise and YFP decay from at least nine runs. Data obtained from the stopped-flow measurements were fitted by a single (left column, red traces) or double (right column, red traces) exponential function.

Traces of TN-L15 are much noisier reflecting the overall reduced fractional fluorescence change compared to those that can be obtained with TN-XL and TN-XXL. It is not surprising that the fastest decay time constant is achieved with TN-XL since this indicator shows the highest Kd value of all three sensors. A higher Kd value should yield a higher K_{off} value and therefore a faster decay time constant. On the other hand TN-L15 and TN-XXL displayed almost the same Kd value but have different decay time constants. This in turn supposes a different K_{on} value for these two indicators.

Construct	Kd [M] (measured)	T_{decay, single} [s] (measured)	T_{decay, double} [s] (measured)	K_{off} [s ⁻¹] (measured)	K_{on} [M ⁻¹ s ⁻¹] (calculated)
TN-L15	0.71*10 ⁻⁶	1.23 (r ² = 0.993)	0.897 (74 %)/ 2.62 (26 %) (r ² = 0.996)	0.81	1.1*10 ⁶
TN-XL	2.20*10 ⁻⁶	0.180 (r ² = 0.989)	0.143 (91 %)/ 0.867 (9 %) (r ² = 0.997)	5.56	2.5*10 ⁶
TN-XXL	0.80*10 ⁻⁶	0.527 (r ² = 0.983)	0.287 (73 %)/ 1.34 (27 %) (r ² = 0.999)	1.90	2.4*10 ⁶

Figure 24: Comparison of the parameters obtained from TnC-based GECIs.

Figure 24 gives a summary of all measured and calculated parameters of the TnC-based GECIs TN-L15, TN-XL and TN-XXL

4.6. Performance of TN-XXL in cell culture

The upcoming paragraph depicts calcium imaging with TN-XXL in cell culture. Calcium imaging was performed in primary hippocampal neurons and HEK293 cells from which stable calcium signals were recorded.

4.6.1. Detection of calcium signals in primary hippocampal neurons with TN-XXL

As a first test of TN-XXL dissociated primary hippocampal cell cultures were transfected. It is known that these neurons become spontaneously active after two weeks in culture. This activity can be reliably detected with TN-XXL as is shown in Figure 25. Primary hippocampal neuron displayed oscillations in its cytosolic calcium level within a timescale of minutes that are reflected by a change in the $\Delta R/R$ values (red curve). Neurons were imaged at a frame rate of 0.5 Hz. Intensity traces of the donor and acceptor are plotted with colors according to their emission (CFP, blue line and Citrine cp174, yellow line).

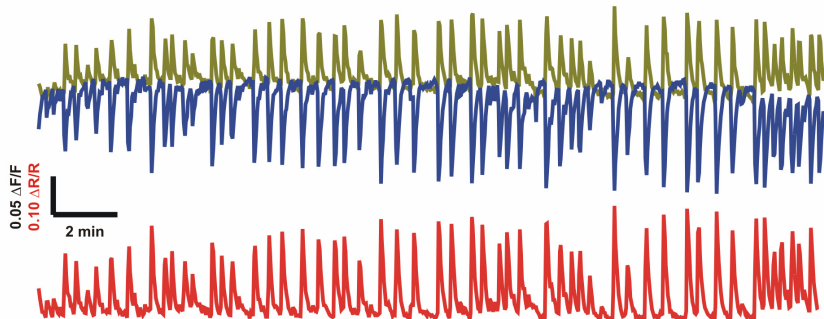


Figure 25: Activity of a primary hippocampal cell reported by TN-XXL.

A single primary hippocampal neuron was recorded after two weeks in cell culture. Red trace represents the $\Delta R/R$ in [%] obtained from that cell within a recording time of 25 minutes. Each peak corresponds to a decrease in the CFP channel and an increase in the YFP (Citrine cp174) channel depicted as $\Delta F/F$ in [%] in the upper traces resembling the FRET-mechanism of TN-XXL. Acquisition was at 0.5 Hz. Excitation was at 440/20 nm and the individual channels were recorded at 535/25 nm (for Citrine cp174) and 485/35 nm (for CFP).

To test if the signals are promoted by neuronal activity, 1 μM TTX was applied to the cultures to inhibit voltage gated sodium channels and thereby the initiation of action potentials. Figure 26A shows the response of a neuron before and after treatment with TTX. One can observe calcium transients that are prevented during treatment with 1 μM TTX. After washout of the drug, the neuron starts again to produce calcium oscillations. Figure 26B shows a blowup of the experiment in Figure 26A (black box). Signals are produced by

the FRET-mechanism as can be seen by reciprocal behavior of the individual wavelengths corresponding to the donor (CFP, blue line) and acceptor protein (Citrine cp174, yellow line).

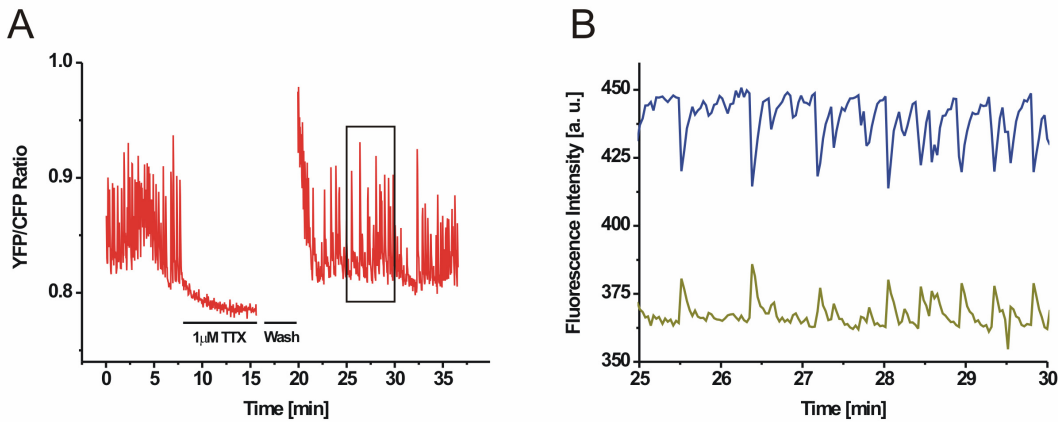


Figure 26: Inhibition of the calcium signals produced by primary hippocampal neurons with TTX.

(A) Calcium signals in primary hippocampal neurons are inhibited by TTX indicating a dependency on active neuronal processes. After applying 1 μ M of TTX signals are diminished and are re-initiated after removal of the drug by washing. (B) Amplification of data presented in A (black box) shows the response of CFP (blue) and Citrine cp174 (yellow). Imaging conditions were the same as in Figure 25.

4.6.2. Imaging calcium oscillations in HEK293 cells

In contrast to primary hippocampal neurons, HEK293 cells are not spontaneously active. In these cells, calcium oscillations can be induced by stimulating their muscarinic receptors via the agonist Carbachol. After transfecting HEK293 with TN-XXL 1 mM Carbachol to the cell culture was added. As it can be seen in Figure 27 stimulation of the muscarinic receptor system indeed led to calcium oscillations that were reported by the calcium indicator TN-XXL (red trace). As the calcium signals measured in the primary hippocampal neurons, signals obtained from HEK293 cells are based on the FRET-mechanism, as it can be seen in the individual traces of the donor (CFP, blue trace) and acceptor emission respectively (Citrine cp174, yellow trace)

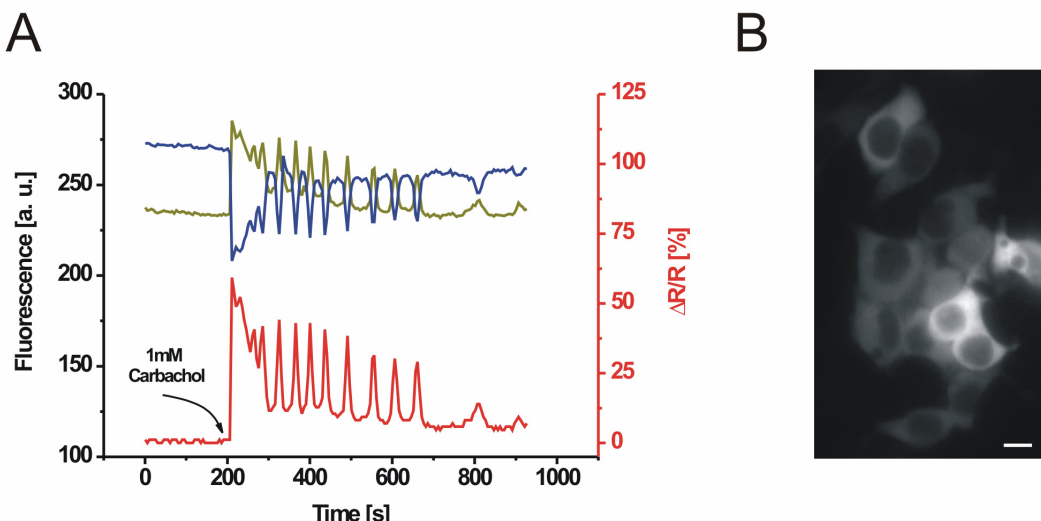


Figure 27: Eliciting calcium oscillations in HEK293 cells.

(A) A HEK293 cell expressing the genetically-encoded calcium indicator TN-XXL shows calcium oscillations after stimulation with 1 mM Carbachol. Red trace shows the $\Delta R/R$ as it can be calculated from the individual wavelengths depicted in blue (CFP) and yellow (Citrine cp174). Imaging conditions were the same as in Figure 25. (B) Fluorescence image of Citrine cp174 (535/25 nm) elicited upon excitation at 440/20 nm of HEK293 cells expressing TN-XXL. Scale bar, 10 μ m.

For a profound *in vivo* comparison of TN-L15, TN-XL and TN-XXL the reader is referred to the ‘Discussion – *In vivo* comparison of troponin C-based GECIs at the *Drosophila* NMJ’ chapter. There, all troponin C-based genetically-encoded calcium indicators were compared under the same *in vivo* conditions using the *Drosophila* neuromuscular junction as a reliable *in vivo* test system.

4.7. Applying different strategies to improve the troponin C-based GECI TN-XXL

The improvement that has been achieved with the development of TN-XXL so far mostly relied on a structural re-arrangement of the troponin C backbone of the calcium indicator. Three additional strategies were performed to further modulate the response properties of TN-XXL in order to enhance the signal strength. First the ‘doubling strategy’ was expanded to TnC’s from different animals, second the amount of calcium binding sites in TN-XXL was reduced

and third, specific positions inside the calcium binding loops of EF III and EF IV were target of point mutations to directly lower the Kd value for calcium of TN-XXL.

4.7.1. Expanding the C-terminal doubling strategy to variants of troponin C from different species

In order to further increase the signal strength of TN-XXL I tried to apply the C-terminal doubling strategy to variants of troponin C from different species. For that purpose I chose chicken skeletal TnC (**C**), mouse skeletal TnC (**M**) and zebrafish skeletal TnC (**Z**). In all TnC's I introduced mutations that led to the disruption of the Z-acid pair in the according EF-hand III. For mouse and zebrafish TnC these mutations refer to as N105D and D107N. The corresponding I130T mutation of csTnC was omitted since mouse and zebrafish TnC already posses a threonine or serine at that position ('127'). It has been shown that there is no difference in the effect of calcium binding whether this position is occupied by a threonine or serine (67). Figure 28 shows an alignment of the C-terminus from the different wild type troponin C variants

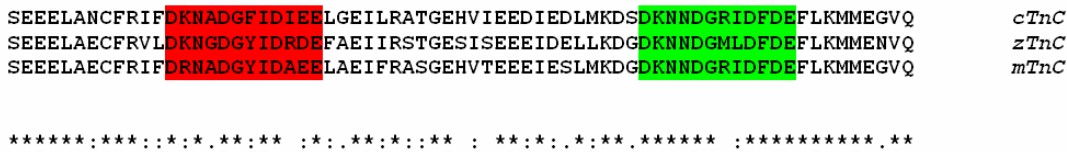


Figure 28: Amino acid alignment of the C-terminal parts of wild type chicken skeletal, mouse skeletal and zebrafish skeletal troponin C.

Red and green boxes highlight the calcium binding loops of EF-hand III and IV respectively. Alignment was performed using the TCoffee multiple sequence alignment tool.

All C-terminal lobes display a high similarity although there is variation in the region between the two calcium binding loops (red and green). For the doubling C-terminal parts were used as follows: csTnC (S94-Q162), zTnC

Results

(S91-Q159) and mTnC (S91-Q159). All nine permutations were cloned and calcium titration was performed to determine the calcium dissociation constant and to obtain the $\Delta R/R$ values at calcium concentrations from zero to 1.35 μM . Figure 29A gives a summary of the normalized titration curves that were used to determine the K_d value of all doublings.

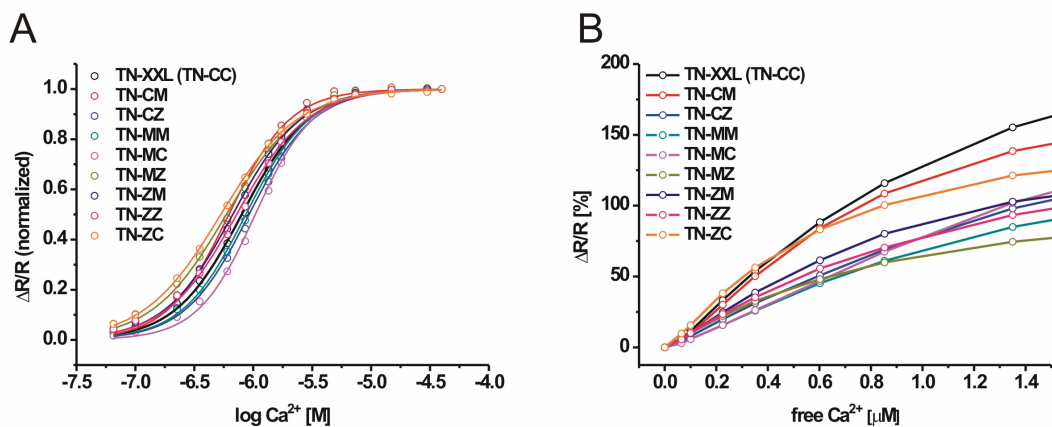


Figure 29: Titration curves of nine different indicators based on the C-terminal doubling of troponin C from different animals.

(A) Titration curves of nine different indicators based on doubling of the C-terminal domain of troponin C from different animals. To obtain the calcium sensors all possible permutations of csTnC (chicken, C), mTnC (mouse, M) and zTnC (zebrafish, Z) were created (S94-Q162 for csTnC and S91-Q159 for m/zTnC). As reference TN-XXL is plotted in black (mean of four titrations, refers to as TN-CC since it resembles the doubling of csTnC). All other curves represent individual titrations and are indexed according to their architecture, e.g. in TN-CM the csTnC part precedes the mTnC part in the artificial construct. (B) The graph shows a blow up of signals in [%] obtained at free calcium values from zero to 1.35 μM . None of the eight constructs significantly exceeds the signal strength obtained with TN-XXL. Only TN-ZC and TN-CM roughly display the same signal properties as TN-XXL. Except for TN-XXL (four titrations of four purified proteins) data represent one titration.

Different indicators are named according to their building scheme meaning which parts of the different C-terminal variants are used as building blocks between CFP and Citrine cp174. For example in TN-CM the C-terminal part of csTnC (C) precedes the C-terminal part of mTnC (M). All of the doublings yielded indicators that display a calcium dependent FRET change. As it can be seen in Figure 29B none of the doublings significantly exceed the actual $\Delta R/R$ values of TN-XXL although TN-CM and TN-ZC roughly displays the same signal strength.

Interestingly, all indicators that display the highest signals of all permutations posses at least one chicken skeletal troponin C part (two parts in TN-XXL, one part in TN-CM and TN-ZC). Figure 30 summarizes the calcium dissociation constants and the $\Delta R/R_{max}$ values of all nine variants. Among these permutations TN-ZC displays the lowest Kd value of all indicators (with four EF-hands) mentioned so far in this thesis (530 nM).

Construct	Kd [nM]	$\Delta R/R [\%, 39.8 \mu M Ca^{2+}]$
TN-XXL (= CC)	800	230
CM	620	180
CZ	920	160
MM	860	130
MC	1040	170
MZ	590	100
ZZ	720	130
ZC	530	160
ZM	670	140

Figure 30: Kd and $\Delta R/R$ values obtained from the C-terminal doubling of troponin C from different species.

(A) Calcium dissociation constants were extracted by a dose response fit of the curves depicted in Figure 29A. $\Delta R/R$ represents the ratio change obtained from the variants at 39.8 μM free Ca^{2+} . Except for TN-XXL (average of four different titrations of four purified proteins) data represents one titration.

4.7.2. Reducing the calcium binding site in TN-XXL to one C-terminal domain

One major concern using genetically-encoded calcium indicators is a possible buffering effect due to overexpression of a protein that is capable to bind calcium in the physiological relevant range. Additionally most of the GECIs have more than one calcium binding site meaning a possible stoichiometry of more than one bound calcium ion per molecule of indicator (usually 4 mol calcium per mol indicator). In order to prevent a calcium buffering effect I tried to reduce the overall amount of calcium binding sites in our troponin C-based GECIs. For that reason I used a single C-terminal domain (S94-Q162) of the

Results

mutated csTnC (N108D D110N I130T) and sandwiched this part between the CFP and Citrine cp174 variants of GFP. Due to the reduction of the overall amino acid linker between the two FRET chromophores this indicator displayed a huge FRET even in the absence of calcium.

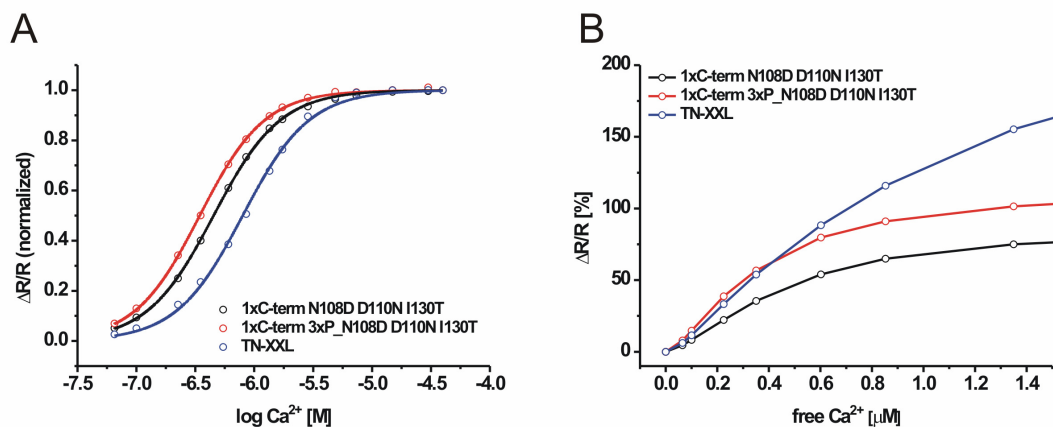


Figure 31: Reducing the calcium binding moiety of TnC-based GECIs to one EF-hand domain.

(A) Dose response fits to the calcium titration curves obtained from different single EF-hand domain indicators. Depicted are two variants that use the mutated C-terminal part from csTnC (including mutations N108D D110N I130T). Again the C-terminal domain from serine94 to glutamine162 was used and sandwiched between CFP and Citrine cp174 (1xC-term N108D D110N I130T). In case of 1xC-term 3xP_N108D D110N I130T, three proline residues precede the C-terminal domain. Kd values are 450 nM (1xCterm N108D D110N I130T) and 350 nM (1xC-term 3xP_N108D D110N I130T). (B) Signals obtained from the different variants depicted in A according to the calcium regime from zero to 1.35 μM . 1xC-term 3xP_N108D D110N I130T displays roughly the same signal strength up to 600 nM free calcium as TN-XXL. Except for TN-XXL (average of four different titrations of four purified proteins) data represents one titration.

For that reason I tried to tune the FRET by introducing additional prolines that are known to promote kinks of a protein backbone in order to change the orientation of the two chromophores and therefore change the FRET-efficiency according to the dependency on the orientation factor (see 'Introduction - FRET'). Figure 31 displays calcium titrations performed on two calcium sensors with reduced calcium binding sites.

Although both indicators showed a reduction in the Kd value for calcium compared to TN-XXL (450 nM and 350 nM vs. 800 nM), none of them significantly exceeded the actual signals obtained with TN-XXL (Figure 31B).

4.7.3. Introducing aspartic acid to glutamic acid (D_{to}E) conversion to the -X position of chelating loops III and IV in the TnC backbone of TN-XXL

The transition of soluble calcium that is ligated by seven water molecules to a coordinated ion inside the loop region of a given EF-hand is achieved by replacing the water shell by the chelating residues. For that reason one determinant of calcium affinity is the increase of solvent entropy, i.e. the amount of exchanged water molecules by the residues. An increase of the solvent energy should therefore provide an increase in calcium affinity of a calcium binding domain (47).

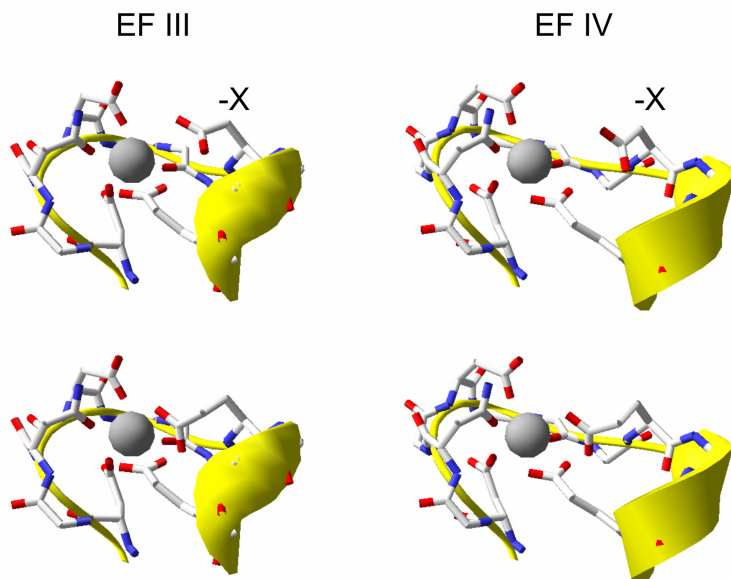


Figure 32: Schematic drawing of the aspartic acid to glutamic acid substitution in -X position of chelating loops in EF-hand III and IV of csTnC.

Upper row shows the chelating loops and involved amino acid residues of the two C-terminal EF-hands III and IV of csTnC. Position -X is highlighted. This position coordinates the calcium ion in wt₊csTnC via a water bridge since it is too far away for direct interaction with the ion. Bottom row shows a theoretical picture with substituted residues in the -X position. This substitution refers to as an aspartic acid to glutamic acid exchange. Structures were redrawn according to the pdb entry 1TOP using DeepView/SwissPdbViewer 3.7.

The calcium ion of EF III and EF IV of csTnC coordinates the ion by seven ligands, although one chelating position (-X) binds the ion via a water bridge

Results

(68). According to the solvent entropy hypothesis a direct binding of the ion by the chelating residue in position -X should increase the affinity of this EF-hand due to the additional release of a water molecule from the coordination sphere of calcium to the solvent. For that reason I introduced an aspartic acid to glutamic acid substitution in both -X positions of EF-hand III and IV of the mutated csTnC backbone of TN-L15 N108D D110N I130T Citrine cp174. The aim was to elongate the acidic side chain into the loop region, so that direct coordination of the calcium ion can occur.

Figure 32 illustrates a theoretical diagram of the aspartic acid to glutamic acid substitution according to the C-terminal calcium binding loops of wild type csTnC. As it can be seen in the bottom row, the longer side chain should diminish the distance to the calcium ion. In order to further increase calcium affinity of TN-XXL, I introduced the DtoE conversion in both EF-hands independently and in parallel. This led to the mutated C-terminal parts that were used to build all possible permutations.

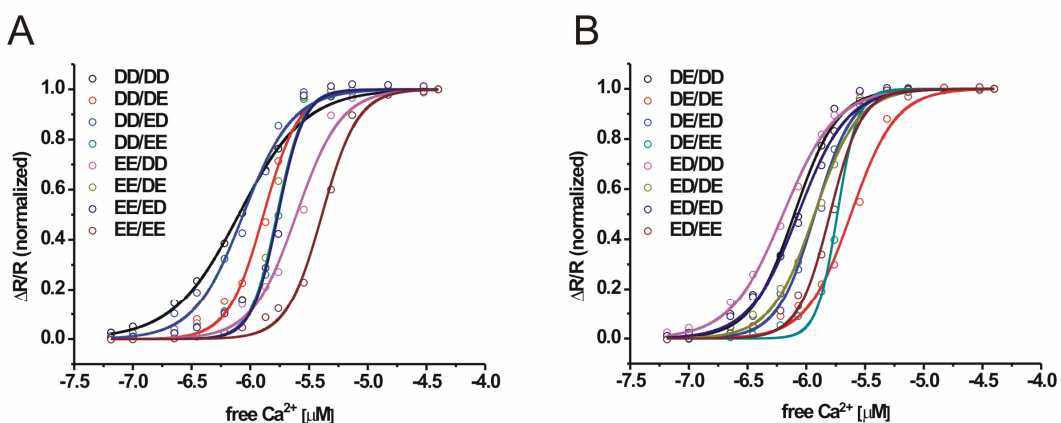


Figure 33: Titration curves obtained from the different aspartic acid to glutamic acid substitutions in EF III and IV of TN-XXL.

(A) Dose response fits to the normalized $\Delta R/R$ values elicited by variants with unmutated (DD) and double mutated (EE) C-terminal part of csTnC as first block. (B) Dose response fits to the normalized $\Delta R/R$ values elicited by variants with single mutated (ED and DE) C-terminal part of csTnC as first block. Except for TN-XXL (DD/DD, average of four titrations from four independently purified proteins) all data represents one titration.

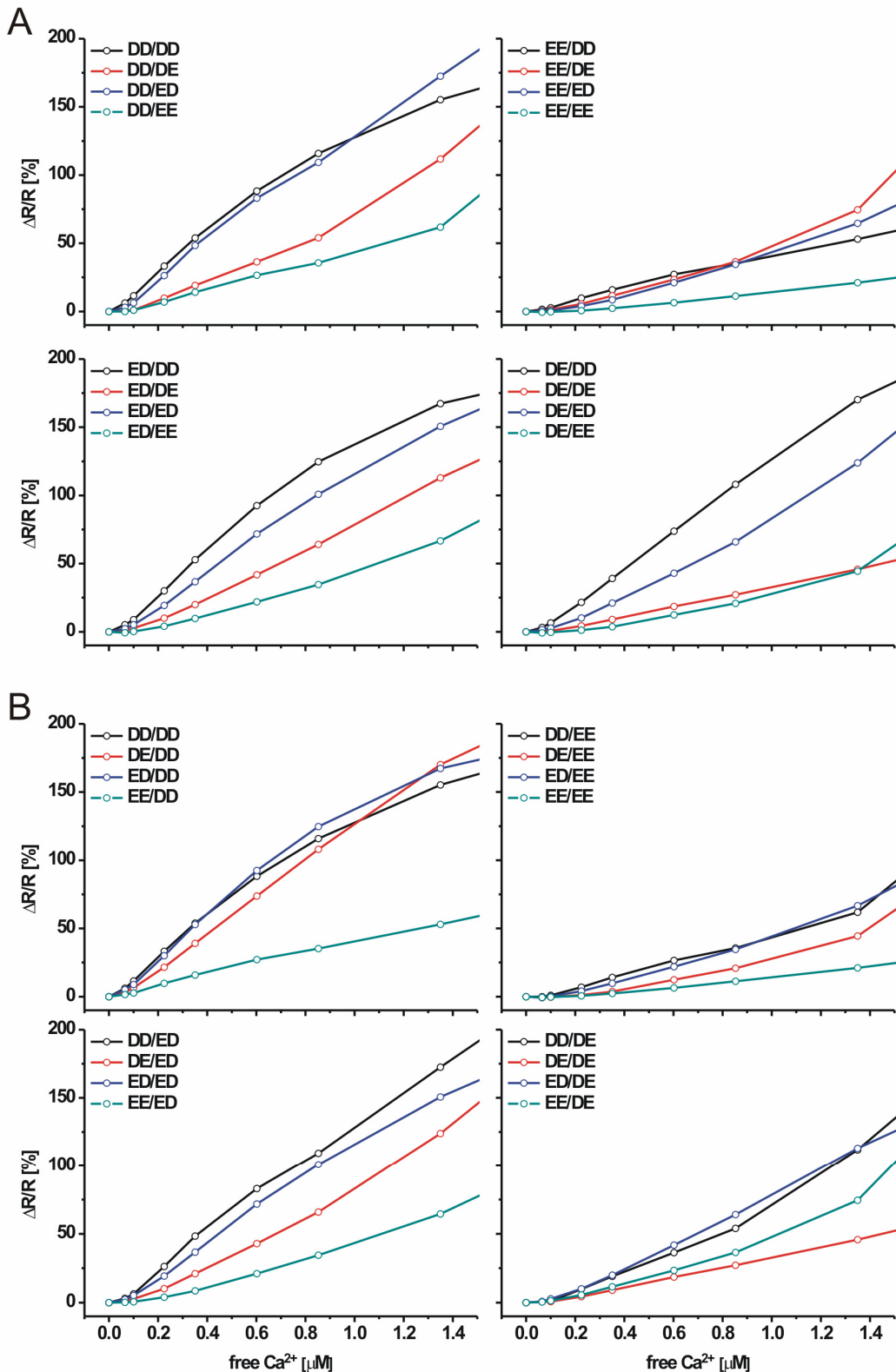
 Results


Figure 34: Comparison of the actual $\Delta R/R$ values in [%] of the aspartic acid to glutamic acid substitutions elicited by all permutations.

(A) Values obtained from the 16 variants sorted according to the first block. (B) Values obtained from the 16 variants sorted according to the second block.

Results

These mutated C-terminal parts referred to as:

csTnC N108D D110N D114E I130T (substitution in EF III, **ED**)

csTnC N108D D110N I130T D150E (substitution in EF IV, **DE**)

csTnC N108D D110N D114E I130T D150E (substitution in EF III and IV, **EE**)

As seen from Figure 33 none of the substitutions yielded a significant enhancement in calcium affinity. Only the DE/DD ($K_d = 790 \text{ nM}$) and ED/DD ($K_d = 630 \text{ nM}$) showed roughly the same or a slightly lowered K_d value in comparison to TN-XXL ($K_d = 800 \text{ nM}$). To have a more detailed insight in signal strength Figure 34 shows the actual signals in [%] of the variants according to the calcium regime of zero to $1.35 \mu\text{M}$ free Ca^{2+} . Figure 34A shows the response of the variants sorted according to the first block meaning the first C-terminal part of csTnC that has been used to create the doubling. Figure 34B shows the same 16 variants sorted according to the second part of the doubling.

A closer look at the data depicted in Figure 34 reveals a dramatic decrease in signal strength of a given indicator that is in line with the amount of aspartic acid to glutamic acid substitutions. Interestingly it can be observed that introducing the DtoE substitution in the already mutated EF-hand III of csTnC did not yield such a dramatic loss in signal strength than introducing the glutamic acid in the wild type EF-hand IV. For example DD/ED elicited much higher signals than DD/DE as it can be seen in Figure 34A.

Of all tested variants only DD/ED, DE/DD, ED/DD and ED/ED displayed similar signals in the calcium range of zero to $1.35 \mu\text{M}$ free calcium (Figure 35) than TN-XXL (DD/DD). Signals obtained from the variant EE/EE, in which all -X positions are substituted with glutamic acid, displayed the smallest values of all 16 permutations. Except for DE/DD, all of the well working variants comprise the DtoE conversion in the mutated EF-hand III of csTnC either in the first, the second or both blocks.

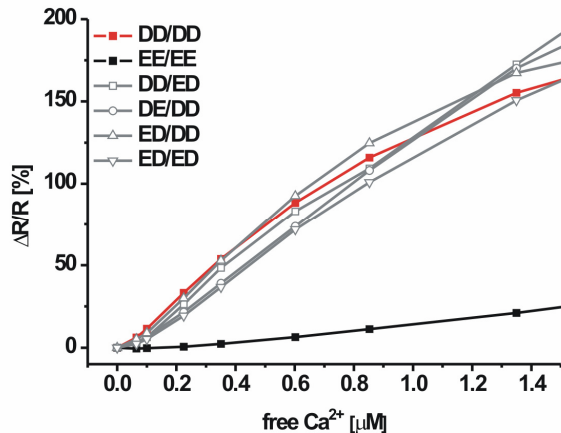


Figure 35: Selected variants of the aspartic acid to glutamic acid substitution compared to TN-XXL.

4.8. Comparison of TnC-based with CaM-based GECIs and one synthetic calcium indicator (OGB-1)

Different genetically-encoded calcium indicators have been developed in the past few years that can be used to measure calcium fluctuations inside living cells. In order to integrate our TnC-based calcium indicators I performed calcium titrations of different GECIs and one synthetic calcium indicator, namely Oregon Green BAPTA (OGB-1). The goal was to compare signal strength at the same defined calcium concentrations. For that purpose I investigated the genetically-encoded calcium indicators Yellow Cameleon 3.60 (YC3.60) (57), GCaMP 1.6 (69) and D3cpv (39) and set the resulting signals in relation to our TnC-based GECIs. Figure 36 shows the results of the titrations and the resulting signals according to the calcium regime of zero to 1.35 μM . Data for OGB-1 and GCaMP 1.6 reflects $\Delta F/F$ values since these indicators belong to the family of single wavelength sensors. All the other indicators (TN-L15, TN-XL, TN-XXL, YC3.60, D3cpv) belong to the family of ratiometric indicators and their signals therefore reflect a $\Delta R/R$. The most striking observation that is seen in Figure 36A is the dramatic difference in the actual signal that is achieved with the synthetic dye (OGB-1) compared to all

Results

GECIs. Figure 36B shows a zoom of the y-axis so that the actual signals of each GECI can be more easily seen. None of the genetically-encoded sensors displays a comparable sharp rise in the signal as it can be seen with OGB-1.

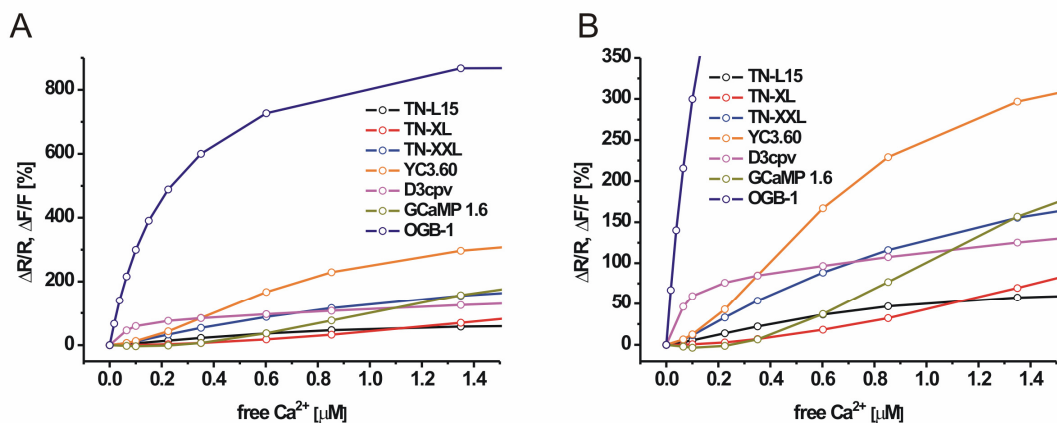


Figure 36: Comparison of TnC-based with CaM-based GECIs and OGB-1.

(A) Signals obtained from the different calcium indicators according to calcium concentrations from zero to 1.35 μM . Signals for GCaMP 1.6 and OGB-1 are depicted as $\Delta F/F$ values according to their single wavelength nature. All signals from the other indicators are indicated as $\Delta R/R$ since they exploit the FRET-mechanism and therefore reflect ratiometric sensors. (B) A zoom in of the data in A along the y-axis. Note the huge signal strength that is produced with OGB-1. Except for OGB-1 (average of three titrations) the data represent an average of four experiments on four independently purified proteins.

Construct	$\Delta R/R, \Delta F/F [\%]$ at 65 nM free Ca^{2+}
TN-L15	3.1 ± 0.3
TN-XL	-0.1 ± 0.7
TN-XXL	6.1 ± 1.4
YC3.60	6.5 ± 0.5
D3cpv	46.3 ± 0.4
GCaMP 1.6	-2.3 ± 0.5
OGB-1	215.6 ± 5.6

Figure 37: Comparison of $\Delta F/F$ and $\Delta R/R$ values from different calcium indicators at 65 nM free Ca^{2+} .

Signals obtained from the depicted calcium sensors according to a $\Delta[\text{Ca}^{2+}]$ of 65 nM. Signals were calculated as the fluorescence/ratio change in [%] ($\pm \text{SDM}$) of peak values from zero to 65 nM calcium. For peak values 524 nm (OGB-1), 510 nm (GCaMP 1.6) and 527 nm/475 nm for all FRET-based sensors were used.

Already at a ΔCa^{2+} of 17 nM this indicator displays a significant $\Delta F/F$ of ~70 %. Apart from D3cpv none of the GECIs elicit a significant signal for $\Delta\text{Ca}^{2+} = 17$ nM. This is the reason why the smallest free calcium change for titration was set to $\Delta\text{Ca}^{2+} = 65$ nM. Signals of all investigated calcium indicators that were obtained for this value are depicted in Figure 37.

4.9. Transgenic animals

Generation of two different transgenic animal models were attempted during this research. Transgenic flies were successfully created using the Gal4/UAS-system (UAS-TN-XXL) that expressed TN-XXL in a pan neuronal manner using the elac^{C155}-driver line. In addition I attempted to generate a transgenic mouse line that expresses TN-XXL in glial cells using the human GFAP-promoter, however this was unsuccessful.

4.9.1. Transgenic expression of TN-XXL in *Drosophila melanogaster*

The improvement of troponin C-based calcium indicators that were achieved with TN-XXL have been so far just been demonstrated by titration of the indicator in the cuvette. To have a more profound idea on how good this achievement can be translated *in vivo* I decided to generate transgenic animals. For that purpose the fruit fly *Drosophila melanogaster* was chosen since a reliable *in vivo* test system exists in that species that had been previously used to compare different GECIs in a defined *in vivo* environment (60). For that purpose the larval neuromuscular junction provides a reliable test system that allows comparison of the different GECIs with a defined stimulation paradigm (and therefore with defined cytosolic $\Delta[\text{Ca}^{2+}]_i$). I made use of the Gal4/UAS-system that allows expression of a transgene of interest under the control of a genomic enhancer (70). Creation of a UAS-TN-XXL

Results

reporter line was achieved by injection of the construct into fertilized eggs of *Drosophila melanogaster*.

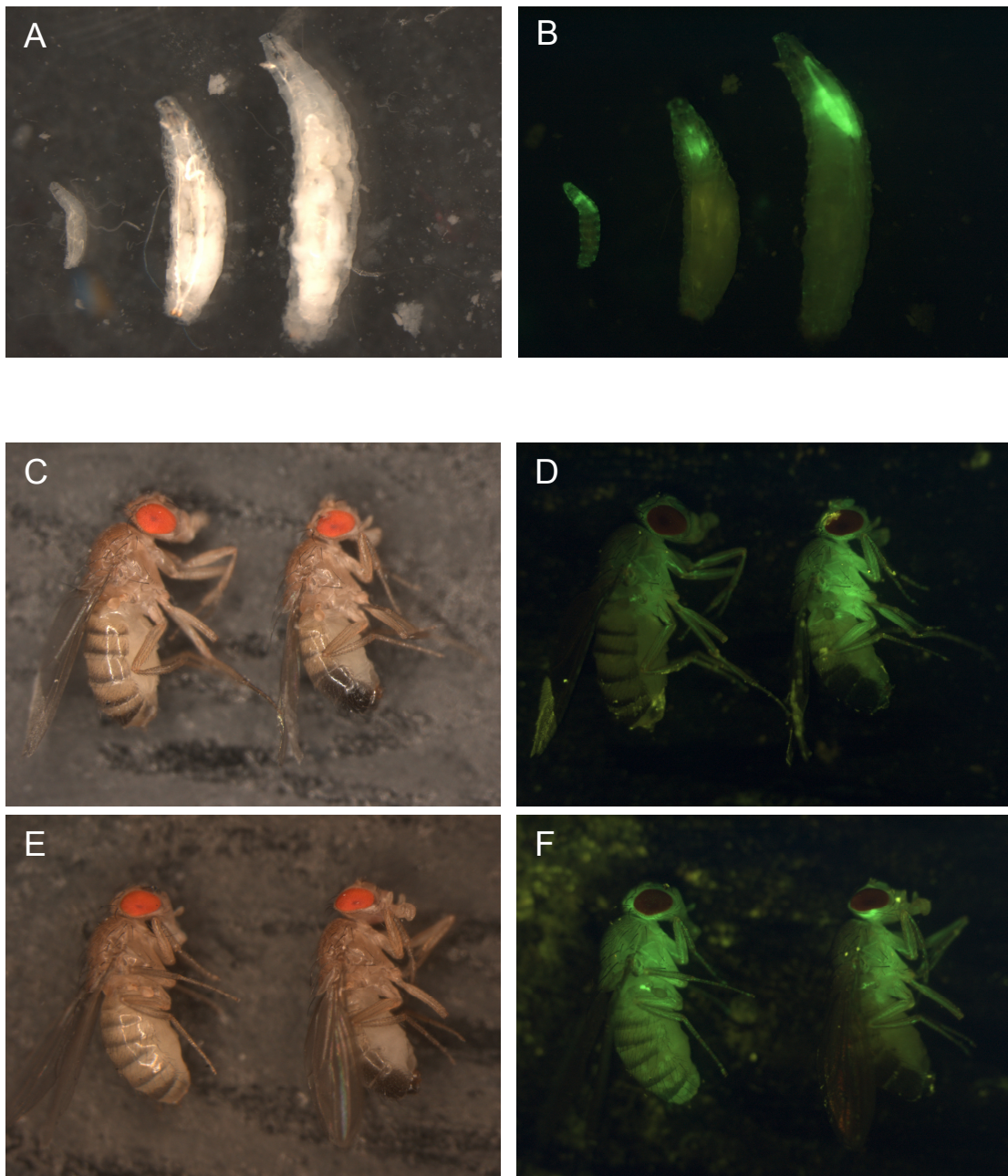


Figure 38: Transgenic expression of TN-XXL in *Drosophila melanogaster* using the Gal4/UAS-system.

Flies are of the genotype $\text{elav}^{\text{C}155}\text{-Gal4}/\text{elav}^{\text{C}155}\text{-Gal4}$; UAS-TN-XXL/UAS-TN-XXL indicating their homozygous nature. (A) Light microscopy picture of first, second and third instar larval stage. (B) Fluorescent picture (YFP-channel) of the larvae depicted in A. (C) and (E) Light microscopy picture of adult flies of both sexes. In each picture female flies are on the left, male flies on the right side. (D) and (F) Fluorescent images of the flies depicted in C and E.

Crossing of these transgenic flies with the driver line $\text{elav}^{\text{C}155}$ -Gal4 allows the expression of the GECI TN-XXL in a pan neuronal manner (71). Figure 38 shows light and fluorescence images of the double mutant $\text{elav}^{\text{C}155}$ -Gal4/ $\text{elav}^{\text{C}155}$ -Gal4; UAS-TN-XXL/UAS-TN-XXL that showed expression of TN-XXL in the nervous system of the larval and adult flies.

These flies were used to compare all three troponin C-based calcium indicators TN-L15, TN-XL and TN-XXL *in vivo*. Hereby the reader is referred to section ‘Discussion - *In vivo* comparison of troponin C-based GECIs at the *Drosophila* NMJ’.

4.9.2. Creating transgenic mice with TN-XL and TN-XXL using the human GFAP-Promoter

Astrocytes can be regarded as ‘bridging units’ that connect different types of cells and structures in their vicinity e.g. neurons and blood vessels (72). They are able to promote signaling from neurons to blood vessels to regulate blood flow and therefore the energy support of neurons (73) or to modulate neuronal transmission via the so-called ‘gliotransmitters’ (e.g. glutamate and ATP) (72). Although electrically excitable, astrocytes are not able to produce action potentials and therefore their signaling mechanism exclusively relies on fluctuations in the cytosolic calcium level (72).

To investigate calcium signaling in glial cells, I made use of the human GFAP-promoter successfully used to drive expression of transgenes in this cell type (74, 75). Starting DNA for generating transgenic mice was the (human) hGFAP_CFP plasmid kindly provided by Frank Kirchhoff. The CFP was excised with restriction enzymes AgeI/EcoRI and replaced by TN-XL and TN-XXL respectively. Figure 39 shows a schematic of the constructs used to create transgenic animals.

As a first test primary hippocampal cell cultures were transfected with the plasmid encoding TN-XL under the GFAP promoter. Glial cells were labeled and stimulated with ATP leading to an activation of purinergic receptors (76).

Results

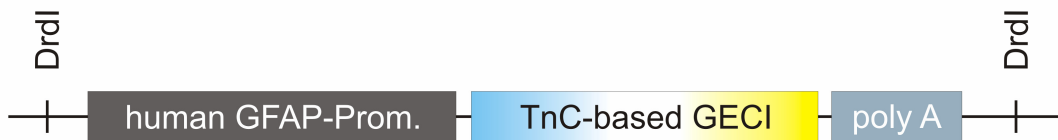


Figure 39: Schematic of the constructs used to create transgenic mice.

The subsequent calcium rise in the glial cells was detected with TN-XL, showing a functional expression of the GECI using the GFAP promoter. Figure 40 depicts an example of a glial cell in which TN-XL reports calcium signaling.

After successfully testing the promoter in cell culture, the plasmids containing hGFAP_TN-XL/TN-XXL were linearized with DrdI. The 4.7 kb fragment containing the promoter, the GECI and a poly-adenylation signal was purified and microinjected into pronuclei of fertilized oocytes. From all injections 9 PCR-positive founders with hGFAP_TN-XL and 30 PCR-positive founders with hGFAP_TN-XXL were obtained. After breeding of these 39 founders, 36 offspring producing lines could be established.

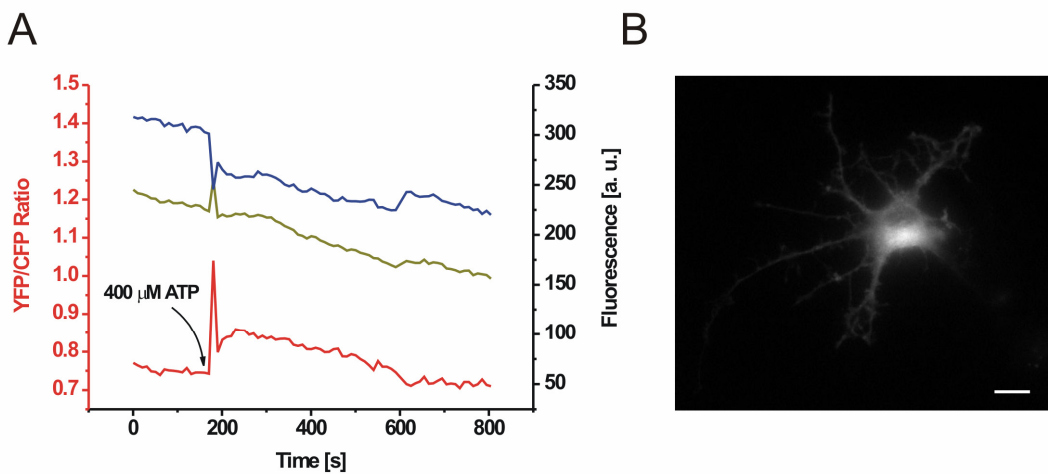


Figure 40: Glial calcium signals detected with TN-XL using the hGFAP promoter.

(A) Responses of a glial cell transfected with hGFAP_TN-XL after stimulation with 400 μ M ATP. Red trace depicts the Citrine cp174/CFP ratio obtained during the recording session. Blue line (CFP) and yellow line (Citrine cp174) correspond to the behavior of the individual chromophores from which an increase in FRET could be extracted after the stimulation with ATP. (B) Citrine cp174 image of a glial cell transfected with hGFAP_TN-XL. Scale bar, 10 μ m.

All lines were checked for glial expression of the indicators by extracting the brains of PCR-positive offspring (from two animals) or by extracting the brains of at least two litters of PCR-positive founders (on average 18 individuals per founder). All prepared brains were screened for expression using a fluorescence microscope but none of these lines showed expression of one of the GECIs in the nervous system.

Discussion

5.1. Enhancing signal strength in TN-L15

The central aim of my research was to increase the signal strength of the first generation of genetically-encoded calcium indicator based on troponin C, namely TN-L15. As mentioned before this indicator is suitable to detect calcium transients elicited in cell culture (41) and in transgenic animals (60, 61, 77). The major drawback of TN-L15 however was the lack of this indicator to detect small calcium transients especially those elicited by single action potentials when expressed in neurons (61).

In order to overcome this lack of sensitivity I applied various strategies to enhance the signal strength of TN-L15. As a first approach I exchanged the acceptor protein in TN-L15. The YFP derivative Citrine was used to create different circularly permuted variants (58). Among the different variants two distinct versions showed similar spectral characteristics as the wild type Citrine molecule. These variants referred to as Citrine cp174 and Citrine cp158. When replacing the original Citrine with Citrine cp174 in TN-L15 I yielded an enhanced signal of the calcium indicator. On the other hand no significant enhancement in FRET-efficiency was achieved with the Citrine cp158 variant. A circularly permuted variant presumably shows the same structure as the wild type protein. The only difference is that the wild type termini are linked together (which reflects a closure in the protein backbone) and new termini are created at a different site in the protein. When a cp variant is fused to a protein the most dramatic effect should be a new orientation of the cp variant according to the tagged protein. In case of having a FRET sensor this rearrangement should lead to a reorientation of the transition dipoles of the two fluorescent proteins and so to a change in FRET-efficiency according to its dependency on the orientation that is reflected by the orientation factor κ^2 . Unfortunately no crystal structure of a FRET-based

genetically-encoded calcium indicator is available so far. In that respect it can only be speculated that the dramatic increase in FRET-efficiency that can be observed with the Citrine cp174 variant is based on a change of the orientation. It can not be excluded that introduction of a cp variant to our sensors also changes distance of the two chromophores which affects the FRET-efficiency in a more dramatic way since latter one depends on the inverse of the sixth power of the distance. FRET-efficiency has also been improved by use of circular permuted variants in so-called Yellow Cameleons a family of genetically-encoded calcium indicators that are based on calmodulin (57). Interestingly the authors also used a similar position for the circular permutation of the acceptor protein Venus (an YFP derivative). In that approach position 173 was used that corresponds to the preceding amino acid of the 174 position in the Citrine variant. This shows that usage of cp variants of fluorescent proteins represents a robust and general possibility to improve efficiency in FRET-based biosensors.

However, a problem that arose in this approach to improve the indicator was a non-restricted increase in FRET-efficiency to calcium. Unfortunately, wild type troponin C also binds magnesium that is present in the low millimolar range inside a cell (78). Magnesium binding in troponin C is promoted by the high affinity C-terminal lobe that is capable of binding both ions (calcium and magnesium) (51). As shown in Figure 8 both indicators (TN-L15 and TN-L15 Citrine cp174) elicited a significant signal with 1 mM magnesium that is pronounced in TN-L15 Citrine cp174 showing that magnesium is not only bound by troponin C but also elicits a structural change of the binding moiety. Given the fact that a GECI faces a similar free magnesium concentration inside a cell, this would diminish the overall signal that can be obtained by this calcium indicator since the baseline is shifted to an increased FRET which reduces the residual FRET response that can be elicited by calcium. This magnesium sensitivity of troponin C-based calcium indicators displayed the major contribution to the overall reduction in signal strength of troponin C-based calcium biosensors. The acid pair hypothesis proposes that maximum calcium affinity by an EF-hand is elicited with four acidic residues in positions 1(+X), 5(+Z), 9(-X) and 12(-Z) (79). On the other hand it was demonstrated in

Discussion

synthetic peptides that magnesium binding occurs if the Z-axis is occupied with two acidic residues (80). In order to prevent the magnesium binding to our sensors I tried to combine the results of the two studies mentioned before by disruption of the Z-acid pair, and at the same time maintain the four acidic residues in the calcium binding loop of the C-terminal EF-hands III and IV present within the csTnC. For disruption of the Z-acid pair only position 5(+Z) was considered to be exchanged since the glutamic acid in position 12(-Z) is essential for calcium coordination (47). As it can be seen in TN-XL magnesium-induced FRET (elicited by 1 mM Mg²⁺) is almost absent. The price that had been paid for the reduced magnesium affinity was also a reduced calcium affinity (0.7 µM for TN-L15 and 2.2 µM for TN-XL). The disadvantage becomes clear when actual values of signal strength are compared to a calcium regime that can be found in an activated cell (up to 1 µM). Here one finds an almost complete loss in signal strength of TN-XL especially for calcium values up to 350 nM (Figure 22B). Only above this calcium value TN-XL produces significant FRET signals. From this data one can derive that TN-XL is not a suitable calcium indicator to detect small cytosolic calcium changes that are elicited by e.g. a single action potential in neurons. Nevertheless one advantage can be found in TN-XL namely the high Kd value of TN-XL causes fast off-kinetics. This in turn can be useful when investigating calcium transients with higher temporal resolution at sites where calcium reaches elevated concentrations. For example, TN-XL would be a suitable indicator for studying calcium dynamics at entry sites by attaching to a calcium channel.

All the work done so far did not yield the desired improvement of troponin C-based calcium indicators according to their signal strength. Therefore I tried to increase calcium affinity of TN-XL in order to gain enhanced signals especially in the low nanomolar calcium regime. A lot of mutagenesis studies have been performed on troponin C which reported increased calcium affinity when replacing hydrophobic with more polar groups. The idea is to increase the solvent accessibility of the csTnC's N-terminal part and thereby promote the structural transition of the apo to the calcium bound state by reducing the

energy that is needed for this transition (65, 66). Unfortunately none of the introduced substitutions significantly enhanced the FRET signals of TN-XL. Especially the mutations F22Q ($K_d = 0.99 \mu\text{M}$), V45Q ($K_d = 0.17 \mu\text{M}$), M46Q ($K_d = 0.88 \mu\text{M}$), L49Q ($K_d = 0.17 \mu\text{M}$), M82Q ($K_d = 0.69 \mu\text{M}$) and M86Q ($K_d = 2.6 \mu\text{M}$) decreased the K_d value of TnC ($K_d = 3.2 \mu\text{M}$) as shown by Tikunova and colleagues (65). At this point one should comment on the different determination of K_d values that were used in this study compared to the approach used by the other research group. In our case the K_d value reflects an apparent K_d value since we use the FRET signal to determine the calcium dissociation constant. In other words the K_d values presented in this thesis reflect the values at which the FRET signal reaches half maximum according to the calcium concentration. Since the FRET-mechanism is a highly non-linear system (especially due to the dependency on distance) the K_d values not necessarily reflect a direct calcium binding to troponin C. One can easily imagine that calcium is bound to our indicator and promote a structural change of the troponin C backbone that is not converted into a FRET signal because the chromophores are too far away to produce a significant energy transfer. Only around the Förster radius one can find an almost linear relation between distance and FRET-efficiency (Figure 41).

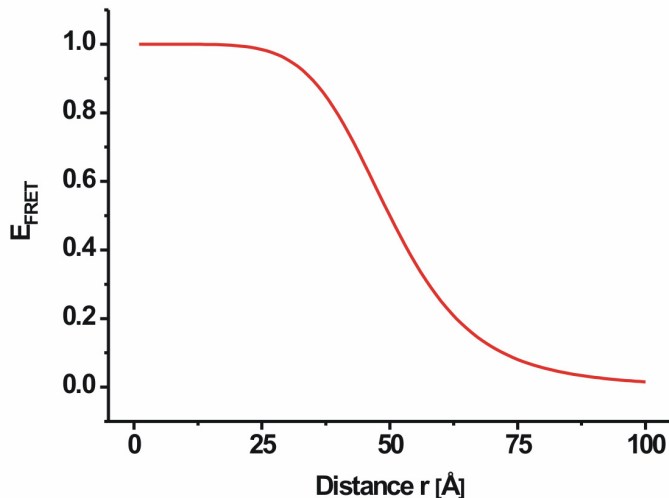


Figure 41: Dependency of FRET-efficiency on the distance of two chromophores with a Förster radius (R_0) of 50 Å.

Points were calculated using the formula $E_{\text{FRET}} = R_0^6 / (R_0^6 + r^6)$.

Discussion

On the other hand studies on calcium binding are almost exclusively done by point mutating a distinct amino acid residue that allows for a more direct fluorescent readout of calcium binding. When studying the calcium binding of the N-terminal part of troponin C the so called TnC^{F29W} mutant is used that produces an intrinsic fluorescent signal due to the incorporation of the aromatic tryptophan residue that is more directly changed upon calcium binding (65). Therefore it is not necessarily surprising that the same mutations applied to the troponin C backbone of our sensor did not produce the same decrease in the apparent calcium dissociation constant. Nevertheless our goal is not the study of direct calcium binding to troponin C. The interest of this research is to generate a genetically-encoded calcium indicator that is suitable to pick up small calcium changes that are converted to a fluorescent readout - a change in FRET-efficiency between CFP and Citrine. For that reason my intention was to compare FRET signals with given free calcium values.

As mentioned in the previous paragraph enhancing signal strength in TN-XL by means of single mutations did not lead to success. Thus, a more profound way of changing the calcium binding moiety by doubling of the csTnC's C-terminal part aimed to increase signal strength. This domain was chosen as it is known that the C-terminal lobe of troponin C exhibits a higher calcium affinity than the N-terminal counterpart. The doubling was performed since most of the calcium binding proteins come along as a multitude of an EF-hand domain that exists of two EF-hands. The idea was to preserve the high affinity of the C-terminal lobe and in parallel - by doubling this domain - yield enough structural rearrangement that can be converted to a high FRET readout. Different doublings of the csTnC's C-terminal part in TN-XL I130T led to adequate start- and ending points at which the doubling of the C-terminal lobe worked best. These were (according to csTnC) serine94 (as start) and glutamine162 (as stop). Most important this doubling variant preserved the overall $\Delta R/R_{max}$ values obtained with TN-XL. At this point the reader should be pointed to the effect of a particular single amino acid substitution performed on the TN-XL backbone. This mutation corresponds to csTnC I130T. Introduction of this mutation to the N-cap residue of the G-helix of chicken

skeletal troponin C is thought to stabilize the C-terminal domain and therefore enhance their calcium affinity (67). Figure 42 shows the result of the I130T mutation in different variants.

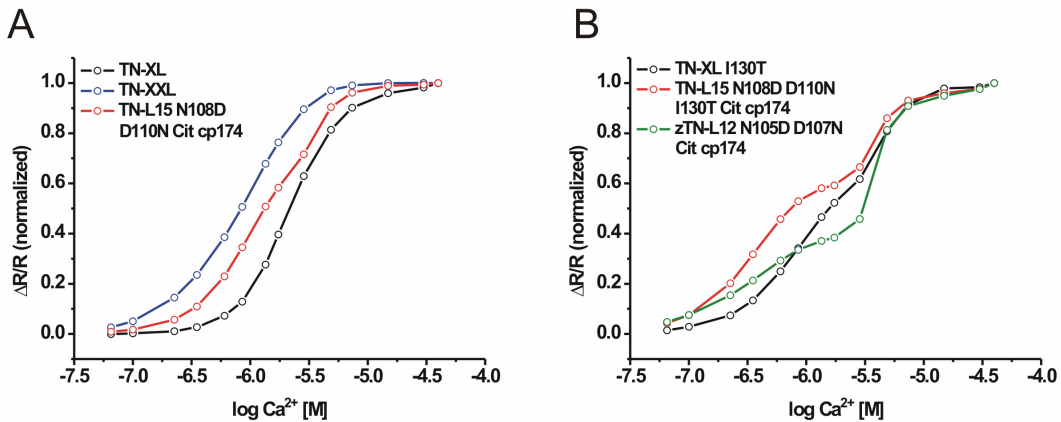


Figure 42: Effect of the I130T mutation in csTnC -based calcium indicators.

(A) Titration curves obtained from TN-XL, TN-XXL and TN-L15 N108D D110N Citrine cp174. Note that TN-XXL is built by a doubling of the same C-terminal domain (csTnC N108D D110N I130T). (B) Curves obtained from TN-XL I130T, TN-L15 N108D D110N I130T and zTN-L12 N105D D107N (that uses a shortened TnC variant from zebrafish as calcium binding moiety. Except for TN-XL and TN-XXL (average of four independent measurements performed on four independently purified proteins) the data represent a single titration.

As mentioned before, csTnC is composed of two EF-hand domains with different calcium affinities. A comparison of the calcium titration curves of TN-XL (Figure 42A) and TN-XL I130T (Figure 42B) shows an almost perfect sigmoidal curve for TN-XL and a slightly pronounced double sigmoidal for TN-XL I130T. The double sigmoidal curve might reflect different calcium affinities of the two EF-hand domains in TN-XL I130T. On the other hand disruption of the Z-acid pairs in the loops of EF III and EF IV without the additional I130T mutation - as it is been displayed by TN-XL - gives rise to a perfect sigmoidal. In other words introduction of the mutations to diminish magnesium binding led to equalization of the calcium affinity of the N- and C-terminal EF-hand domains. This observation is further promoted when the single EF-hand mutant TN-L15 N108D D110N Citrine cp174 and its I130T variant are compared. These indicators have only one disrupted Z-acid pair namely in EF-hand III. TN-L15 N108D D110N Citrine cp174 shows a slightly double

Discussion

sigmoidal titration curve meaning the restoring of two EF-hand domains with different calcium affinities (Figure 42A). This difference is dramatically increased by adding the I130T substitution (Figure 42B). The calcium titration curve for TN-L15 N108D D110N I130T Citrine cp174 clearly shows double sigmoidal characteristics with high responsiveness in the low calcium regime. Interestingly, the difference in calcium affinity of the two lobes can also be observed in troponin C derived from zebrafish which shows that this is a common feature of troponin C. As depicted in Figure 42B, one finds a clear double sigmoidal characteristic for zTN-L12 N105D D107N which already posses one of the two N-cap residues that stabilizes the C-terminal EF-hand domain (serine127, Figure 28).

Due to the high signals obtained with TN-L15 N108D D110N I130T Citrine cp174 that still possesses the low affinity N-terminal lobe, doubling of its C-terminal part was considered to be fruitful. Taking the part of the mutated csTnC (N108D D110N I130T) from amino acid S94 to Q162 and double it between CFP and the Citrine cp174 variant led to the calcium sensor TN-XXL that exceeded all other indicators' signals according to concentrations between zero and 1.35 μ M free Ca^{2+} . A closer look at the titration curve obtained with TN-XXL reveals a perfect sigmoidal characteristic. This reflects the uniformity that has been achieved by doubling the same (affine) C-terminal EF-hand domain (Figure 42A).

TN-XXL represents the best performing troponin C-based genetically-encoded calcium indicator so far. According to TN-L15 it displays on average a 2.4 fold enhancement in signal strength according to calcium concentrations from zero to 1.35 μ M which was also confirmed by a detailed *in vivo* comparison at the *Drosophila* NMJ (see 5.3.). Nonetheless TN-XXL surely does not display the ultimate GECI not even with respect to signal strength. For that reason two different strategies were applied in order to improve TN-XXL. On the one hand the doubling strategy was expanded to variants of troponin C from different species. On the other hand I tried to enhance calcium affinity by exchanging a particular aspartic acid residue in each of the two EF-hands with glutamic acid (-X position).

Applying the doubling strategy to troponin C from different species did not yield an indicator with superior signal strength. Nevertheless this approach shows that it is indeed possible to shuffle different C-terminal domains that always yielded functional indicators. The C-terminal part can therefore be regarded as an autonomous building block. It would be interesting to go further down and try to shuffle even smaller parts especially from different calcium binding proteins like troponin C, calmodulin or calmodulin related proteins.

A more direct approach to increase signal strength was trying to enhance calcium affinity of TN-XXL by direct mutagenesis of the residue that contributes to calcium coordination at position -X in the calcium binding loops III and IV. As mentioned in the results part the exchange of aspartic acid with the longer side chain of glutamic acid should promote a direct co-ordination of the calcium ion and therefore an additional release of the last water molecule in the coordination sphere of calcium to the solvent. This in turn would increase the solvent entropy and thereby display and energetically favored state meaning an enhanced affinity of the mutated EF-hand. Unfortunately none of the permutations showed any significant increase in signal strength. Quite the contrary was observed mostly a significant loss in signal strength. The data suggests that the signals decrease by increasing the amount of EF-hands with a glutamic acid residue in the -X position. An easy explanation for this observation would be an unfavorable accumulation of negative charges in close vicinity. This might lead to repulsion of the side chains and a conformation that does not prefer calcium chelation. Interestingly the decrease in signal strength was not as promoted when the -X position in the already mutated EF-hand III was occupied by a glutamic acid. This observation can only be stated descriptively. It might well be that the wild type EF-hand III is able to handle the DtoE conversion per se or that the change in position of negative charges in the mutated EF-hand III (N108D D110N) stabilizes the introduction of the longer side chain. Alternatively it might be that the desired effect of releasing the last water molecule to the solvent only takes place when glutamic acid is introduced in EF-hand III and not in EF-hand IV.

5.2. Reducing the calcium binding moiety in troponin C-based GECIs to a single EF-hand domain

A major concern by using genetically-encoded calcium indicators is a possible effect on the calcium dynamics of a cell that might arise from the additional expression of a calcium binding protein. In the case of our troponin C-based calcium indicators this could be 'in the worst case' a stoichiometry of four calcium ions per indicator molecule. This might be a more pronounced effect when the indicator is transiently expressed e.g. when using transfection or infection (via a virus) techniques. In contrast - by using a transgenic approach - one could imagine that the organism has the ability to overcome this imbalance in calcium homeostasis by adopting expression of endogenous buffers or the calcium turnover rate. This might be the fact since in a transgenic animal the organism has to encounter the additional buffer during the whole lifetime which sets a longer timeline to overcome a possible buffering effect.

Nevertheless an indicator with lowered calcium binding sites would be an interesting tool - also with respect to kinetic characteristics. Therefore I tried to lower the overall calcium binding sites in TnC-based GECIs by using only one C-terminal domain of the mutated csTnC (N108D D110N I130T). As mentioned in the results section replacement of existing four hand moieties with shortened calcium binding domains always led to an increased basal FRET i.e. in the absence of calcium which can be seen in Figure 43.

Comparison of the actual $\Delta R/R$ values obtained from TN-XXL and 1xC-term 3xP_N108D D110N I130T shows that both indicators display the same signals from 65 nM to 600 nM free Ca^{2+} (Figure 31B). Since one would expect small calcium changes - especially when trying to detect small signals like elicited by one or a few action potentials in neurons - usage of the shortened variant would be favorable due to the reduced amount of calcium binding sites. At this point I would like to stress the difference of the two variants depicted in Figure 43 that might show the superiority of TN-XXL. As seen in Figure 43B the shortened variant displays a much higher basal FRET. In that aspect the basic

fluorescence in the CFP channel is much more reduced according to TN-XXL, which could lead to serious problems when performing *in vivo* experiments. Our sensors are constructed in a way that upon calcium binding the FRET-efficiency is enhanced.

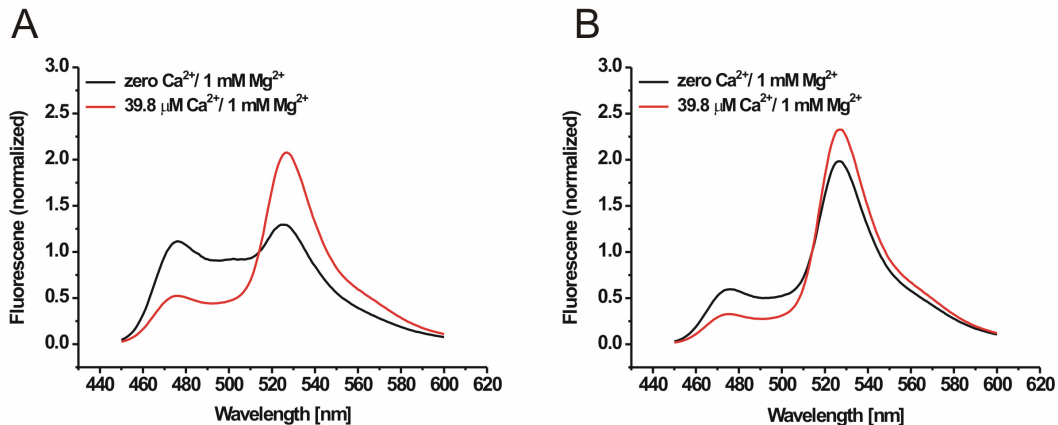


Figure 43: Comparison of the basal FRET in two TnC-based GECIs with different amount of calcium binding sites.

(A) Representative fluorescence spectrum obtained with TN-XXL that has four calcium binding sites (in presence of 1 mM Mg²⁺). (B) Representative fluorescence spectrum of a shortened variant of troponin C-based calcium indicators with just two EF-hands (1xC-term. 3xP_N108D D110N I130T). Note the dramatic increase of basal FRET in the shortened variant.

This is reflected by a reduction in the CFP and an increase in the YFP channel. Depending on the expression level one can imagine that signals obtained from the donor channel of the shortened variant can be low. This in turn would cause serious problems in detecting signals since the change in fluorescence of the CFP channel could be around background fluorescence. As a result signals calculated as ratio changes would be noisier.

5.3. *In vivo* comparison of troponin C-based GECIs at the *Drosophila* NMJ

Comparison of the genetically-encoded calcium indicators were so far achieved by measuring the recombinantly expressed purified protein in the

Discussion

cuvette. This allowed a precise comparison of the individual calcium indicators in a defined environment. Since the ultimate goal of developing GECIs is *in vivo* calcium imaging one would like to have a precise *in vivo* test system to compare and define the response properties of different calcium indicators. For that reason one can make use of the *Drosophila* neuromuscular junction as a test system where stimulus frequency and $\Delta[\text{Ca}^{2+}]_i$ show linear relation (60) and (T. Hendel, personal communication). Experiments were performed in the third instar larvae of transgenic animals that express the GECI at nerve terminals that innervate muscle 6/7 in the abdominal segment 2 or 3 using the elav^{C155} driver line. Stimulation of presynaptic boutons was achieved by delivering voltage pulses of 5.5 V to the innervating fiber through a suction electrode eliciting one action potential per pulse. Imaging of boutons was performed by 2P-microscopy (with 485/40 nm bandpass filter for CFP and 535/30 nm bandpass filter for Citrine/Citrine cp174) within a period of eight seconds at a rate of 8 Hz. Stimulation was applied for two seconds that allow reaching a steady state calcium value in the boutons. Response properties of the different GECIs were investigated at stimulation frequencies of 10, 20, 40, 80 and 160 Hz.

The transgenic reporter line UAS-TN-XXL was generated by Alexandra Ihring and myself at the MPI of Neurobiology. Generation of the reporter lines UAS-TN-L15 and UAS-TN-XL were performed by Alexandra Ihring and Maximilian Jösch-Krotki. Experiments at the *Drosophila* NMJ and data analysis were completed by Thomas Hendel at the MPI of Neurobiology. Calcium titrations of the TnC-based GECIs and OGB-1 were performed by myself.

Figure 44 shows the *in vivo* responses of TN-L15, TN-XL and TN-XXL expressed at the NMJ.

The results obtained at different stimulus intensities demonstrate a significant improvement of TN-XXL, just as has been seen before in the cuvette. For all stimulus intensities signals from TN-XXL clearly exceed all the other indicators' responses and especially at low stimulations (10 and 20 Hz) one

can find a major improvement in sensitivity when using TN-XXL a as calcium reporter.

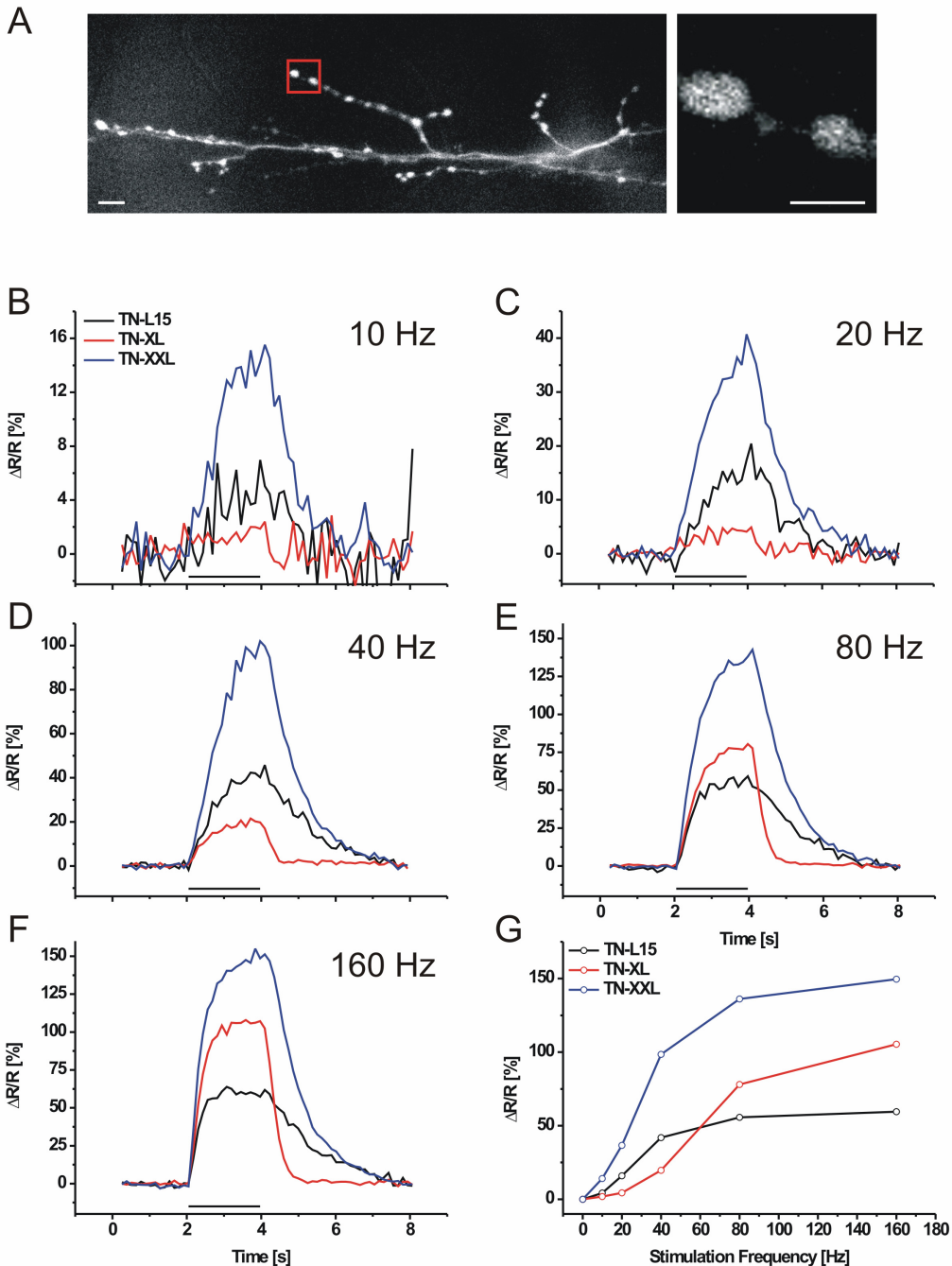


Figure 44: *In vivo* comparison of troponin C-based GECIs at the *Drosophila* NMJ.

(A) 2P-image of presynaptic boutons innervating muscle 6/7 of the *Drosophila* larval NMJ. Fluorescence acquired from the YFP channel. Right: Blow up of the red rectangular. Scale bars: 10 μm (left) and 5 μm (right). (B-F) Responses of the three GECIs at different stimulation frequencies ranging from 10 Hz to 160 Hz. Black bars between 2 s and 4 s indicate the stimulation. (G) $\Delta R/R_{\max}$ values in [%] obtained with these indicators plotted against the stimulation frequency.

Discussion

Two observations should be highlighted that correspond to the cuvette data shown. Firstly, as seen before in the stopped-flow experiments, TN-XL displays the shortest decay time constant of the troponin C-based GECIs and this also holds true for the indicator performance at the NMJ. Independent of stimulation frequency, TN-XL follows the calcium fluctuation with the most precise time resolution that can be obtained with troponin C-based sensors. Secondly, TN-XL is almost ‘blind’ to small changes in the cytosolic calcium concentration as can be seen for stimulus intensities of 10 or 20 Hz. This is also consistent with the data obtained from the calcium titrations. As mentioned before stimulation frequency and $\Delta[\text{Ca}^{2+}]_i$ at the *Drosophila* NMJ reveal a linear dependency. Therefore the data in Figure 44G can be compared to the $\Delta R/R$ values obtained from the calcium titrations that are plotted versus the linear calcium concentration.

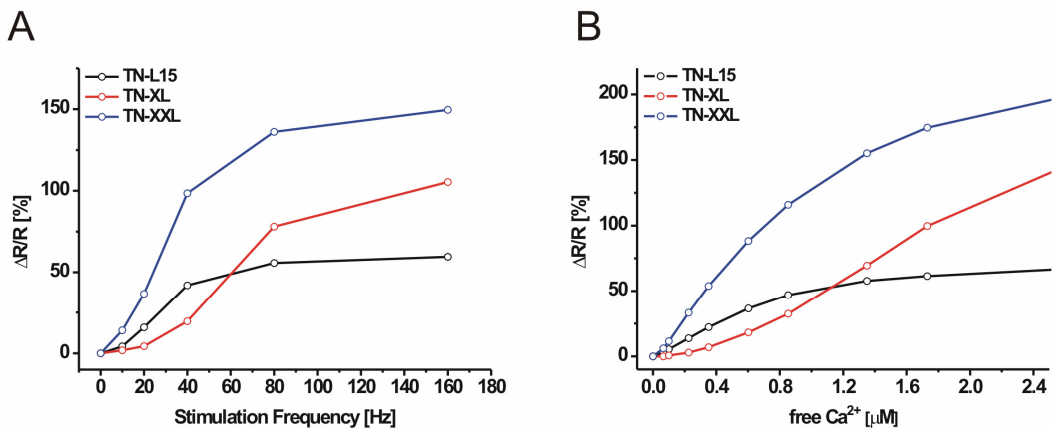


Figure 45: Comparison of actual $\Delta R/R$ values in [%] obtained from different csTnC-based GECIs in two different systems.

(A) Data obtained from the stimulation of motoneurons innervating the *Drosophila* NMJ. (B) Data obtained from calcium titrations of the purified indicators in the cuvette.

As seen in Figure 45 the overall appearance of the curves obtained from fly and the cuvette correspond remarkably well representing a conserved response no matter if the indicators are investigated *in vitro* or cuvette measurements. This is an important observation since it allows assessing possible improvements of an indicator in the cuvette without the need to perform detailed *in vivo* studies.

Nevertheless, as it can also be seen in Figure 45, there exist some discrepancies between the *in vivo* and titration data obtained from the cuvette. For example TN-XXL, the indicator seems to saturate at a $\Delta R/R$ value of ~200 % in the cuvette. In contrast, TN-XXL saturates *in vivo* at a value of ~150 %. To explain this inconsistency, it is important to realize that the cuvette data represents an actual $\Delta R/R$ in [%] calculated from the two peak values of the spectra (475 nm for donor and 527 nm for acceptor). In an *in vivo* experiment one uses bandpass filters that broaden the values obtained in both channels. Secondly a cell at rest displays a given intracellular calcium level. This has also to be considered since any resting calcium will set the calcium indicator to a different resting FRET ratio R_0 from which the corresponding $\Delta R/R$ values are calculated. This will also diminish the signal that can be obtained from an indicator *in vivo*. Figure 46 shows the consequences on the actual $\Delta R/R$ values from calcium titration of TN-XXL if these two parameters are taken into account.

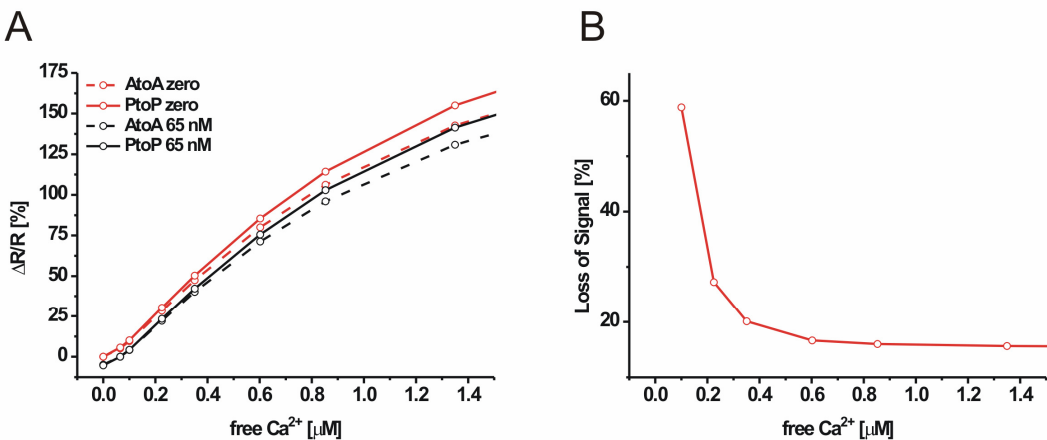


Figure 46: Effect of mimicking *in vivo* conditions to the spectra of the calcium titrations of purified TN-XXL obtained from cuvette data.

(A) Drop of signal strength in TN-XXL for different parameters. PtoP reflects peak to peak ratio changes in [%] according to 475 nm for CFP and 527 nm for Citrine cp174. AtoA reflects area to area ratio changes in [%] when integrating the spectra from 520 - 550 nm for Citrine cp174 and 465 - 505 nm for CFP. Depicted are the values calculated at two different resting calcium concentrations (zero and 65 nM). (B) Loss of signal in [%] when PtoP (zero calcium) values are compared to AtoA (65 nM) values. This corresponds to the signal loss when ideal cuvette conditions are compared to *in vivo* imaging conditions.

Discussion

One can observe a decrease in the overall signal strength if *in vivo* imaging conditions are mimicked (65 nM resting calcium, bandpass filters: 485/40 nm for CFP and 535/30 nm for YFP as integration limits of the spectra to yield new values for each channel). Figure 46B shows the loss in signal strength when the peak to peak values and zero calcium are compared to the area to area values obtained with 65 nM resting calcium. The initial loss of ~60 % at a given free calcium value of 100 nM is due to the overall small signals obtained at that calcium concentration and therefore overestimated.

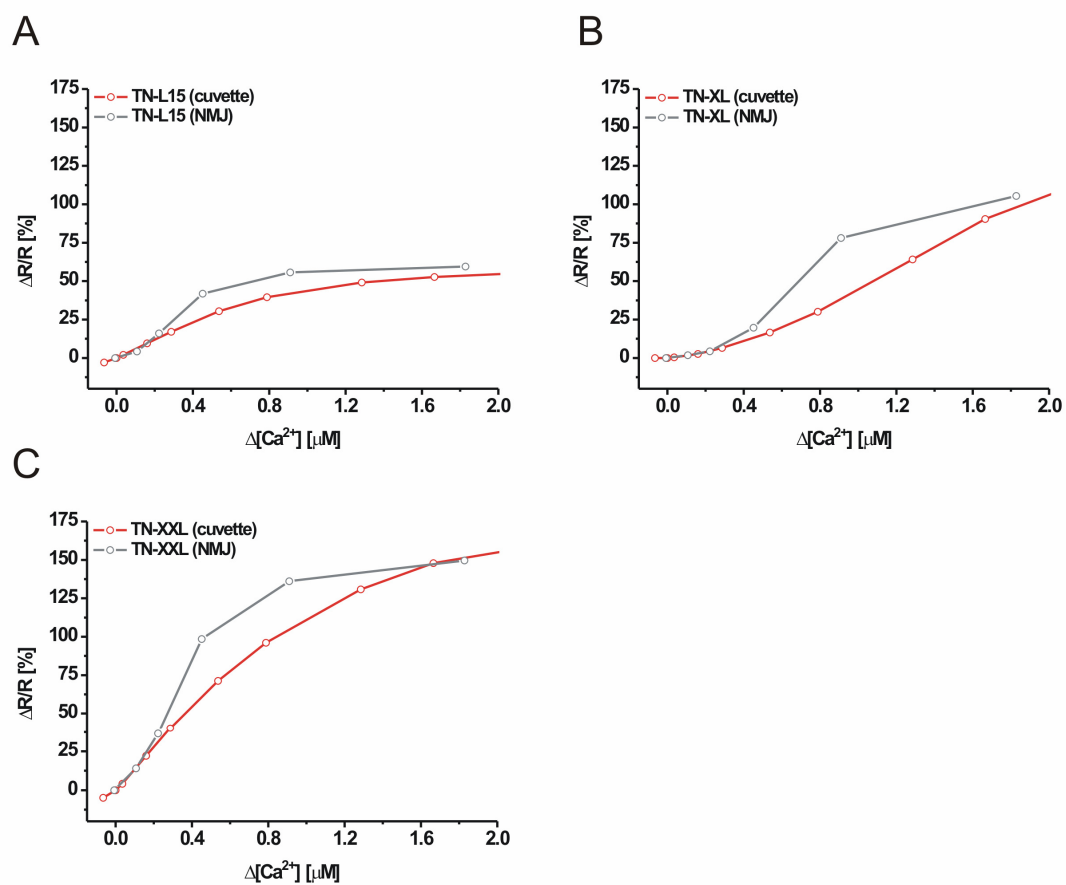


Figure 47: Comparison of *in vivo* mimicked data of calcium titrations to *in vivo* data obtained at the *Drosophila* NMJ for three TnC-based GECIs.

Signals acquired from the two systems for (A) TN-L15, (B) TN-XL and (C) TN-XXL. The x-axis depicts the deflection in the calcium concentration. For the cuvette data baseline is set to 65 nM to mimic resting calcium inside the boutons. Additionally all signals are calculated according to the loss of bandpass filters. *In vivo* data refer to 0, 10, 20, 40, 80 and 160 Hz stimulation that give rise to a deflection in the intracellular calcium level of 0, 0.11, 0.22, 0.45, 0.91 and 1.83 μM.

Nevertheless, when the ideal cuvette data (peak to peak, zero resting calcium) above 100 nM free Ca^{2+} are compared to the *in vivo* mimicked data (area to area, 65 nM resting calcium), one finds a robust overall 15 - 30 % loss in signal strength. Comparing the *in vivo* mimicked data of the titrations with the signals obtained at different stimulation frequencies acquired at the fly's NMJ, the discrepancy in signal strength observed in the two systems vanishes. Figure 47 depicts a comparison of the data obtained in the two systems. Cuvette data correspond to $\Delta R/R$ values in [%] that were calculated accounting for the use of bandpass filters and a resting calcium concentration of 65 nM. The x-axis depicts the deflection of calcium from this resting value. To compare the cuvette data to the *in vivo* data, an intracellular calcium estimation was performed using the synthetic calcium indicator OGB-1. The method used here has been described by Maravall and colleagues (81) and was performed by Thomas Hendel. A resting calcium concentration of 31 nM has been determined in the unstimulated boutons with a deflection of calcium ($\Delta[\text{Ca}^{2+}]$) of 110 nM (10 Hz), 220 nM (20 Hz), 450 nM (40 Hz), 910 nM (80 Hz) and 1.83 μM (160 Hz). Since all TnC-based GECIs displayed poor or absent signals to calcium concentrations from zero to 65 nM in cuvette titrations, fly data were aligned with the bandpass filtered data according to 65 nM from cuvette measurements which displayed the best estimation for the resting state in the boutons. When the corrected data are compared, one finds a good agreement of cuvette and *in vivo* data. For 10, 20 and 160 Hz both systems yield the same $\Delta R/R$ values for all three indicators. Interestingly data obtained from the *Drosophila* NMJ shows slightly bigger signals for 40 Hz and 80 Hz stimulation. Nevertheless, if these considerations are taken into account (usage of bandpass filters and a resting calcium concentration), a dramatic loss in performance of a GECI may not necessarily be due to folding problems or inactivation of the protein-based calcium indicator in *in vivo* applications. Quite the contrary, the loss of signal strength of a calcium indicator can be easily explained by the basic conditions that are faced in *in vivo* calcium imaging experiments like the use of bandpass filters and the resting calcium state of a cell as it is clearly demonstrated by Figure 47. Especially for high affinity calcium indicators the resting calcium concentration can have a

Discussion

dramatic effect on the signal strength that can be obtained *in vivo* applications. When determining the peak $\Delta F/F$ values in [%] of OGB-1 in cuvette titrations starting from baseline levels of zero, 38 nM and 65 nM free calcium, the maximum signal drops from 800 % to below 200 % (Figure 48).

Since most of the GECIs do not belong to high affinity calcium indicators and therefore show only moderate responsiveness to really small absolute calcium values (up to 50 - 100 nM), the drawback of having a resting calcium state inside a cell does not diminish the signals of GECIs in that way as it would affect high affinity synthetic calcium indicators. One exception might be D3cpv which already shows a significant signal at 65 nM (46 % $\Delta R/R$). Although OGB-1 encounters a dramatic reduction in signal strength when considering a resting calcium level, the overall high fractional fluorescence change of this synthetic indicator is able to buffer this drawback.

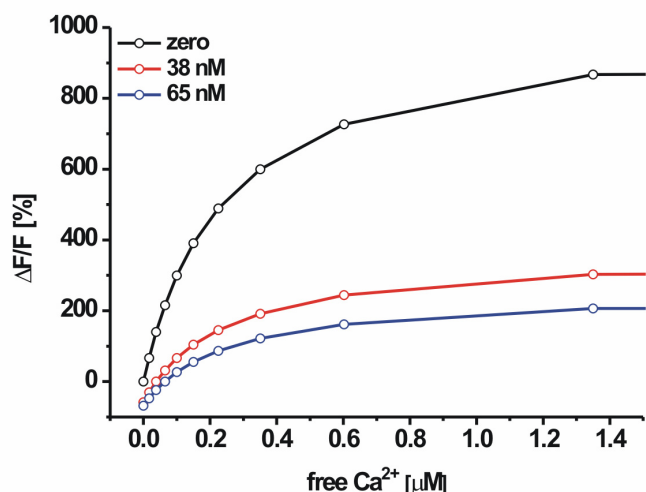


Figure 48: Signal strength of OGB-1 obtained at different resting calcium values.

5.4. Determination of TN-XXL's detection threshold in organotypic hippocampal slices

As mentioned before the first generation of troponin C-based calcium indicators (TN-L15) failed to report cytosolic calcium changes that are elicited by single action potentials (61). Therefore we considered the possibility that the new generation TN-XXL indicator could close that gap. For that reason we expressed TN-XXL by infecting organotypic hippocampal slices with the Semliki Forest Virus (SFV) (82, 83). Expression of the GECI is driven by the genomic promoter of that particular virus which is able to infect various cell types. To elicit different stimuli whole cell patch clamp recordings of hippocampal CA1 pyramidal neurons were performed. Cells were held in current clamp configuration and action potentials elicited by current pulses of 0.2 - 0.4 nA for 10 ms injected through the recording electrode. All experiments were performed at room temperature. Wide field fluorescence imaging was performed with a CCD camera at a rate of 25 Hz. Individual channels were recorded using appropriate bandpass filters (480/30 nm for CFP and 535/30 nm for YFP) upon excitation with 420/30 nm.

I performed subcloning of TN-XXL into the pSCA vector that has been used to create virus particles. Generation of virus particles, data analysis, patch-clamping and imaging of organotypic hippocampal slices were accomplished by Stephan Direnberger at the MPI of Neurobiology.

Figure 49A represents traces obtained from four independently measured cells stimulated with 1, 2, 5, 10 and 20 action potentials elicited at 20 Hz. As it can be seen calcium transients evoked by a single action potential are detected with TN-XXL that can be seen even in single experiments. According to the investigation at the *Drosophila* NMJ, signals seem to saturate when the number of action potentials was increased (Figure 49B).

Discussion

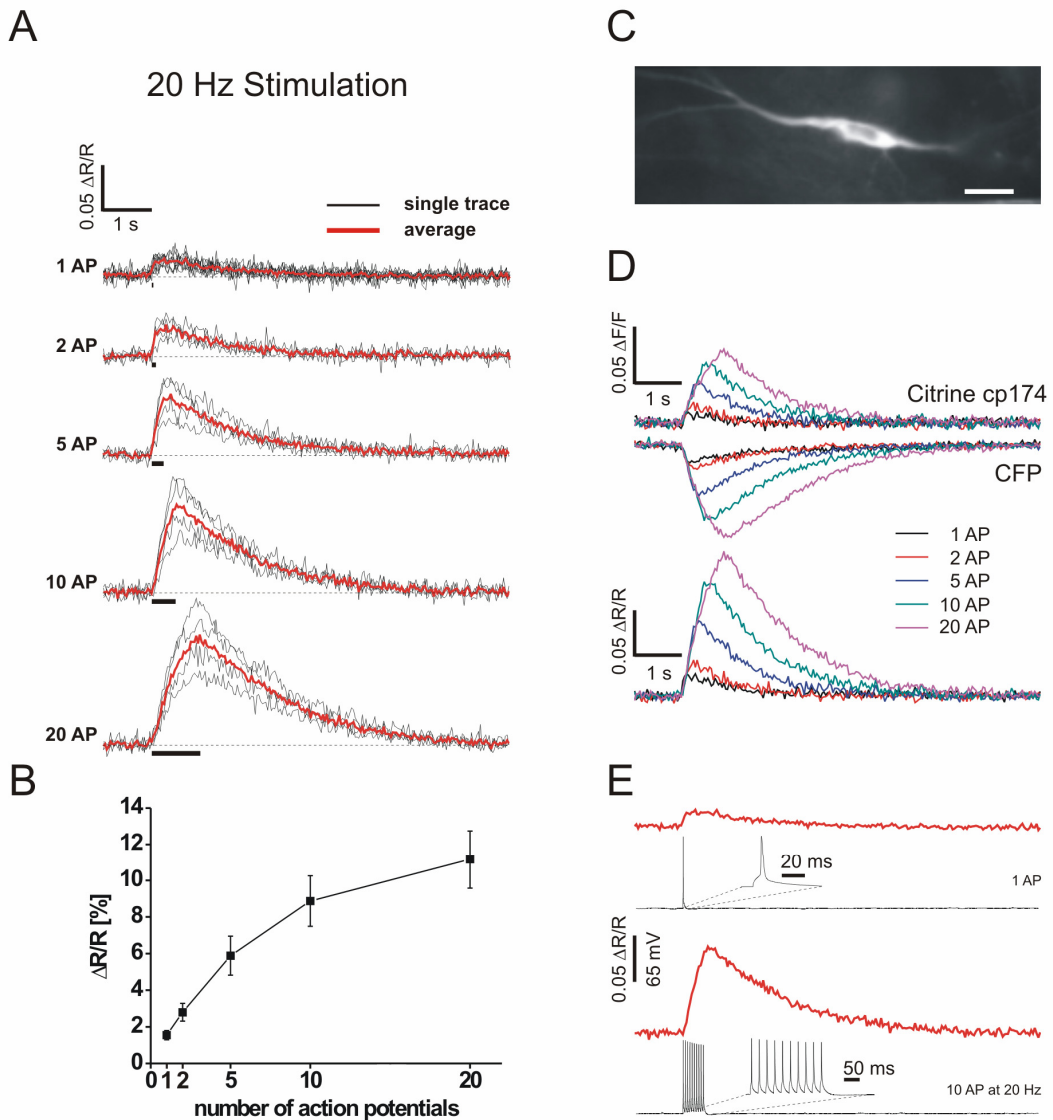


Figure 49: *In vitro* responses of TN-XXL in organotypic hippocampal slices.

(A) 20 Hz stimulation for 1, 2, 5, 10 and 20 action potentials (APs) for patched CA1 neurons. The APs are evoked by short triggered current pulses (0.2 - 0.4 nA for 10 ms/pulse). Each pulse elicits one action potential. The black bar below each trace displays the time of the electrical stimulation. The black lines show the $\Delta R/R$ in [%] of a single trial of each cell, the red line depicts the average of four individual cells. (B) Overview of the $\Delta R/R_{\max}$ dependence for 1, 2, 5, 10 and 20 AP at 20 Hz stimulation ($n = 4$, \pm SEM). (C) A CA1 pyramidal neuron of a cultured hippocampal slice expressing TN-XXL. Scale bar, 5 μ m. (D) Recordings of a single train for one patched CA1 neuron are plotted. Current injections evoke 1, 2, 5, 10 and 20 action potentials. The upper graph displays the change of fluorescence intensity $\Delta F/F$ in [%] for the single channels (Citrine cp174 and CFP) during and after current injection. The graph combines all recordings from 1 to 20 AP. The lower graph shows the ratio $\Delta R/R$ in [%] calculated from the background subtracted single channels. (E) Electrophysiology data for a stimulation protocol of 1 AP and 10 AP at 20 Hz (black lines, with blow up) and the respective average $\Delta R/R$ in [%] ($n = 4$) (red lines).

Clear responses of TN-XXL were visible in single runs as it can be seen in Figure 49D that depicts the time course of the individual channels and the calculated $\Delta R/R$ value in [%] of a single measured cell (and therefore one trial per stimulus at 20 Hz). Average signals obtained from four different cells and example electrophysiology traces for one action potential and ten action potentials (at 20 Hz) are shown in Figure 49E with the enlarged images depicting typical deflections in membrane potential that has been elicited by a single action potential or a burst of ten APs.

Detection of a single action potential has not been achieved with one of the troponin C-based calcium indicators TN-L15 and TN-XL and sets a milestone in the development of GECIs and the usage of these indicators in *in vivo* experiments.

It would be interesting to extend the stimulation paradigm and to investigate if synaptically evoked action potentials - by stimulation of a presynaptic cell and simultaneously recording of the indicator response in the postsynaptic cell - can also be detected by the use of TN-XXL. On the other hand it would be interesting to apply single action potentials at different interstimulus intervals to determine the minimum frequency at which these individual signals can be separated by the indicator.

5.5. *In vivo detection of sensory evoked calcium transient in mouse visual cortex*

Since TN-XXL displayed outstanding performance at the *Drosophila* NMJ and it was possible to sense single action potentials in organotypic hippocampal slices, this indicator should fulfill all the requirements needed for *in vivo* imaging of neuronal activity.

In mice, sensory afferents project from the retina to the dLGN (dorsal laterale geniculate nucleus) before entering the V1 region of the primary visual cortex that consists of a major monocular and a minor (lateral) binocular region (84, 85). Within the mouse primary visual cortex one can find orientation selective

Discussion

neurons i.e. neurons that respond best to moving bars or gratings of a particular orientation or a subset of orientations in the receptive field (85). It was now, after the promising results reported above, of highest interest to see if this orientation tuning of neurons could be detected by means of calcium imaging performed on single cells using our GECI TN-XXL.

For that reason expression of TN-XXL in the V1 region was achieved by infection with the semliki forest virus or by in utero electroporation. Cells in the monocular region were imaged using 2P-microscopy (with a 480/40 nm filter for CFP and a 535/30 nm filter for Citrine cp174) upon stimulation of the contralateral eye with moving bars of different orientations. Images were acquired at 1 Hz and the stimulus was applied for 5 s (separated by an inter stimulus interval of 5 s).

I performed subcloning of TN-XXL into the pSCA vector that has been used to create virus particles. Generation of virus particles was carried out by Stephan Direnberger at the MPI of Neurobiology. In utero electroporation was accomplished by Christiaan Levelt at the Netherlands Institute for Neuroscience, Amsterdam (Netherlands). Infection of mouse visual cortex with the semliki forest virus, *in vivo* imaging and data analysis were performed by Alexandre Ferrao Santos at the MPI of Neurobiology.

Figure 50 shows *in vivo* fluorescent responses of TN-XXL expressing neurons in V1. Detection of calcium signals was achieved no matter if the expression was driven by virus infection (Figure 50A and Figure 50B, two different cells each infected with the semliki forest virus) or by in utero electroporation (Figure 50C). As it can be extracted from the data depicted in Figure 50 one could indeed find cells that responded to a variety of different orientations which were detected using calcium imaging with genetically-encoded calcium indicators. To stress one major advantage of using GECIs the cell in Figure 50C was repeatedly measured over several days. In contrast to the semiliki forest virus infection the in utero electroporation lead to a stable expression of the indicator in the neurons and therefore allows for chronic imaging. Expression obtained by virus delivery usually comes along with a change of

morphology of the cell and eventually cell death due to the overexpression that is promoted by the viral genomic promoter.

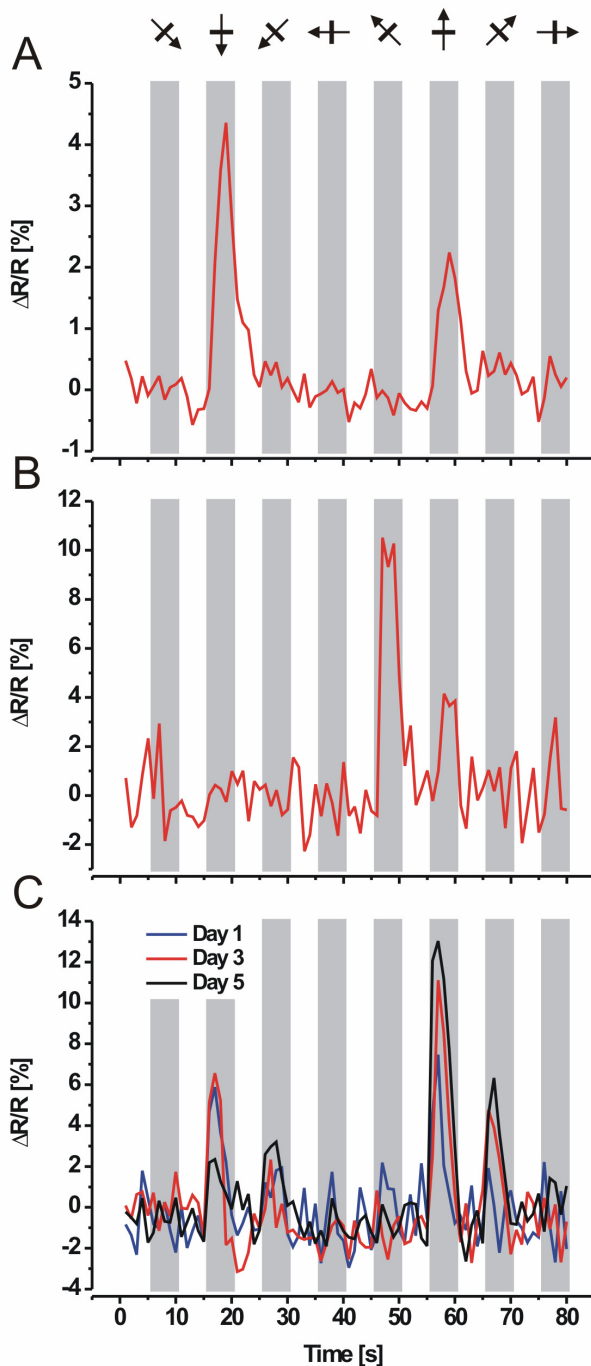


Figure 50: *In vivo* detection of sensory evoked calcium transients using TN-XXL.

(A) and (B) *In vivo* responses of two different cortical neurons in the V1 region (layer 2/3) of mice expressing TN-XXL after infection with the semliki forest virus. Grey bars indicate the time at which the given stimulation (depicted as arrows above) was applied. (C) Responses of a cortical neuron expressing TN-XXL after in utero electroporation. Chronic imaging was performed on that individual neuron for three successive sessions separated by one day. Data represent the average of six runs.

Calcium responses were recorded at three consecutive sessions separated by one day. In each session calcium transients could be detected with a stable major orientation for upward motion and with slightly varying signals for downward, downward-left and upper-rightward motion.

These data represents - at least to our knowledge - the first example of functional and chronic *in vivo* calcium imaging using genetically-encoded calcium indicators reporting sensory evoked calcium transients in mice.

5.6. Outlook

All the data presented in this thesis clearly demonstrate the significant improvement obtained with the development of TN-XXL compared to the previous generation of troponin C-based calcium indicators. Detection of single action potentials in hippocampal slices and the detection of sensory evoked calcium transients *in vivo* are a basic prerequisite of functional calcium imaging that can now be performed with genetically-encoded calcium indicators. Although there is still room for improvement of TN-XXL e.g. in signal strength especially to small changes in the calcium level, our next step will be the generation of a transgenic mouse that expresses TN-XXL in neurons. Therefore I will use the Thy1.2 promoter that has been successfully applied to drive expression of various transgenes in the nervous system (61, 86).

Our group recently created transgenic mice that express a derivative of TN-L15 using the Thy1.2 promoter. As already mentioned these transgenic mice showed a lack of sensitivity to single action potential evoked calcium transients. The goal is to close that gap by generating a transgenic mouse expressing the improved GECI TN-XXL that will allow for more sensitive and robust *in vivo* calcium imaging. This in turn would be a next step to realize the advantage of calcium imaging based on genetically-encoded calcium indicators - a 'ready to image' animal.

References

1. Klar TA, Jakobs S, Dyba M, Egner A, Hell SW (2000) Fluorescence microscopy with diffraction resolution barrier broken by stimulated emission. *Proc Natl Acad Sci U S A* 97: 8206-8210.
2. Betzig E, Trautman JK, Harris TD, Weiner JS, Kostelak RL (1991) Breaking the Diffraction Barrier: Optical Microscopy on a Nanometric Scale. *Science* 251: 1468-1470.
3. Westphal V, Hell SW (2005) Nanoscale resolution in the focal plane of an optical microscope. *Phys Rev Lett* 94: 143903.
4. Denk W, Strickler JH, Webb WW (1990) Two-photon laser scanning fluorescence microscopy. *Science* 248: 73-76.
5. Flusberg BA, Jung JC, Cocker ED, Anderson EP, Schnitzer MJ (2005) In vivo brain imaging using a portable 3.9 gram two-photon fluorescence microendoscope. *Opt Lett* 30: 2272-2274.
6. Griffin BA, Adams SR, Tsien RY (1998) Specific covalent labeling of recombinant protein molecules inside live cells. *Science* 281: 269-272.
7. Tour O, Adams SR, Kerr RA, Meijer RM, Sejnowski TJ, Tsien RW, Tsien RY (2007) Calcium Green FlAsH as a genetically targeted small-molecule calcium indicator. *Nat Chem Biol* 3: 423-431.
8. Tsien RY (1998) The green fluorescent protein. *Annu Rev Biochem* 67: 509-544.
9. Lichtman JW, Conchello JA (2005) Fluorescence microscopy. *Nat Methods* 2: 910-919.

10. Shimomura O, Johnson FH, Saiga Y (1962) Extraction, purification and properties of aequorin, a bioluminescent protein from the luminous hydromedusan, *Aequorea*. *J Cell Comp Physiol* 59: 223-239.
11. Prasher DC, Eckenrode VK, Ward WW, Prendergast FG, Cormier MJ (1992) Primary structure of the *Aequorea victoria* green-fluorescent protein. *Gene* 111: 229-233.
12. Chalfie M, Tu Y, Euskirchen G, Ward WW, Prasher DC (1994) Green fluorescent protein as a marker for gene expression. *Science* 263: 802-805.
13. Shimomura O (2006) Discovery of green fluorescent protein. *Methods Biochem Anal* 47: 1-13.
14. Cubitt AB, Heim R, Adams SR, Boyd AE, Gross LA, Tsien RY (1995) Understanding, improving and using green fluorescent proteins. *Trends Biochem Sci* 20: 448-455.
15. Ormo M, Cubitt AB, Kallio K, Gross LA, Tsien RY, Remington SJ (1996) Crystal structure of the *Aequorea victoria* green fluorescent protein. *Science* 273: 1392-1395.
16. Yang F, Moss LG, Phillips GN, Jr. (1996) The molecular structure of green fluorescent protein. *Nat Biotechnol* 14: 1246-1251.
17. Jung G, Wiegler J, Zumbusch A (2005) The photophysics of green fluorescent protein: influence of the key amino acids at positions 65, 203, and 222. *Biophys J* 88: 1932-1947.
18. Brejc K, Sixma TK, Kitts PA, Kain SR, Tsien RY, Ormo M, Remington SJ (1997) Structural basis for dual excitation and photoisomerization of the *Aequorea victoria* green fluorescent protein. *Proc Natl Acad Sci U S A* 94: 2306-2311.

References

19. Heim R, Prasher DC, Tsien RY (1994) Wavelength mutations and posttranslational autoxidation of green fluorescent protein. Proc Natl Acad Sci U S A 91: 12501-12504.
20. Wachter RM, Remington SJ (1999) Sensitivity of the yellow variant of green fluorescent protein to halides and nitrate. Curr Biol 9: R628-R629.
21. Wachter RM, Yarbrough D, Kallio K, Remington SJ (2000) Crystallographic and energetic analysis of binding of selected anions to the yellow variants of green fluorescent protein. J Mol Biol 301: 157-171.
22. Llopis J, McCaffery JM, Miyawaki A, Farquhar MG, Tsien RY (1998) Measurement of cytosolic, mitochondrial, and Golgi pH in single living cells with green fluorescent proteins. Proc Natl Acad Sci U S A 95: 6803-6808.
23. Jayaraman S, Haggie P, Wachter RM, Remington SJ, Verkman AS (2000) Mechanism and cellular applications of a green fluorescent protein-based halide sensor. J Biol Chem 275: 6047-6050.
24. Griesbeck O, Baird GS, Campbell RE, Zacharias DA, Tsien RY (2001) Reducing the environmental sensitivity of yellow fluorescent protein. Mechanism and applications. J Biol Chem 276: 29188-29194.
25. Nagai T, Ibata K, Park ES, Kubota M, Mikoshiba K, Miyawaki A (2002) A variant of yellow fluorescent protein with fast and efficient maturation for cell-biological applications. Nat Biotechnol 20: 87-90.
26. Kuner T, Augustine GJ (2000) A genetically encoded ratiometric indicator for chloride: capturing chloride transients in cultured hippocampal neurons. Neuron 27: 447-459.

27. Matz MV, Fradkov AF, Labas YA, Savitsky AP, Zaraisky AG, Markelov ML, Lukyanov SA (1999) Fluorescent proteins from nonbioluminescent Anthozoa species. *Nat Biotechnol* 17: 969-973.
28. Campbell RE, Tour O, Palmer AE, Steinbach PA, Baird GS, Zacharias DA, Tsien RY (2002) A monomeric red fluorescent protein. *Proc Natl Acad Sci U S A* 99: 7877-7882.
29. Shaner NC, Campbell RE, Steinbach PA, Giepmans BN, Palmer AE, Tsien RY (2004) Improved monomeric red, orange and yellow fluorescent proteins derived from Discosoma sp. red fluorescent protein. *Nat Biotechnol* 22: 1567-1572.
30. Wang L, Jackson WC, Steinbach PA, Tsien RY (2004) Evolution of new nonantibody proteins via iterative somatic hypermutation. *Proc Natl Acad Sci U S A* 101: 16745-16749.
31. Siegel MS, Isacoff EY (1997) A genetically encoded optical probe of membrane voltage. *Neuron* 19: 735-741.
32. Guerrero G, Siegel MS, Roska B, Loots E, Isacoff EY (2002) Tuning FlaSh: redesign of the dynamics, voltage range, and color of the genetically encoded optical sensor of membrane potential. *Biophys J* 83: 3607-3618.
33. Smith JC (1990) Potential-sensitive molecular probes in membranes of bioenergetic relevance. *Biochim Biophys Acta* 1016: 1-28.
34. Gross D, Loew LM (1989) Fluorescent indicators of membrane potential: microspectrofluorometry and imaging. *Methods Cell Biol* 30: 193-218.
35. Tsien RY (1980) New calcium indicators and buffers with high selectivity against magnesium and protons: design, synthesis, and properties of prototype structures. *Biochemistry* 19: 2396-2404.

References

36. Gryniewicz G, Poenie M, Tsien RY (1985) A new generation of Ca²⁺ indicators with greatly improved fluorescence properties. *J Biol Chem* 260: 3440-3450.
37. Minta A, Kao JP, Tsien RY (1989) Fluorescent indicators for cytosolic calcium based on rhodamine and fluorescein chromophores. *J Biol Chem* 264: 8171-8178.
38. Stosiek C, Garaschuk O, Holthoff K, Konnerth A (2003) In vivo two-photon calcium imaging of neuronal networks. *Proc Natl Acad Sci U S A* 100: 7319-7324.
39. Palmer AE, Giacomello M, Kortemme T, Hires SA, Lev-Ram V, Baker D, Tsien RY (2006) Ca²⁺ indicators based on computationally redesigned calmodulin-peptide pairs. *Chem Biol* 13: 521-530.
40. Miyawaki A, Llopis J, Heim R, McCaffery JM, Adams JA, Ikura M, Tsien RY (1997) Fluorescent indicators for Ca²⁺ based on green fluorescent proteins and calmodulin. *Nature* 388: 882-887.
41. Heim N, Griesbeck O (2004) Genetically encoded indicators of cellular calcium dynamics based on troponin C and green fluorescent protein. *J Biol Chem* 279: 14280-14286.
42. Moldoveanu T, Jia Z, Davies PL (2004) Calpain activation by cooperative Ca²⁺ binding at two non-EF-hand sites. *J Biol Chem* 279: 6106-6114.
43. Rizo J, Sudhof TC (1998) C2-domains, structure and function of a universal Ca²⁺-binding domain. *J Biol Chem* 273: 15879-15882.
44. Verdaguer N, Corbalan-Garcia S, Ochoa WF, Fita I, Gomez-Fernandez JC (1999) Ca(2+) bridges the C2 membrane-binding domain of protein kinase Calpha directly to phosphatidylserine. *EMBO J* 18: 6329-6338.

45. Shao X, Fernandez I, Sudhof TC, Rizo J (1998) Solution structures of the Ca²⁺-free and Ca²⁺-bound C2A domain of synaptotagmin I: does Ca²⁺ induce a conformational change? *Biochemistry* 37: 16106-16115.
46. Kretsinger RH, Nockolds CE (1973) Carp muscle calcium-binding protein. II. Structure determination and general description. *J Biol Chem* 248: 3313-3326.
47. Gifford JL, Walsh MP, Vogel HJ (2007) Structures and metal-ion-binding properties of the Ca²⁺-binding helix-loop-helix EF-hand motifs. *Biochem J* 405: 199-221.
48. Grabarek Z (2006) Structural basis for diversity of the EF-hand calcium-binding proteins. *J Mol Biol* 359: 509-525.
49. Tikunova SB, Black DJ, Johnson JD, Davis JP (2001) Modifying Mg²⁺ binding and exchange with the N-terminal of calmodulin. *Biochemistry* 40: 3348-3353.
50. Filatov VL, Katrukha AG, Bulargina TV, Gusev NB (1999) Troponin: structure, properties, and mechanism of functioning. *Biochemistry (Mosc)* 64: 969-985.
51. Potter JD, Gergely J (1975) The regulatory system of the actin-myosin interaction. *Recent Adv Stud Cardiac Struct Metab* 5: 235-244.
52. Lewit-Bentley A, Rety S (2000) EF-hand calcium-binding proteins. *Curr Opin Struct Biol* 10: 637-643.
53. Jurado LA, Chockalingam PS, Jarrett HW (1999) Apocalmodulin. *Physiol Rev* 79: 661-682.
54. Baird GS, Zacharias DA, Tsien RY (1999) Circular permutation and receptor insertion within green fluorescent proteins. *Proc Natl Acad Sci U S A* 96: 11241-11246.

References

55. Nagai T, Sawano A, Park ES, Miyawaki A (2001) Circularly permuted green fluorescent proteins engineered to sense Ca²⁺. *Proc Natl Acad Sci U S A* 98: 3197-3202.
56. Tallini YN, Ohkura M, Choi BR, Ji G, Imoto K, Doran R, Lee J, Plan P, Wilson J, Xin HB, Sanbe A, Gulick J, Mathai J, Robbins J, Salama G, Nakai J, Kotlikoff MI (2006) Imaging cellular signals in the heart *in vivo*: Cardiac expression of the high-signal Ca²⁺ indicator GCaMP2. *Proc Natl Acad Sci U S A* 103: 4753-4758.
57. Nagai T, Yamada S, Tominaga T, Ichikawa M, Miyawaki A (2004) Expanded dynamic range of fluorescent indicators for Ca(2+) by circularly permuted yellow fluorescent proteins. *Proc Natl Acad Sci U S A* 101: 10554-10559.
58. Mank M, Reiff DF, Heim N, Friedrich MW, Borst A, Griesbeck O (2006) A FRET-based calcium biosensor with fast signal kinetics and high fluorescence change. *Biophys J* 90: 1790-1796.
59. Gordon AM, Homsher E, Regnier M (2000) Regulation of contraction in striated muscle. *Physiol Rev* 80: 853-924.
60. Reiff DF, Ihring A, Guerrero G, Isacoff EY, Joesch M, Nakai J, Borst A (2005) In vivo performance of genetically encoded indicators of neural activity in flies. *J Neurosci* 25: 4766-4778.
61. Heim N, Garaschuk O, Friedrich MW, Mank M, Milos RI, Kovalchuk Y, Konnerth A, Griesbeck O (2007) Improved calcium imaging in transgenic mice expressing a troponin C-based biosensor. *Nat Meth* 4: 127-129.
62. Spradling AC, Rubin GM (1982) Transposition of cloned P elements into *Drosophila* germ line chromosomes. *Science* 218: 341-347.
63. Taketo M, Schroeder AC, Mobraaten LE, Gunning KB, Hanten G, Fox RR, Roderick TH, Stewart CL, Lilly F, Hansen CT, . (1991) FVB/N: an

- inbred mouse strain preferable for transgenic analyses. *Proc Natl Acad Sci U S A* 88: 2065-2069.
64. Lin DM, Goodman CS (1994) Ectopic and increased expression of Fasciclin II alters motoneuron growth cone guidance. *Neuron* 13: 507-523.
 65. Tikunova SB, Rall JA, Davis JP (2002) Effect of hydrophobic residue substitutions with glutamine on Ca(2+) binding and exchange with the N-domain of troponin C. *Biochemistry* 41: 6697-6705.
 66. Pearlstone JR, Borgford T, Chandra M, Oikawa K, Kay CM, Herzberg O, Moult J, Herklotz A, Reinach FC, Smillie LB (1992) Construction and characterization of a spectral probe mutant of troponin C: application to analyses of mutants with increased Ca²⁺ affinity. *Biochemistry* 31: 6545-6553.
 67. Trigo-Gonzalez G, Awang G, Racher K, Neden K, Borgford T (1993) Helix variants of troponin C with tailored calcium affinities. *Biochemistry* 32: 9826-9831.
 68. Rao ST, Satyshur KA, Greaser ML, Sundaralingam M (1996) X-ray structures of Mn, Cd and Tb metal complexes of troponin C. *Acta Crystallogr D Biol Crystallogr* 52: 916-922.
 69. Ohkura M, Matsuzaki M, Kasai H, Imoto K, Nakai J (2005) Genetically encoded bright Ca²⁺ probe applicable for dynamic Ca²⁺ imaging of dendritic spines. *Anal Chem* 77: 5861-5869.
 70. Brand AH, Perrimon N (1993) Targeted gene expression as a means of altering cell fates and generating dominant phenotypes. *Development* 118: 401-415.
 71. Lin DM, Goodman CS (1994) Ectopic and increased expression of Fasciclin II alters motoneuron growth cone guidance. *Neuron* 13: 507-523.

References

72. Volterra A, Meldolesi J (2005) Astrocytes, from brain glue to communication elements: the revolution continues. *Nat Rev Neurosci* 6: 626-640.
73. Jakovcevic D, Harder DR (2007) Role of astrocytes in matching blood flow to neuronal activity. *Curr Top Dev Biol* 79: 75-97.
74. Nolte C, Matyash M, Pivneva T, Schipke CG, Ohlemeyer C, Hanisch UK, Kirchhoff F, Kettenmann H (2001) GFAP promoter-controlled EGFP-expressing transgenic mice: a tool to visualize astrocytes and astrogliosis in living brain tissue. *Glia* 33: 72-86.
75. Hirrlinger PG, Scheller A, Braun C, Quintela-Schneider M, Fuss B, Hirrlinger J, Kirchhoff F (2005) Expression of reef coral fluorescent proteins in the central nervous system of transgenic mice. *Mol Cell Neurosci* 30: 291-303.
76. Scemes E, Giaume C (2006) Astrocyte calcium waves: what they are and what they do. *Glia* 54: 716-725.
77. Hasan MT, Friedrich RW, Euler T, Larkum ME, Giese G, Both M, Duebel J, Waters J, Bujard H, Griesbeck O, Tsien RY, Nagai T, Miyawaki A, Denk W (2004) Functional fluorescent Ca²⁺ indicator proteins in transgenic mice under TET control. *PLoS Biol* 2: e163.
78. Romani A (2007) Regulation of magnesium homeostasis and transport in mammalian cells. *Arch Biochem Biophys* 458: 90-102.
79. Reid RE, Hodges RS (1980) Co-operativity and calcium/magnesium binding to troponin C and muscle calcium binding parvalbumin: an hypothesis. *J Theor Biol* 84: 401-444.
80. Procyshyn RM, Reid RE (1994) A structure/activity study of calcium affinity and selectivity using a synthetic peptide model of the helix-loop-helix calcium-binding motif. *J Biol Chem* 269: 1641-1647.

81. Maravall M, Mainen ZF, Sabatini BL, Svoboda K (2000) Estimating intracellular calcium concentrations and buffering without wavelength ratioing. *Biophys J* 78: 2655-2667.
82. DiCiommo DP, Bremner R (1998) Rapid, high level protein production using DNA-based Semliki Forest virus vectors. *J Biol Chem* 273: 18060-18066.
83. Ehrengruber MU, Lundstrom K, Schweitzer C, Heuss C, Schlesinger S, Gahwiler BH (1999) Recombinant Semliki Forest virus and Sindbis virus efficiently infect neurons in hippocampal slice cultures. *Proc Natl Acad Sci U S A* 96: 7041-7046.
84. Hofer SB, Mrsic-Flogel TD, Bonhoeffer T, Hubener M (2006) Lifelong learning: ocular dominance plasticity in mouse visual cortex. *Curr Opin Neurobiol* 16: 451-459.
85. Hubener M (2003) Mouse visual cortex. *Curr Opin Neurobiol* 13: 413-420.
86. Caroni P (1997) Overexpression of growth-associated proteins in the neurons of adult transgenic mice. *J Neurosci Methods* 71: 3-9.

Acknowledgements

First of all I would like to thank my supervisors Oliver Griesbeck and Axel Borst - not only for giving me the opportunity (and the salary) to perform the research presented in this thesis, but also for just having fun in the lab. Both were and are able to create one of the best working atmospheres I was allowed to experience.

Of course, I want to express a special gratitude to my parents for always believing in and giving their boundless support to me.

I also want to thank all the members of the 'Griesbeck lab family' for having (un)fruitful discussions and sharing a good time, especially Anja for outstanding technical support during the last four years. Furthermore I have to mention Stephan 'the HiWianer' Direnberger who made his way from the 'interesting' life of a HiWi and fighter in the 'Tierhaus' to a very talented PhD student providing the world with more genetically-encoded biosensors - you'll do it, mate!

Thanks to all the guys in the Borst department, especially those who shared a lot of time drinking coffee with me (yes it's you Nina, Adrian, Alex, Nicola and Jones - 'the Chilean').

Special greetings will also be sent to Würzburg. It always was and will be a pleasure for me having nice days in lovely Franconia - thank you Mirijam and Fenz, Jochen and, of course, Holger - 'the Bocuse'.

Last but not least I want to thank all the people that 'believed' in the indicator and therefore provided nice pictures to this thesis. Thank you Thomas and Dierk for letting the fly blink and Alexandre and Mark for seeing what a mouse sees.

Curriculum Vitae

Education:

Since January 05: PhD thesis at the Max-Planck-Institute of Neurobiology, Martinsried, Germany under supervision of Dr. Oliver Griesbeck and Prof. Dr. Alexander Borst: 'Improved Genetically-Encoded Calcium Indicators Based on Troponin C'.

January 04 - December 04: Diploma thesis at the Max-Planck-Institute of Neurobiology, Martinsried, Germany under supervision of Dr. Oliver Griesbeck and Prof. Dr. Alexander Borst: 'Zirkulär permutierte Varianten des Grün Fluoreszierenden Proteins zur Steigerung der FRET-Effizienz von genetisch-codierten Biosensoren'.

October 99 - December 03: Undergraduate studies in Biology at the University of Würzburg, Germany.

July 97: Graduation from High School (Schiller-Gymnasium, Hof, Germany).

Publications:

Mank M, Griesbeck O (2008) Genetically Encoded Calcium Indicators. Chem Rev (in press).

Griesbeck O, **Mank M** Genetically encoded calcium sensors comprising the C-terminal lobe of troponin C and a fluorescence tag. Internationale Patentanmeldung: PCT/EP2007/007463.

Heim N, Garaschuk O, Friedrich MW, **Mank M**, Milos RI, Kovalchuk Y, Konnerth A, Griesbeck O (2007) Improved calcium imaging in transgenic mice expressing a troponin C-based biosensor. Nat Meth 4: 127-129.

Mank M, Reiff DF, Heim N, Friedrich MW, Borst A, Griesbeck O (2006) A FRET-based calcium biosensor with fast signal kinetics and high fluorescence change. Biophys J 90: 1790-1796.

Versicherung

Ehrenwörtliche Versicherung

Ich versichere hiermit ehrenwörtlich, dass die vorgelegte Dissertation von mir selbständig und ohne unerlaubte Hilfe angefertigt ist.

München, den _____

Marco Mank

Erklärung

Hiermit erkläre ich, dass die Dissertation nicht ganz oder in wesentlichen Teilen einer anderen Prüfungskommission vorgelegt worden ist und dass ich mich anderweitig einer Doktorprüfung ohne Erfolg nicht unterzogen habe.

München, den _____

Marco Mank